HYDRODYNAMIC ANALYSIS AND COMPUTER SIMULATION APPLIED TO SHIP INTERACTION DURING MANEUVERING IN SHALLOW CHANNELS

by

Sankaranarayanan Kizakkevariath

Thesis submitted to the Faculty of
Virginia Polytechnic Institute and State University
in partial fulfillment of the requirements for the degree of
Doctor of Philosophy
in
Aerospace Engineering

APPROVED:

Dr. Paul Kaplan, Chairman

Dr. J.A.Schetz

Dr. W.L.Neu

Dr. A.G. Szeless

Dr. L .Nikolaidis

May 1989

Blacksburg, Virginia

Hydrodynamic Analysis and Computer Simulation Applied to Ship Interaction During Maneuvering in Shallow Channels

by

Sankaranarayanan Kizakkevariath

Dr. Paul Kaplan, Chairman
Aerospace Engineering

(ABSTRACT)

A generalized hydrodynamic interaction force model is combined with a ship maneuvering simulator to provide a free-running, closed loop ship simulation capable of trajectory predictions of ships operating in close proximity in a shallow, asymmetric canal. The interaction force model is based on the generalized Lagally's theorem, properly accounting for the orientations and dynamic motions of the ships. Also included are the lift forces and the cross-flow drag forces, which are found to be important for bank suction phenomena. A simplified method is implemented for box shapes, applicable for barge-tows operating in rivers. Results of the calculations are found to be generally in good agreement with experimental and other theoretical results.

This work would have utility in studying maneuvers involving ships and barges in close proximity and can be used in training pilots who operate in canals, harbors and rivers, and also in studying the effects of various steering control systems in the early design stages.

Acknowledgements

I am indebted to Dr. Paul Kaplan for his help and guidance in furthering this work. I also wish to thank Dr. Schetz, Dr. Neu, Dr. Nikolaidis and Dr. Szeless for serving in my committee.

I am grateful to who was my link with the University during the last phase of this project, when I was working in-absentia. Also I am indebted to of Florida Atlantic University who helped me with computations and word processing with a personal computer, without which this work would be incomplete. Finally I thank , , , , , , , and all other friends for their help and encouragement.

To my father...

Table of contents

LIST OF ILLUSTRATIONS

NOMENCLATURE

A_{22}		Lateral sectional added mass coefficient.
A_{66}		Added inertia coefficient in yaw.
B		Displacement of ship.
CB		Block coefficient.
C_D		Cross-flow drag coefficient.
C_{L_α}		Rate of C_L with change in α.
H_i		Water depth in i^{th} channel.
F_x	$F_x' = \frac{2F_x}{\rho L^2 U^2}$	Hydrodynamic force along X-direction.
F_y	$F_Y' = \frac{2F_y}{\rho L^2 U^2}$	Hydrodynamic force along Y- direction.
I_X	$I_X' = \frac{2I_x}{\rho L^5}$	Moment of inertia of ship about X-axis.
I_Y	$I_Y' = \frac{2I_Y}{\rho L^5}$	Moment of inertia of ship about Y-axis.
I_Z	$I_Z' = \frac{2I_z}{\rho L^5}$	Moment of inertia of ship about Z-axis.
	K_2	Lateral added mass coefficient of ship.
	K_3'	Added inertia coefficient in yaw of ship.
m	$m' = \frac{2m}{\rho L^3}$	Mass of ship.

N	$N' = \frac{2N}{\rho L^3 U^2}$	Hydrodynamic yawing moment.
N_L	$N'_L = \frac{2N_L}{\rho L^3 U^2}$	Contribution to the total hydrodynamic yaw moment from Lagally terms.
N_t	$N'_t = \frac{2N_t}{\rho L^3 U^2}$	Contribution to the total hydrodynamic yaw moment from unsteady terms.
$N_{\dot{v}}$	$N'_{\dot{v}} = \frac{2N\dot{v}}{\rho L^4}$	First order coefficient used in representing N as a function of $\dot{v}$.
N_v	$N'_v = \frac{2Nv}{\rho L^3 U}$	First order coefficient used in representing N as a function of v.
$N_{v\|v\|}$	$N'_{v\|v\|} = \frac{2Nv\|v\|}{\rho L^3}$	Second order coefficient used in representing N as a function of v^2.
$N_{r\|v\|}$	$N'_{r\|v\|} = \frac{2Nr\|v\|}{\rho L^4}$	Second order coefficient used in representing N as a function of vr.
N_r	$N'_r = \frac{2Nr}{\rho L^4 U}$	First order coefficient used in representing N as a function of r.
$N_{r\|r\|}$	$N'_{r\|r\|} = \frac{2Nr\|r\|}{\rho L^5}$	Second order coefficient used in representing N as a function of r^2.
$N_{\dot{r}}$	$N'_{\dot{r}} = \frac{2N\dot{r}}{\rho L^5}$	First order coefficient used in representing N as a function of $\dot{r}$.
N^*	$N'^* = \frac{2N^*}{\rho L^3 U^2}$	Yaw moment when $\beta = \delta = 0$.
N_δ	$N'_\delta = \frac{2N_\delta}{\rho L^3 U^2}$	First order coefficient used in representing N as a function of δ.
N_{vvv}	$N'_{vvv} = \frac{2Nvvv}{\rho L^3 / U}$	Third order coefficient used in representing N as a function of v^3.

$N_{\delta\delta\delta}$	$N'_{\delta\delta\delta} = \frac{2N_{\delta\delta\delta}}{\rho L^3 U}$	Third order coefficient used in representing N as a function of δ^3.
n		Propeller revolutions per minute.
q		Source strength
r		Yaw rate (radians per second)
S		Sectional Area (square feet)
T		Sectional Draught (feet)
U		Forward speed of ship (feet per sec.)
u_i	$u'_i = \frac{u_i}{U}$	Induced velocity in the X-direction of ship-i.
v_i	$v'_i = \frac{v_i}{U}$	Induced velocity in the Y-direction of ship-i.
X_o	$X'_o = \frac{X_o}{L}$	X-Coordinate of the c.o.g of ship.
X_G	$X'_G = \frac{X_G}{L}$	Distance of c.o.g from mid-ship.
X	$X' = \frac{2X}{\rho L^2 U^2}$	Hydrodynamic force along the X-direction.
X_L	$X'_L = \frac{2X_L}{\rho L^2 U^2}$	Contribution to the total hydrodynamic X-Force from Lagally terms.
X_t	$X'_t = \frac{2X_t}{\rho L^2 U^2}$	Contribution to the total hydrodynamic X-Force from unsteady terms.
X_u	$X'_u = \frac{2X_u}{\rho L^2 U}$	First order coefficient used in representing X as a function of u.
$X_{\dot{u}}$	$X'_{\dot{u}} = \frac{2X_{\dot{u}}}{\rho L^3}$	First order coefficient used in representing X as a function of $\dot{u}$.

$X_{v\|v\|}$	$X'_{v\|v\|} = \frac{2X_{v\|v\|}}{\rho L^2}$	Second order coefficient used in representing X as a function of v^2.
$X_{v\|r\|}$	$X'_{v\|r\|} = \frac{2X_{v\|v\|}}{\rho L^3}$	Second order coefficient used in representing X as a function of vr.
$X_{r\|r\|}$	$X'_{r\|r\|} = \frac{2X_{r\|r\|}}{\rho L^4}$	Second order coefficient used in representing X as a function of r^2.
$X_{\delta\delta}$	$X'_{\delta\delta} = \frac{2X_{\delta\delta}}{\rho L^2 U^2}$	Second order coefficient used in representing X as a functiion of δ^2.
Y_0	$Y'_0 = \frac{Y_0}{L}$	Y-coordinate of the c.o.g. of ship. distance of c.o.g. from canal centerline.
Y	$Y' = \frac{2Y}{\rho L^2 U^2}$	Hydrodynamic lateral force.
Y_L	$Y'_L = \frac{2Y_L}{\rho L^2 U^2}$	Contribution to the total hydrodynamic lateral force from Lagally terms.
Y_t	$Y'_t = \frac{2Y_t}{\rho L^2 U^2}$	Contribution to the total hydrodynamic lateral force from unsteady terms.
Y_v	$Y'_v = \frac{2Y_v}{\rho L^2 U}$	First order coefficient used in representing Y as a function of v.
$Y_{v\|v\|}$	$Y'_{v\|v\|} = \frac{2Y_{v\|v\|}}{\rho L^2}$	Second order coefficient used in representing Y as a function of v^2.
$Y_{v\|r\|}$	$Y'_{v\|r\|} = \frac{2Y_{v\|v\|}}{\rho L^3}$	Second order coefficient used in representing Y as a function of vr.
$Y_{\dot{v}}$	$Y'_{\dot{v}} = \frac{2Y_{\dot{v}}}{\rho L^3}$	First order coefficient used in representing Y as a function of $\dot{v}$.

Y_r	$Y'_r = \frac{2Y_r}{\rho L^3 U}$	First order coefficient used in representing Y as a function of r.
$Y_{r\|r\|}$	$Y'_{r\|r\|} = \frac{2Y_{r\|r\|}}{\rho L^4}$	Second order coefficient used in representing Y as a function of r^2.
Y^*	$Y'^* = \frac{2Y^*}{\rho L^2 U^2}$	Lateral force when $\beta = \delta = 0$.
$Y_{\dot{r}}$	$Y'_{\dot{r}} = \frac{2Y_{\dot{r}}}{\rho L^4}$	First order coefficient used in representing Y as a function of $\dot{r}$.
Y_δ	$Y'_\delta = \frac{2Y_\delta}{\rho L^2 U^2}$	First order coefficient used in representing Y as a function of δ.
Y_{vvv}	$Y'_{vvv} = \frac{2Y_{vvv}}{\rho L^2/U}$	Third order coefficient used in representing Y as a function of v^3.
$Y_{\delta\delta\delta}$	$Y'_{\delta\delta\delta} = \frac{2Y_{\delta\delta\delta}}{\rho L^2 U^2}$	Third order coefficient used in representing Y as a function of δ^3.

β	Drift angle
δ	Rudder deflection angle.
ψ	Heading angle.
ϕ	Velocity potential
μ	Doublet strength
ξ	Stagger or longitudinal separation
η	Lateral separation
ρ	Mass density of sea water

INTRODUCTION

Navigation of ships in confined waters, particularly in narrow channels has received considerable attention in recent years. Sound knowledge of the behavior of ships operating in close proximity in canals and harbors is very important for ship owners, operators and everyone at large. It is well known that ships passing in canals are extremely difficult to control because of strong hydrodynamic interaction forces and moments. There is also considerable interest in problems concerning the navigation of barge flotillas in rivers and inland waters. These barge-tows are highly susceptible to collision which in recent years have resulted in millions of dollars lost in damages. Another related maneuver is the procedure of replenishing ships while they move along parallel course. As the ships move close to each other for a considerable amount of time, the interaction forces come to play which makes them difficult to maneuver.

Free running model experiments as well as computer simulations are widely used to study the behavior

of ships under the above circumstances. Free running model tests with radio controlled models in shallow water are very expensive to conduct and the small models which are usually employed in such tests are susceptible to large scale effects. The number of parameters involved in the study of maneuvering of ships in restricted channels are too large (dimensions of the canal, vessel speed, proximity of second ship, vessel orientation, steering control ...) to permit a complete model experiment investigation. Computer simulation on the other hand can be used very efficiently for simulation of all types of maneuvers under different conditions, permitting study of the contributions to maneuvering forces made by various changing parameters, once the basic data for the hydrodynamic coefficients are available.

Computer simulators presently running at research stations like the Army Corps of Engineers Waterways Experiment Station, Vicksburg, MS, and Computer Aided Operations Research Facility, Great Neck, New York, employ empirical modeling of interaction and shallow water phenomena, based on model experiments. The present work combines a generalized hydrodynamic force model with a ship maneuvering model to provide a complete closed-loop ship trajectory prediction system. This would have utility in

studying maneuvers involving ships and barges in close proximity in restricted waters. Such a model can be used in training pilots who operate in harbors, canals and rivers, and also in studying the effects of various control systems in the early design stages.

There have been a number of theoretical studies and a few experimental investigations concerning the hydrodynamic interactions between ships in close proximity in restricted waters. A brief survey of these works can be found in Sankaranarayanan [39]. The analyses range from simple two-dimensional approximations to more complex analyses involving matched asymptotic expansions and integral equations (as in Ref. 2,10 and 45).

All of these models and numerical results show that respective methods provide reasonable qualitative predictions of both lateral force and yaw moment. However all of them need further improvement in order to give acceptable quantitative predictions. It is known that two-dimensional theories are especially objectionable because of the fact that the two-dimensional assumption breaks down even with a small clearance between the ship and the canal bottom. The flow beneath the ship reduces the pressure difference across the hull resulting in smaller

forces and moments. Neglecting this flow as in the case of two-dimensional analysis is not considered as appropriate.

All of these analyses have considered the ships to be moving parallel to each other, as well as parallel to the canal walls. The degree of agreement between theory and model experimental data varies, with better agreement shown by the more complicated analyses-computational studies. The form of the results as well as the effort required for the computations, precluded their utility for simulator studies. This was a major motivation in carrying out experimental studies of forces on passing ships, as was carried out for the Panama Canal simulation study recently carried out by CAORF (Computer Aided Operations Research Facility) [41].

In a recent theoretical study carried out at VPI&SU [39] (also published in [22]), a theoretical analysis was carried out for the case of passing ships in an asymmetric canal. The ships were constrained to be moving parallel to each other and to the canal walls. The method of analysis used the Lagally theorem for unsteady flow, as well as a slender body theory lift force model, with the results determined in the form of triple integrals and summations in terms of the body geometries of the ships. This form of the results is relatively simple for

computation, in contrast to earlier approaches. Comparisons of the calculated results for passing ship cases in the Panama Canal tests at (Swedish Ship Model Testing Tank) SSPA [41], as well as for passing a moored tanker in NSMB (Netherlands Ship Model Basin) tests [38], showed good agreement with the test data. Some limited comparison with test data on steady forces on a single ship in an asymmetric shallow canal (as given in [29]) also showed fairly good agreement, with some features of the results indicating a possible need for further refinement.

All of the work referred to above did not consider arbitrary motions of the ships, which would properly reflect their behavior in realistic cases, but only the constraint of parallel motion at fixed lateral separation distances. The most useful tool for a simulation study would be a mathematical model that would remove that constraint and also include the interaction effects due to the ship dynamic motions.

1.1 PROBLEM DEFINITION

The problem studied herein involves the interaction forces between two ships, or between two barge-tows, during their relative motion with respect to each other, when they are travelling in a shallow canal or

river. The first part of this work describes the interaction force model and the second part deals with motion simulations. The canal (or channel) can have asymmetric depth conditions since export-oriented ports can consider deeper dredged regions for out-going cargo-laden ships. The intent is to calculate the generalized hydrodynamic forces acting on each ship due to the effects of the other ship, including the influence of the dynamic motions of that ship (i.e. sway and yaw), as well as the influence of the canal walls, when the ships operate in shallow water. The case of a single ship in a canal or the so-called bank suction problem is also covered in the scope of this work.

The forces to be found represent the generalized forces due to another ship and the physical boundaries, and are those not included when modeling the conventional hydrodynamic forces acting on a ship in either deep or shallow water. The inclusion of these forces, when also accounting for the effects of the dynamic motions of the ships on the forces, allows full modeling of ship interactions which is not completely carried out at present in ship simulation studies. Aside from cases of ships passing and/or overtaking, the influence of ship orientation, "crabbing" motion, etc. for the case of two ships as well as for a single ship near a canal wall have

not been either fully analyzed or placed in a form readily adaptable for use in a simulator. The application to simulator studies, which provide information appropriate to the problems of ship control and navigation, as well as to harbor and waterway development, are illustrations of the prospective use of the results of the present investigation.

CHAPTER-2

METHODS AND ASSUMPTIONS USED IN THE ANALYSIS

The method of approach will be similar to that in [24] and [39], where each ship was initially represented by a two-dimensional vertical center plane distribution of sources. This was done since that procedure was initially considered to be a way to reflect the effect of the finite draft of the ship relative to the canal depth, which is not done when one-dimensional center line source distributions are used, e.g., [1] and [31]. Associated vertical and lateral images are established to account for the influence of the finite depth, canal walls, and the free surface rigid wall boundary conditions. While satisfying these boundary conditions, the boundary condition on the ship hulls is no longer satisfied so that correcting dipole distributions are established whose strengths are proportional to the induced velocities arising from the image system and the other ship. The effect of the asymmetric canal (different depths in the two different regions, with a "step" in the depth illustrated in the canal cross-section) is represented by use of a piece wise potential function using Heaviside unit functions to indicate the region of validity of the

functional representations.

The basic analysis assumes an inviscid incompressible fluid, for which ideal potential flow concepts are applicable. Since ships in close proximity in canals and other restricted waterways move at low forward speeds, it is assumed that wave making effects are negligible. The bounding free surface condition then assumes the limit condition of a rigid free surface, so that double-body reflected models are used for the ships being considered (just as in the work of [24] and [39], as well as earlier studies represented by [2,10 and 45]).

In the mathematical modeling in [24] and [39], an important procedure is the use of the lateral added mass term applicable to shallow water in the establishment of the correcting dipole strength. This is a heuristic extension of Taylor's theorem [42], relating the dipole strength and added mass, to the case of a bounded fluid region. Since the major hydrodynamic force in the case of passing ships is the unsteady inertial-type force due to the dipole terms, that dominant term is the quantity that reflects the effect of vessel draft relative to the water depth. Another item of importance in the prior analysis in [24] and [39] is the inclusion of lift force effects, as determined by use of

slender body theory results, since such terms were found to be dominant when considering bank suction forces for a single ship in a canal (for the cases considered in [24] and [39]).

On the basis of the procedures and results in [24] and [39], where the major influence of finite depth was manifested in the added mass dependence on depth, the influence of the vertical distribution of source strength for the ship representation was found to be relatively unimportant. As a consequence of this result, it will be assumed that the initial source distribution for the body can be represented in terms of a one-dimensional center line distribution. This will reduce the integrations required for the final force results, thereby reducing computation time considerably. For the present problem it will also be necessary to include dipole distributions for both ships to represent their sway and yaw motions. The formulation allows an arbitrary orientation of each ship relative to the canal walls (which will be assumed to be parallel to each other). First all of the necessary images to account for the bottom, walls and free surface are established for the source distribution for each ship. The correcting dipole distributions in each ship are then determined, recognizing the effects of varying orientation and changing positions

that are possible due to the motions of each ship.

Further improvements in the modeling of [24] and [39] are also applied to the slender body lift force representation. The procedure used had followed a method similar to that of Jacobs [19], which contained certain semi- empirical features. Such features are inherent in the application of slender body theory modeling for ship stability derivatives, and generally represent the present state-of-the-art in such estimation procedures. However the application in [24] and [39] treated the sectional added mass and resulting lift force at the after end of the ship separately for the ship hull, the effective skeg addition, and the rudder, with each considered as a vertical flat plate. The same type of shallow water and free surface influence function was applied for each element, which is not appropriate for all ships. A more refined treatment of the slender body lift force, in terms of the proper model of the added mass effects of their envisioned trailing edge or stern end in a shallow water region, is provided here as an improved model.

In addition another effect often used in slender body theory analysis of transverse forces on bodies, viz. the influence of cross-flow drag, is included in the

analysis of the hydrodynamic forces. This effect, using the distribution of induced lateral cross-flow velocities due to images, is expected to have its major influence on problems associated with single ship bank suction effects due to the dominance of inertial effects in the unsteady passing ship case. This viscous cross-flow drag effect is expected to have a primary influence on the yaw moment rather than the side force, since the local cross-force representation will tend to cancel when integrated over the hull length. Similar type results have been found in other cases where cross-flow drag is considered for determining lateral forces and moments, as an adjunct to the pure potential slender body theory results (e.g. see [21]).

While these different improvements are useful refinements, the major effort involves the treatment of the effects of varying orientation and the inclusion of ship dynamic motion effects on the resulting generalized hydrodynamic forces. The mathematical model includes all of these effects and will therefore reflect the influence of the maneuvering of each ship. The generalized force module is structured so that it can be linked to an overall simulation model that will feed the ship dynamic motions to the force module. The changing interaction forces can then be included in the total dynamic model of the ship motion

responses, so that they will in turn influence the subsequent responses. Thus a coupling exists which is considered to be a realistic modeling of ship interaction in a purely dynamic sense, which is not present in existing simulator models.

The present analysis is intended to represent these interaction effects in the most complete manner possible. Results for a single ship are also expected to be a more realistic representation of the forces acting on a ship near a wall, since the analysis represents the influence of ship heading orientation as well as the ship sway and yaw motions. The model that is established as the end product of this work is expected to be the most complete possible for generalized interaction forces, and will be in a form suitable for direct utilization in a simulator system.

The computer program for determining the forces on both ships will also be established in this work, with the intent to have a rapid computation capability so that it can have greater utility in fast time off-line simulation (it is expected to be definitely capable for use in real time on-line simulation). The input requirements will only be ship geometry; speed; canal geometry; etc., without any

need for additional special experimental or empirical data. In this way the force module will be similar to the major elements that are used in predicting ship motions in waves (e.g., as in [37]), with only similar type input data necessary to apply such a theoretical model. This is a definite improvement in the field of maneuverability analysis that has relied largely on experimental data to establish hydrodynamic force models.

CHAPTER-3

PROBLEM FORMULATION AND ANALYSIS

The problem considered here is that of two slender bodies moving through an ideal fluid; the method is general and is applicable to ships moving in shallow and asymmetric canals. The ships may have arbitrary orientations and velocities, both of which may be changing with time. All possible maneuvers such as ships moving close to each other in shallow harbors, a single ship in a canal (or the bank suction problem), replenishment at sea, ships passing a moored vessel, etc. are all special situations which can be investigated using the general procedure developed here.

3.1) REFERENCE SYSTEMS

In order to develop convenient analytical expressions, three coordinate systems are used in the analysis. Two of these [(x_1,y_1,z_1) and (x_2,y_2,z_2)] are body fixed coordinates, and the third one (x_0,y_0,z_0) is fixed at the sea or canal surface. The body fixed reference system

on each ship has its respective origin at the intersection of the mid-ship plane, center-plane, and the load water-plane of the corresponding ship. The x-axis points forward, y-axis points starboard and the z-axis is positive downwards, in accordance with the right hand convention. The earth fixed coordinate system (x_0, y_0, z_0) has its x-axis along the vertical step in the canal bottom. These reference systems are illustrated in Fig. 1. The positions and heading angles of both ships are measured with respect to the earth fixed reference system.

When evaluating various quantities it is frequently required to transform variables between x_0-x_1-x_2-systems. If we denote the origins of body axes as (x_{01}, y_{01}) and (x_{02}, y_{02}), and the respective heading angles as ψ_1 and ψ_2, any point (x_1, y_1) or (x_2, y_2) can be expressed in terms of the fixed coordinate system as below:

$$x_0 = x_{01} + x_1 \cos \psi_1 - y_1 \sin \psi_1 \qquad (3.1)$$

$$y_0 = y_{01} + x_1 \sin \psi_1 + y_1 \cos \psi_1 \qquad (3.2)$$

This lead to the following transformation between i and j reference systems where i and j take on values 1 or 2 and $i \neq j$.

$$x_i = (x_{oj} - x_{oi}) \cos \psi_i + x_j \cos(\psi_j - \psi_i)$$
$$+ (y_{oj} - y_{oi}) \sin \psi_i + y_j \sin(\psi_i - \psi_j) \qquad (3.3)$$

$$y_i = (x_{oi} - x_{oj}) \sin \psi_i + x_j \sin(\psi_j - \psi_i)$$
$$+ (y_{oj} - y_{oi}) \cos \psi_i + y_j \cos(\psi_j - \psi_i) \qquad (3.4)$$

We also have the following relationships for the derivatives with respect to the various coordinate directions:

$$\frac{\partial x_i}{\partial x_j} = \cos(\psi_i - \psi_j) \qquad (3.5)$$

$$\frac{\partial x_i}{\partial y_j} = \sin(\psi_i - \psi_j) \qquad (3.6)$$

$$\frac{\partial y_i}{\partial y_j} = \cos(\psi_i - \psi_j) \qquad (3.7)$$

$$\frac{\partial y_i}{\partial x_j} = \sin(\psi_j - \psi_i) \qquad (3.8)$$

3.2) Potential Flow Description:

As a first approximation, the flow field around the ships are represented by continuous center-line distribution of sources and sinks moving with the ships in a fluid at rest. The source strengths for axi-symmetric flow about a slender body are obtained as:

$$q_i(x) = -\frac{U_i}{4\pi}\frac{dS_i}{dx_i} \qquad (3.9)$$

where U_i is the forward speed, S_i is the local sectional area and the subscript 'i' stands for the ship under consideration. This represents the flow around the double bodies obtained by considering the ships and their reflection at the free surface. Then the velocity potentials for the longitudinal flow about these double body models are given by

$$\phi_j(x_i,y_i,z_i) = \int_{x_{sj}}^{x_{bj}} \frac{q_j(\xi_j)}{\sqrt{(x_i-\xi_j)^2 + y_i^2 + z_i^2}}\, d\xi_j \qquad (3.10)$$

where the subscript 'i' stands for the reference system considered and 'j' stands for the ship on which the sources are located.

The boundary condition on the body surface requires that the normal component of the velocity of the body be equal to the normal component of the velocity of the fluid in contact with the body at all points on the surface. This condition will be satisfied by the above potential only if the incident flow is longitudinal. In order to allow for the lateral motions of the body, doublets are introduced along the body center-line. The strengths of these lateral doublets for the appropriate ship are given by the following expression.

$$\mu_{yi} = \frac{(1 + k_{2i})}{4\pi} S_i(x_i)(V_i + r_i x_i) \tag{3.11}$$

where k_{2i} is the lateral added mass coefficient, S_i is the local sectional area, V_i is the lateral velocity and r_i is the yaw rate of the corresponding ship. The potential due to the dipoles along the center line of ship-i is then

$$\phi_i^d = \int_{x_{si}}^{x_{bi}} \frac{y_i \mu_{yi}}{r_i^3} \, d\xi_i \tag{3.12}$$

where,

$$r_i^2 = (x_i - \xi_i)^2 + y_i^2 \tag{3.13}$$

The combined potential due to these sources and

doublets represents the motion of a double body model in the horizontal plane, in an infinite fluid. However this potential does not account for the boundaries in the flow like the canal walls and the shallow bottom. The wall and bottom conditions of zero normal velocity are satisfied by introducing arrays of image bodies reflected on the canal bottom and the walls.

To determine the image locations, consider a source or a doublet on the center line of ship-i, at a longitudinal position ξ_i. Then the image locations of this source or doublet in the body fixed reference frame are given by:

$$x_i = \xi_i + n(w_1 + w_2) \sin \psi_i \qquad (3.14)$$

$$y_i = n(w_1 + w_2) \cos \psi_i \qquad (3.15)$$

for n an even number, and

$$x_i = \xi_i \cos 2\psi_i + [(n+1)w_1 + (n-1)w_2 - 2y_{0i}] \sin \psi_i \qquad (3.16)$$

$$y_i = -\xi_i \sin 2\psi_i + [(n+1)w_1 + (n-1)w_2 - 2y_{0i}] \cos \psi_i \qquad (3.17)$$

for n an odd number.

$$z_i = 2mh_i \qquad (3.18)$$

where h_i is the water depth of the region in which the ship is moving. The quantities "m" and "n" are the number of images in the vertical or lateral directions respectively. They take on values from $-\infty$ to ∞, where

m = n = 0 corresponds to the double body itself (i takes on values 1 and 2 which corresponds to the ship under consideration).

The potential functions for the image system are to be expressed in such a way that they are applicable when the ships are in either of the two channels. The water depth h depends on the location of the ship with respect to the step in the canal bottom, [j=1 for $y_0>0$; j=2 for $y_0<0$]. The potential is expressed, allowing for the different water depth regions relative to the step location, by making use of the Heaviside unit step function, which has the value unity when the argument is positive and zero when the argument is negative. The potential field due to the sources and its images on ship-i can then be expressed as:

$$\phi^s = \sum_{m=-\infty}^{\infty} \sum_{\substack{n=-\infty \\ n \text{ even}}}^{\infty} \int_{x_{si}}^{x_{bi}} q_i (DXE_i^2+DYE_i^2+DZ_i^2)^{-1/2} d\xi_i$$

$$+ \sum_{m=-\infty}^{\infty} \sum_{\substack{n=-\infty \\ n \text{ odd}}}^{\infty} \int_{x_{si}}^{x_{bi}} q_i (DXO_i^2+DYO_i^2+DZ_i^2)^{-1/2} d\xi_i$$

(3.19)

$$DXE_i = [x_i - \xi_i - n(w_1 + w_2) \sin \psi_i] \quad (3.20)$$

$$DXO_i = [x_i - \xi_i \cos 2\psi_i - [(n+1)w_1 + (n-1)w_2 - 2y_{01}] \sin \psi_i \quad (3.21)$$

$$DYE_i = [y_i - n(w_1 + w_2)] \cos \psi_i \quad (3.22)$$

$$DYO_i = [y_i + \xi_i \sin 2\psi_i - [(n+1)w_1 + (n-1)w_2 - 2y_{01}] \cos \psi_i \quad (3.23)$$

$$DZ_i = z_i - 2m [h_1 H(Y_{oi}) + h_2 H(-Y_{oi})] \quad (3.24)$$

In these expressions, we have neglected the image sources reflected on the relatively small vertical face of the step in the canal bottom. Since the effects of all image flows are evaluated at the center of the double body, and also because the difference in water depths is relatively small, the influence of the images due to the vertical face of the step can be assumed to be negligible.

Combining the source potentials corresponding to both of the ships, the total source potential is then given by

$$\phi^s = \sum_{i=1}^{2} \sum_{m=-\infty}^{\infty} \sum_{\substack{n=-\infty \\ n \text{ even}}}^{\infty} \int_{x_{si}}^{x_{bi}} q_i (DXE_i^2 + DYE_i^2 + DZ_i^2)^{-1/2} d\xi_i$$

$$+ \sum_{i=1}^{2} \sum_{m=-\infty}^{\infty} \sum_{\substack{n=-\infty \\ n \text{ odd}}}^{\infty} \int_{x_{si}}^{x_{bi}} q_i (DXO_i^2 + DYO_i^2 + DZ_i^2)^{-1/2} d\xi_i$$

(3.25)

This system of self image potentials and the "other-body" potentials will induce lateral and longitudinal velocities on the center lines of both the ships. Considering also the lateral and angular (yaw rate) velocities of the ships, we can obtain the net induced fluid velocity at the center line of both ships. In calculating these induced velocities, contributions from the internal singularities of the corresponding ship are not considered as their effect on the forces and moments identically cancel out as pointed out by Landweber and Yih [25]. Proper consideration is given to the potential functions in their respective regions of applicability, as expressed by the Heaviside unit step functions.

The induced lateral velocity on ship-i center

line due to the total source potential field can be expressed in its local moving reference system as

$$v_i^s = - \left. \frac{\partial \phi^s}{\partial y_i} \right|_{y_i = 0} \tag{3.26}$$

Substituting the expression for the potential (Eq. 3.25) we obtain

$$\begin{aligned} v_1^s = & \sum_{m=-\infty}^{\infty} \sum_{\substack{n=-\infty \\ n \text{ even}}}^{\infty} \int_{x_{s1}}^{x_{b1}} q_1 [DYE_1] (DXE_1^2 + DYE_1^2 + DZ_1^2)^{-3/2} d\xi_1 \\ & + \sum_{m=-\infty}^{\infty} \sum_{\substack{n=-\infty \\ n \text{ odd}}}^{\infty} \int_{x_{s1}}^{x_{b1}} q_1 [DYO_1] (DXO_1^2 + DYO_1^2 + DZ_1^2)^{-3/2} d\xi_1 \\ & + \sum_{m=-\infty}^{\infty} \sum_{\substack{n=-\infty \\ n \text{ even}}}^{\infty} \int_{x_{s2}}^{x_{b2}} q_2 \left[DXE_2 \frac{\partial x_2}{\partial y_1} + DYE_2 \frac{\partial y_2}{\partial y_1} \right] (DXE_2^2 + DYE_2^2 + DZ_2^2)^{-3/2} d\xi_2 \\ & + \sum_{m=-\infty}^{\infty} \sum_{\substack{n=-\infty \\ n \text{ odd}}}^{\infty} \int_{x_{s2}}^{x_{b2}} q_2 \left[DXO_2 \frac{\partial x_2}{\partial y_1} + DYO_2 \frac{\partial y_2}{\partial y_1} \right] (DXO_2^2 + DYO_2^2 + DZ_2^2)^{-3/2} d\xi_2 \end{aligned} \tag{3.27}$$

where $m \neq 0$ when $n = 0$ because internal singularities are not considered here. These induced velocities are evaluated at the center lines of both the ships by putting either y_1 or y_2 equal to zero, as the case

may be. Appropriate coordinate transformations are used to express these equations in either of the two ship-fixed reference systems.

By a similar procedure we can obtain the expression for the induced velocity in the longitudinal direction due to the source potential as given below.

$$u_1^s = \sum_{m=-\infty}^{\infty} \sum_{\substack{n=-\infty \\ n \text{ even}}}^{\infty} \int_{x_{s1}}^{x_{b1}} q_1 [DXE_1] \, (DXE_1^2+DYE_1^2+DZ_1^2)^{-3/2} d\xi_1$$

$$+ \sum_{m=-\infty}^{\infty} \sum_{\substack{n=-\infty \\ n \text{ odd}}}^{\infty} \int_{x_{s1}}^{x_{b1}} q_1 [DXO_1] \, (DXO_1^2+DYO_1^2+DZ_1^2)^{-3/2} d\xi_1 \qquad (3.28)$$

$$+ \sum_{m=-\infty}^{\infty} \sum_{\substack{n=-\infty \\ n \text{ even}}}^{\infty} \int_{x_{s2}}^{x_{b2}} q_2 \left[DXE_2 \frac{\partial x_2}{\partial x_1} + DYE_2 \frac{\partial y_2}{\partial x_1} \right] (DXE_2^2+DYE_2^2+DZ_2^2)^{-3/2} d\xi_2$$

$$+ \sum_{m=-\infty}^{\infty} \sum_{\substack{n=-\infty \\ n \text{ odd}}}^{\infty} \int_{x_{s2}}^{x_{b2}} q_2 \left[DXO_2 \frac{\partial x_2}{\partial x_1} + DYO_2 \frac{\partial y_2}{\partial x_1} \right] (DXO_2^2+DYO_2^2+DZ_2^2)^{-3/2} d\xi_2$$

Where $m \neq 0$ when $n = 0$. This induced flow along the center lines will disrupt the surface boundary conditions on body surface. In order to satisfy the surface boundary conditions of zero normal velocity at the solid surface, lateral and longitudinal doublets are introduced

along the center lines of both the ships, the strengths of which are determined by use of the following relations, which also take proper account of the body motions.

$$\mu_{yi} = - \frac{(1 + k_{2i})}{4\pi} S_i(x_i)[v_i^s(x_i) - V_i - r_i x_i] \qquad (3.29)$$

$$\mu_{xi} = - \frac{(1 + k_{1i})}{4\pi} S_i(x_i) u_i^s(x_i) \qquad (3.30)$$

where μ_x is the strength of the doublets in the X-direction μ_y is the strength of the doublets in the Y-direction, k_{2i} is the local sectional lateral added mass coefficient and k_{1i} is the local sectional longitudinal added mass coefficient of the ship-i.

The potential field due to these doublets is given by

$$\phi_i^d = \int_{x_{si}}^{x_{bi}} \frac{y_i \mu_{yi}}{r_i^3} d\xi_i + \int_{x_{si}}^{x_{bi}} \frac{x_i \mu_{xi}}{r_i^3} d\xi_i \qquad (3.31)$$

where,

$$r_i^2 = (x_i - \xi_i)^2 + y_i^2 \qquad (3.32)$$

Then the induced lateral velocities on ship-j due

to the doublets on ship-i can be obtained as:

$$v_j^d = -\int_{x_{si}}^{x_{bi}} \frac{\left[\mu_{yi} \frac{\partial y_i}{\partial y_j} + \mu_{xi} \frac{\partial x_i}{\partial y_j} \right]}{r_i^3} d\xi_i \qquad (3.33)$$

Similarly the expression for the induced longitudinal velocity on ship-j due to the doublets on ship-i can be obtained from:

$$u_j^d = -\int_{x_{si}}^{x_{bi}} \frac{\left[\mu_{yi} \frac{\partial y_i}{\partial x_j} + \mu_{xi} \frac{\partial x_i}{\partial x_j} \right]}{r_i^3} d\xi_i \qquad (3.34)$$

The total induced velocities are then obtained as

$$\begin{aligned} v_i &= v_i^s + v_i^d \\ u_i &= u_i^s + u_i^d \end{aligned} \qquad (3.36)$$

The doublet strengths are now recalculated using these values for the induced velocities. However at this time the effects of body motions (per se) are to be excluded as we only need the interaction effects, which will directly include such body motion terms in the induced velocities. In other words, this procedure involves calculating the induced velocities on each ship due to the canal, the 'other ship'

and its motions. The effect of the motions of the 'other ship' is obtained this way as an induced fluid flow. This will give rise to dipole distribution along the center-lines of both the ships. In order to calculate these dipole distribution, the self body motions are not considered as they will only give rise to a 'self' term in the Lagally's expressions. This is so because all the 'self' terms are included in the maneuvering model discribed in Chapter-6, and here we only seek the interaction forces and moments.

Chapter-4

ADDED MASSES

4.1) Added Mass for Sway Acceleration in Shallow Water

The added mass in sway motion (including the effect of shallow water) is needed for establishing the strength of the doublet distribution required to correct for the induced velocities on each ship. The relation between the doublet strength and the lateral added mass is essentially the result of generalizing a relationship first established by Taylor [42]. That relation was applied to an infinite fluid domain, and in the present case the same type of relation is assumed to apply to a body in a shallow bounded fluid region. Thus the added mass is assumed to be that for a body in shallow water, subject to the rigid free surface boundary condition which involves a reflected double-body model.

Two-dimensional, lateral sectional added masses are calculated at each section following the analysis of Flagg and Newman [13] for rectangular sections in shallow

water. Most full ship forms such as those of tankers and bulk carriers can be approximated as rectangular forms. Other sections are represented by an "equivalent" rectangular section where the equivalent draft is calculated by dividing the sectional area by the respective beam.

In order to evaluate the added mass for very shallow water cases, a small parameter ε^* is introduced which is defined as

$$\varepsilon^* = 1 - \frac{T}{H} \tag{4.1}$$

where T is the section draft and H is the water depth. Then the two-dimensional lateral added mass of a rectangular cylinder, of breadth B and depth $2T$, as given by Newman [32] is:

$$\frac{m_y}{4\rho H^2} = \frac{1}{\varepsilon^*}\frac{B}{2H} - \frac{2}{\pi}\log(4\varepsilon^*) + \frac{2}{\pi} - \frac{B}{H} + \frac{\varepsilon^* B}{2H} + \frac{2\varepsilon^{*2}}{3\pi} + O(\varepsilon^{*3}) \tag{4.2}$$

For full ships in very shallow water, this would give a good estimate of the sectional lateral added mass. The resulting expression for the sectional lateral added mass coefficient used in the present analysis is given below, where the division by two reduces to the results for the ship alone without the surface reflected body.

$$k_2 = -\frac{1}{2}\left[\frac{m_y}{\rho S}\right] \tag{4.3}$$

$$= \left[\frac{2H^2}{S}\right]\left[\frac{B}{\varepsilon^* 2H} - \frac{2}{\pi}\log(4\varepsilon^*) + \frac{2}{\pi} - \frac{B}{H} + \frac{B\varepsilon^*}{2H} + \frac{2\varepsilon^{*2}}{3\pi} + O(\varepsilon^{*3})\right]$$

Average value of k_2 has been used for the whole ship in the present analysis, where,

$$k_2(\text{ave.}) = \frac{1}{\text{Vol.}} \int_L k_2 \, S \, dx \tag{4.4}$$

where Vol. is the displaced volume of the ship. The longitudinal added mass coefficient, k_1, is very small for long slender bodies in an infinite fluid. It is assumed in the present study that this added mass term is also relatively small even in the case of shallow water. Hence it will be ignored, i.e. assumed to be effectively zero in any of the calculations carried out using the present theory.

For not so shallow situations, where T/H is less than 0.8, the asymptotic approximation as given in equation (4.3) breaks down. In such cases, a complete solution of Gurevich's [16] equations are needed. This is obtained by the computational scheme outlined in Flagg & Newman [13].

See appendix-A for details.

This method involves the conformal mapping of the fluid domain, bounded by the rectangular section and the canal bottom into a semi-infinite half-plane. Then the added mass coefficient for sway acceleration can be expressed as in Gurevich [16] in terms of elliptic functions and integrals as below:

$$A_{22} = \rho \left[-4BT - \frac{B^2 K'}{K} + 4\frac{H^2}{\pi} \log \left\{ \frac{\pi P \theta_1'(0)}{K\sqrt{(1-P^2)}\sqrt{1-k^2P^2}\,\theta_1(\pi a/K)} \right\} \right] \qquad (4.5)$$

The parameters in this equation are as defined below:

$$\frac{B}{2H} = -\frac{\theta_3'(\alpha,q)}{\theta_3(\alpha,q)} = -4\sum_{n=1}^{\infty} \frac{(-1)^n q^n \sin 2n\alpha}{(1-q)^{2n}} \qquad (4.6)$$

$$\frac{T}{H} = \frac{2\alpha}{\pi} - \frac{K'B}{K(2H)} \qquad (4.7)$$

$$\frac{K'}{K} = -\frac{1}{\pi} \log q \qquad (4.8)$$

$$p = sn\ a \qquad \text{or} \qquad a = \int_0^p \frac{dt}{\sqrt{(1-t^2)(1-k^2t^2)}} \qquad (4.9)$$

$$\alpha = \frac{\pi a}{2K} \qquad \text{and} \qquad K = \int_0^1 \frac{dt}{\sqrt{(1-t^2)(1-k^2t^2)}} \qquad (4.10)$$

$$k' = \sqrt{(1-k^2)} \quad \text{and} \quad K' = \int_0^1 \frac{dt}{\sqrt{(1-t^2)(1-k'^2t^2)}} \tag{4.11}$$

$$\text{and} \quad \theta_1(\alpha,q) = 2\, q^{1/4} \sum_0^\infty (-1)^n q^{n(n+1)} \sin\,(2n+1)\alpha \tag{4.12}$$

where, $0 \le \alpha \le \pi/2$

$0 \le q \le 1$

$$\frac{\pi\ P\ \theta_1'(0)}{K\ \sqrt{(1-P^2)}\sqrt{1-k^2P^2}\ \theta_1(\pi a/K)} = \left[\ \frac{T_2(0).T_3(0)}{T_2(\alpha).T_3(\alpha)}\ \right]^2 \tag{4.13}$$

$$T_2(\alpha) = \sum_{n=0}^{\infty} q^{n(n+1)} \cos\,(2n+1)\alpha \tag{4.14}$$

$$T_3(\alpha) = \frac{1}{2} + \sum_{n=0}^{\infty} q^{n^2} \cos\,(2n\alpha) \tag{4.15}$$

This set of equations is solved iteratively for k_2. See Appendix-A for details.

4.2) Added Fluid Inertia for Yaw Angular Acceleration in Shallow Water:

The added fluid inertia coefficient for yaw is found for each ship by means of strip theory procedure, using the sectional values of the sway added mass coefficient determined above (i.e. as given in Eq. [4.3]). According to this procedure, the value of the added inertia coefficient for yaw is given by

$$k'_{3i} = \frac{\int_{x_{si}}^{x_{bi}} k_{2i} S_i x_i^2 \, dx_i}{\int_{x_{si}}^{x_{bi}} S_i x_i^2 \, dx_i} \qquad (4.16)$$

for each respective ship.

Chapter-5

Computation of the Forces and Moments

Having obtained all the expressions for the strengths of the singularities, their potentials, induced velocities, etc., we can use the generalized Lagally's theorem to determine the forces and moments on both the bodies. For the present singularity distribution, Lagally's theorem for the total force acting on the double-body as given by Landweber and Yih [25] is

$$F_{yi} = F^{s}_{yi} + F^{t}_{yi} \tag{5.1}$$

$$F_{xi} = F^{s}_{xi} + F^{t}_{xi} \tag{5.2}$$

$$N_{i} = N^{s}_{i} + N^{t}_{i} \tag{5.3}$$

where the superscripts s and t stand for the steady and unsteady components, and the subscripts x and y represent the respective components of the total force, respectively. The various components of the force and moment equations found by the method of [25], which also include the forces due to self body motions as well as the interaction effects are:

$$F^s_{yi} = -4\pi\rho \int_{x_{si}}^{x_{bi}} q_i(v_i - V_i - r_i x_i)d\xi_i \tag{5.4}$$

$$F^t_{yi} = -4\pi\rho \int_{x_{si}}^{x_{bi}} \frac{\partial \mu_{yi}}{\partial t} d\xi_i + B_i \frac{\partial V_i}{\partial t} \tag{5.5}$$

$$F^s_{xi} = -4\pi\rho \int_{x_{si}}^{x_{bi}} q_i(u_i - U_i)d\xi_i \tag{5.6}$$

$$F^t_{xi} = -4\pi\rho \int_{x_{si}}^{x_{bi}} \frac{\partial \mu_{xi}}{\partial t} d\xi_i + B_i \frac{\partial U_i}{\partial t} \tag{5.7}$$

$$N^s_i = -4\pi\rho \int_{x_{si}}^{x_{bi}} q_i x_i (v_i - V_i - r_i x_i)d\xi_i + 4\pi\rho \int_{x_{si}}^{x_{bi}} \mu_{yi}(u_i - U_i)d\xi_i \tag{5.8}$$

$$N^t_i = 4\pi\rho \frac{\partial}{\partial t} \int_{x_{si}}^{x_{bi}} \mu_{621}(v_i - V_i)d\xi_i + \frac{\partial}{\partial t}\left[r_i A_{66i} \right] \tag{5.9}$$

where B_i is the displacement of the respective ship. The contributions from the self terms are present in the ordinary maneuvering ship motion mathematical model (see Chapter-6), and the parts desired here are only the interaction effects due to the second ship, canal walls and the shallow water. These interaction force and moment

components are obtained by eliminating the forces and moments that would act if the ship were to move in an unrestricted ocean, from the equations 5.4 to 5.9 as below:

$$F^s_{yi} = -4\pi\rho \int_{x_{si}}^{x_{bi}} q_i v_i \, d\xi_i \tag{5.10}$$

$$F^t_{yi} = -4\pi\rho \int_{x_{si}}^{x_{bi}} \frac{\partial \mu_{yi}}{\partial t} \, d\xi_i \tag{5.11}$$

$$F^s_{xi} = -4\pi\rho \int_{x_{si}}^{x_{bi}} q_i u_i \, d\xi_i \tag{5.12}$$

$$F^t_{xi} = -4\pi\rho \int_{x_{si}}^{x_{bi}} \frac{\partial \mu_{xi}}{\partial t} \, d\xi_i \tag{5.13}$$

$$N^s_i = -4\pi\rho \int_{x_{si}}^{x_{bi}} q_i x_i v_i \, d\xi_i + 4\pi\rho \int_{x_{si}}^{x_{bi}} \mu_{yi} (u_i - U_i) \, d\xi_i \tag{5.14}$$

$$N^t_i = 4\pi\rho \frac{\partial}{\partial t} \int_{x_{si}}^{x_{bi}} \mu_{62i} v_i \, d\xi_i \tag{5.15}$$

where the quantity μ_{62} in Eq. (5.15) is the strength of the doublet distribution that would represent the body with unit yaw rate. Such a term is present regardless of whether the vessel has a yaw rate or not. By analogy with the expressions in Eqs. (3.29) and (3.30), μ_{62} is given by

$$\mu_{62_i} = \frac{(1+k'_{3i})}{4\pi} x_i S_i(x_i) \qquad (5.16)$$

with the value of k'_{3i} found from Eq. (4.16). In the expressions for the steady Lagally force above (Eq. 5.10 and 5.12), terms from $\mu.\Delta v$ is not included as they are of higher order in the slenderness parameter ε (where ε = Beam/Length) compared to other terms considered. For the same reason $\mu_x.v$ term is not included in the steady Lagally moment expression.

5.1) Time Derivatives Operations

As can be seen from the above expressions, the time derivatives of various quantities are needed for calculating the unsteady forces and moments. These are obtained using the following second order backward differencing formula

$$\frac{df_0}{dt} = \frac{3f_0 - 4f_{-1} + f_{-2}}{2\Delta t} + O(\Delta t^2) \qquad (5.17)$$

where Δt is the time step, f_0 is the value of the function at time t, and f_{-n} is the value of the function

at time t - nΔt.

5.2) Lift Force Contribution

All the interaction forces and moments treated so far are of non-lifting nature, and arise from the potential flow representation in terms of singularities. In addition to these forces, slender bodies in steady motion in a lateral flow field also develop a lift force. An expression to evaluate this lifting force using slender body theory is given below.

The force acting on a cross-sectional plane of a slender body moving in an ideal fluid with forward velocity U, in an arbitrary lateral flow field v(x,t), is given by the time rate of change of fluid momentum. This gives the general expression for the strip wise lateral force as

$$\frac{df_y}{dx} = \frac{D}{Dt}\left[A_{22}(x)\ v(x,t) \right] \qquad (5.18)$$

where A_{22} is the sectional added mass. The force associated with unsteady acceleration terms is an added mass self term that is included in the ship equations of motion, so it is not considered here. The remaining part which is

quasi-steady (because v is changing with time), on integrating over the ship length, gives the following:

$$F_y = - U \int_{x_b}^{x_s} \frac{d}{dx}\Big[A_{22}(x)\ v(x,t) \Big]\ dx$$

$$= - U \Big[A_{22}(x_b)\ v(x_b) - A_{22}(x_s)\ v(x_s)\Big] \qquad (5.19)$$

As the bow is almost always pointed, the added mass at the bow can be taken to be zero. There will not be any contribution from this term if the trailing edge also is pointed. For a body with finite trailing edge span, as in the case of skeg in a ship, the steady lifting force is given by

$$F_y = U\ v(x_s)\ A_{22}(x_s) \qquad (5.20)$$

The yaw moment is calculated in a similar manner from the lift force and its assumed point of application, with the general expression for the moment given by

$$N = - U \int_{x_s}^{x_b} x \frac{d}{dx}\Big[v(x)\ A_{22}(x)\Big]\ dx$$

$$= - U \Big[xv(x)A_{22}(x)\Big]_{x_s}^{x_b} + U\int_{x_s}^{x_b} v(x)A_{22}dx \qquad (5.22)$$

$$= x_s (F_y)_{lift} + U \int_{x_s}^{x_b} v(x) A_{22} dx \qquad (5.23)$$

The last term in the above equation is the moment acting on a body moving in an ideal fluid at an angle of attack, which is present even for bodies with a pointed trailing edge. This is included in the Munk moment on a non-lifting body in steady translation. The contribution due to this term is already accounted for in the expression for the steady Lagally moment, so the only additional yaw moment is that due to the lift force acting at the aft end, which is given by the first term in the above equation.

This formulation has not been found to be completely adequate to represent the lateral force and yaw moment on ships, although some of the basic ideas have been adapted in a pragmatic manner in some useful procedures (e.g. [19]). In such cases the separate contributions of the bare hull, the skeg, and the rudder are determined, assuming no interference between each element, and the total force and moment are found by summing the individual terms (including the products by appropriate moment arms). The values of the lateral added masses at appropriate end locations of the ship and the skeg, which are the important terms in the slender body theory model, are determined for

the case of shallow water and the free surface reflection representation of the appropriate end section. By extending these ideas to the present case, where the ship hull and the skeg are considered as two different low aspect ratio airfoils, as interpreted by slender body theory, and the rudder as an effective wing of large aspect ratio, the lateral force is represented by

$$F_{y(lift)} = U\left[v(x_h)A_{22}(x_h) + v(x_s)A_{22}(x_s)\right] + \frac{\rho}{2} S_r U v(x_r) C_{L_{\alpha r}} \qquad (5.24)$$

where x_h, x_s and x_r are the locations of the after ends of the hull and skeg, respectively, and the mid-chord location of the rudder; S_r is the lateral projected area of the rudder; and $C_{L_{\alpha r}}$ is the rudder lift coefficient rate given by

$$C_{L_{\alpha r}} = \frac{2\pi}{1 + 2/AR} \qquad (5.25)$$

with AR the rudder aspect ratio. The yaw moment due to lift forces is given by

$$N_{(lift)} = U\left[v(x_h)A_{22}(x_h)x_h + v(x_s)A_{22}(x_s)x_s\right] + \frac{\rho}{2} S_r U v(x_r) x_r C_{L_{\alpha_r}} \qquad (5.26)$$

The added mass at the end of the skeg $A_{22}(x_s)$ is taken as the two-dimensional lateral added mass of a vertical flat plate section in shallow water which is given in [33] as,

$$A_{22} = -\frac{4\rho H^2}{\pi} \ln\left(\cos\frac{\pi T}{2H}\right) \qquad (5.27)$$

where T is the ship draft, with this quantity considered to be appropriate for the end location of the skeg. Since the ship generally has "fullness", the use of a flat plate representation is not proper for the location of the after end of the hull. This requires a modification to the added mass representation at the location of the effective end of hull, which includes the effect of the ship width, which is also consistent with other models that apply slender body theory to determine ship hydrodynamic force and moment representations (e.g. [7]).

The ship section at the hull after end is not generally rectangular, but an equivalent rectangle method has been utilized earlier in this work. That equivalent

rectangle representation was based on using the effective draft (found by dividing the section area by the section beam) to determine sectional added masses as well as the total vessel added mass coefficient k_2. Since more detail is required to establish these local sectional added mass than the overall total added mass for the vessel, another possible approach is to use the concept of an equivalent rectangle with an effective beam found by dividing the section area by the actual section draft. The formulas given in Eq. 4.3 and 4.16 are used to evaluate the added mass in this way, using the proper effective values. The added mass values found by use of both of these effective-type representations are expected to "bracket" the actual section added mass, so that the value to be used for the added mass at the hull end is then assumed to be the arithmetic mean of the values found by use of the effective draft and effective beam models discussed above.

5.3) Viscosity Effects

All of the preceding analysis is based on potential flow theory, although the presence of a lift force implies the existence of vorticity and a trailing vortex sheet. Since this trailing vortex sheet is only present in the flow field behind the ship, it will not affect the

potential flow modeling although such vorticity arises only as a result of viscous effects in the fluid. One possible effect of the trailing vortex sheet may occur after passing ships start travelling in the wakes of each other. That may possibly be the reason for large oscillatory forces and moments after the models pass each other, which was noted in recent model tests involving passing ships at SSPA [41] as well as similar type model tests at DTNSRDC. No analysis of such effects is made here, as it is beyond the scope of the present work.

A particular manifestation of viscous effects that results in hydrodynamic forces and moments on various bodies (ships, aircraft, missiles, etc.) is that in the concept of cross-flow drag (e.g. see [21] and [43]), with the cross-flow in the present case arising as the induced velocity due to the different image systems and also the other ship. The total lateral force and yaw moment due to cross-flow are given by

$$F_{y_{cfd}} = \frac{\rho}{2} C_D \int_{x_s}^{x_b} T(x)\, v_i(x)\, |v_i(x)|\, dx \qquad (5.28)$$

$$N_{cfd} = \frac{\rho}{2} C_D \int_{x_s}^{x_b} T(x)\, v_i(x)\, |v_i(x)|\, x\, dx \qquad (5.29)$$

where the local draft at each section is represented by T(x). In the above expressions the cross-flow drag coefficient has the suggested value $C_D = 2$ for representative full ship sections, and the absolute value on the induced velocity is used to produce the proper sign of the local force regardless of the flow direction.

5.4) BARGE FORMS

Barges have simple box shape which can be analyzed by a simplified theoretical model. By the procedure established in the previous sections we obtain zero source strength along the length of the barge except at the two extreme ends. The flow field around the barges are thus represented by a source-sink pair along the center line, moving with the barge. These source strengths for axi-symmetric flow about barges can be expressed as:

$$q_i(x) = \frac{U_i S_i}{4\pi} \left[\delta(x_i - x_i^b) - \delta(x_i - x_i^s) \right] \qquad (5.30)$$

where U_i is the forward velocity S_i is the sectional area and the superscripts 's' and 'b' stand for

stern and bow of the barge. This form for the source strength simplifies all the integrations needed to obtain potentials and velocities. As an example, the expression for induced velocity Eq.3.27 becomes:

$$
\begin{aligned}
v_i^s = &\sum_{m=-\infty}^{\infty} \sum_{\substack{n=-\infty \\ n\ even}}^{\infty} U_1 \frac{S_1[DYE_1]}{4\pi} (DXE_1^2+DYE_1^2+DZ_1^2)^{-3/2} \Bigg|_{\xi_1=x_{s1}}^{\xi_1=x_{b1}} \\
&+ \sum_{m=-\infty}^{\infty} \sum_{\substack{n=-\infty \\ n\ odd}}^{\infty} U_1 \frac{S_1[DYO_1]}{4\pi} (DXO_1^2+DYO_1^2+DZ_1^2)^{-3/2} \Bigg|_{\xi_1=x_{s1}}^{\xi_1=x_{b1}} \\
&+ \sum_{m=-\infty}^{\infty} \sum_{\substack{n=-\infty \\ n\ even}}^{\infty} \frac{U_2 S_2 \left[DXE_2 \frac{\partial x_2}{\partial y_1}^2 + DYE_2 \frac{\partial y_2}{\partial y_1} \right]}{4\pi (DXE_2^2+DYE_2^2+DZ_2^2)^{3/2}} \Bigg|_{\xi_2=x_{s2}}^{\xi_2=x_{b2}} \\
&+ \sum_{m=-\infty}^{\infty} \sum_{\substack{n=-\infty \\ n\ odd}}^{\infty} \frac{U_2 S_2 \left[DXO_2 \frac{\partial x_2}{\partial y_1}^2 + DYO_2 \frac{\partial y_2}{\partial y_1} \right]}{4\pi (DXO_2^2+DYO_2^2+DZ_2^2)^{3/2}} \Bigg|_{\xi_2=x_{s2}}^{\xi_2=x_{b2}}
\end{aligned}
\tag{5.31}
$$

This requires only a two term summation in the place of a lengthy integration which cuts down the computation time by a large factor.

Barge flotillas also have a tow boat pushing them from behind. These tow boats are much smaller and lighter than the barge systems themselves. The contribution

to the interaction forces and moments from these tow boats is similar to that of a skeg attached to the barge stern. The location of the tow-boat and its lateral sectional added mass are the only input required for the computation. This can be taken as the sectional added mass at the aft shoulder of the tow-boat. There is also provision in the program to calculate this value at any given section of the tow-boat. The aft end of barge hulls are normally rectangular sections and the added masses at these sections are calculated using the asymptotic approximation given in Eq. [4.3).

Chapter-6

Maneuvering Model

Having established a procedure for obtaining interaction forces and moments on ships while passing or meeting in shallow asymmetric canals, it is now possible to predict their trajectories and study their responses to control. The procedure uses standard mathematical model for vehicle dynamics together with the interaction forces added to all the other forces which would act during an open sea maneuver.

6.1) Equations of Motion

Motions of a ship can be conveniently expressed when referred to a body fixed axes system. The reference system used here is the same right-handed orthogonal system referred in the previous sections, as illustrated in Fig.1.

Our interest here is only in the horizontal plane motions, viz: surge, sway and yaw motions. As we are only concerned with slow speed maneuvers in calm waters, it is reasonable to neglect any heave, pitch or roll motions. Then

the pertinent equations of motion are:

$$X = m(\dot{u}-v\dot{\psi}) - mX_G r^2 \tag{6.1}$$

$$Y = m(\dot{v}+u\dot{\psi}) + mX_G \dot{r} \tag{6.2}$$

$$N = I_Z \dot{r} + mX_G(\dot{v}+ru) \tag{6.3}$$

Y_G is zero because of symmetry with respect to the X-Z plane. The forces X and Y and the moment N have several components which are functions of the properties of the ship, motion of the ship and properties of the fluid. In the case of interaction of ships in canals, X, Y and N are also functions of the orientation of the ships, properties of the meeting or passing ship and the properties of the canal. These contributions are calculated separately and added to the hydrodynamic forces on a single ship in open sea maneuver, to get the total forces and moments. This reduces the hydrodynamic interaction problem to that of maneuvering in unrestricted waters.

Here we chose to use the model equations in which the non-linearities are represented by a 'square absolute' technique wherein all non-linearities are reduced to a linear and quadratic fit, where odd functions are represented by linear and square terms. This is preferred over a third order Taylor expansion representation for the

physical nature of the interaction phenomenon. At large drift angles, which is generally the case for the maneuvers considered here, the dominant part of forces and moments arise due to cross flow drag effect which is proportional to the square of velocity. This is the reason for adopting a 'square absolute' representation of non-linearities as in Goodman et al. [15] and Miller [28]. (Goodman followed the mathematical model of Gertler et al. [48] which is used in the U.S. successfully for a number of years for submarine simulations.)

Then we have the following as our equations of motion:

$$m(\dot{u}-vr-x_G r^2) = 0.5\rho l^3\left[X'_{\dot{u}}\dot{u} + X'_{vr}vr\right] + 0.5\rho l^2 X'_{vv}v^2 + 0.5\rho l^2 u^2 X'_{\delta\delta}\delta^2 + 0.5\rho l^4 X'_{rr}r^2 \qquad (6.4)$$

$$m(\dot{v}+ur+x_G\dot{r}) = 0.5\rho l^4\left[Y'_{\dot{r}}\dot{r} + Y'_{r|r|}r|r|\right] + 0.5\rho l^3 Y'_{\dot{v}}\dot{v} + 0.5\rho l^3\left[Y'_{r}ur + Y'_{v|r|}v\,|r|\right] + 0.5\rho l^2 u^2\left[Y'_{*} + Y'_{\delta}\delta\right] + 0.5\rho l^2\left[Y'_{v}uv + Y'_{v|v|}v\,|v|\right] \qquad (6.5)$$

$$I_z\dot{r} + mX_G(\dot{v} + ur) = 0.5\rho l^5\left[N'_{\dot{r}}\dot{r} + N'_{r|r|}r\,|r|\right] + 0.5\rho l^4 N'_{\dot{v}}\dot{v}$$

$$+ 0.5\rho l^4\left[N'_r ur + N'_{|v|r}r|v|\right] + 0.5\rho l^3 u^2\left[N'_* + N'_\delta\delta\right]$$

$$+ 0.5\rho l^3\left[N'_v uv + N'_{v|v|}v|v|\right] \qquad (6.6)$$

Here it is assumed that the ship is at its self propulsion point (η=1). These equations are solved at every instant for the accelerations ($\dot{u}$,$\dot{v}$ and $\dot{r}$) which are integrated to obtain the velocities u,v and r. Then the trajectories are obtained by integrating the following equations.

$$\dot{x}(t) = u\cos\psi - v\sin\psi \qquad (6.7)$$

$$\dot{y}(t) = u\sin\psi + v\cos\psi \qquad (6.8)$$

$$\dot{\psi}(t) = r \qquad (6.9)$$

In order to provide realistic simulations similar to that of a helmsman steering a ship, it is also necessary to include a rudder control equation along with the above set of equations of motion. The following rudder control algorithm is used in the simulations as an auto-pilot, (See Eda [12]) which is sensitive to change in heading, yaw rate, lateral position and lateral velocity.

$$\delta_c = a\,(\psi - \psi_e) + b'\dot{\psi}' + c'(y' - y_e') + d'\dot{y}' + \delta_e$$
$$= \delta + t_r'\,\dot{\delta}' \qquad (6.10)$$

where t_r' is the time delay in rudder activation, δ_c is the command rudder angle, δ_e is the equilibrium rudder angle and δ is the actual rudder angle. The coefficients in the above equation (a, b', c' and d') are the non-dimensional gain constants which can be varied to simulate different 'personalities' in control of the vessel. This equation is also solved along with the surge, sway and yaw equations to obtain the accelerations $\dot{u},\dot{v},\dot{r}$ and $\dot{\delta}$. For practical considerations maximum rudder angle is limited to ±35 degrees and maximum rudder rate is limited to ±2.7 deg/sec. A typical value of t_r' is about 0.1, which is the value used for the computations presented here.

Eda [12] has performed an eigen value analysis of this set of equations to determine the range of values for the gain constants required to make the system stable, as well as to gain insight into the relative importance of each of the terms for the case of a tanker model in a shallow canal. The results indicate that the ship is directionally stable when $4 < a < 17.5$ and the degree of directional

stability in that channel is maximum when a = 6 for the case where $b'=c'=d'=0$. These guidelines will be followed while choosing gain constants for the simulations with the present model.

Chapter-7

Numerical Computations and Results

Based on the theoretical model described in the previous sections, FORTRAN programs were written to evaluate interaction forces and moments on ships and barge-tows in shallow canals or rivers. The basic hydrodynamic analysis described above includes various improvements and refinements to the original analysis in [24] and [39]. The main effort in the present generalized model involves the treatment of the effects of varying angular orientation of the ships relative to each other (and to the canal walls) as well as the inclusion of ship horizontal plane dynamic motion effects on the resulting hydrodynamic forces. The detailed determination of such effects computationally is only to be considered as involved due to the great care required to represent geometric changes in a proper manner.

Other computational aspects applied to this work include the effects of use of a one-dimensional center line source distribution in place of the earlier two-dimensional center plane source distribution in representing the basic hulls, as well as the method of determining time derivative

terms in the force expressions. The source distribution used has its strength proportional to the longitudinal rate of change of cross-sectional area, while the previous source strength was proportional to the longitudinal rate of change of the lateral section offset. The net result of this change is to eliminate one of the integration operations (in the vertical direction for each term appearing in the final expressions for forces), thereby reducing the computation time (by a large factor since 11 vertical points for integration at every station were used in [24] and [39]).

The time derivative operation in the earlier effort ([24] and [39]) was carried out analytically in terms of the theoretical expressions developed there. However, for the generalized case, there would be too many quantities in the geometric representations of distances between the ships that would be changing with time; viz. longitudinal and lateral separations, angular orientations, other motion variables, etc. to consider an analytic evaluation, from both the analytic formulation effort point of view as well as computationally. The time derivative operations are then represented by a second order backward finite difference formula applied on the values of desired quantities, i.e. integral and summation terms, at different time values, which is a sufficiently accurate method for the present

application (see Eq. (5.17)).

For numerical computations, the center line of the ship is divided into 20 segments by 21 equi-spaced stations along the length. Sectional areas and drafts at these stations are input to the Program, which then evaluates the source strengths and induced velocities at these stations. Computations only involve numerical integrations and summations of algebraic expressions derived in Chapter-3. All integrations are carried out using Simpson's second rule.

The Main Program calls the interaction force module at every time step providing it with velocities and positions of the ships. The force module returns to the Main Program all the hydrodynamic interaction forces and moment acting on both the ships at that instant. These external forces are combined with the four equations of motion and control, which are solved simultaneously to obtain the accelerations. These are integrated to obtain the respective positions, velocities and rudder angle. This process is repeated as we march in time to produce a free-running maneuvering simulation of ships in confined waters. The Program flow-charts are shown in Fig. 14(a) and 14(b).

The number of summations corresponding to images in the vertical and lateral directions are to be controlled by input. Repetitive runs with increased number of summations may be required to see convergence of the solution. For the cases presented here, extreme shallow water occurs when water depth is 1.15 times the draught of the ship. In this case 16 images reflected in the vertical plane (m=17) were found to give adequate convergence (2% relative error). As the clearance between the hull and the canal walls are much more than the bottom clearance, only six images reflected on the canal walls (n=7) were needed to give adequate convergence.

In the program, added masses are calculated using the asymptotic approximation of Flagg and Newman [13]. Wherever needed, added mass can be calculated separately using the full solution and given as input to the program. This is how the computations are carried out here for the barges in intermediate water depth cases.

In order to check the effects of all the changes made to the interaction model since the initial publication [24] several cases analyzed previously for the constrained condition were again evaluated with the present model. Data from cases of passing ships from the tests series in [41] as

well as other cases considered in [24] and [39] will be utilized, as well as steady state bank suction force measurements of a single ship in a shallow canal, to enhance the reliability of the model. Since there have been a number of changes in the analysis method presented here, as compared to the earlier work of [24] and [39], these comparisons also provide further illustrations of the utility of the present analysis.

The following cases of ship-ship-bank interaction phenomena were studied in the proceeding section for model verification and analysis.

1) Verification of the interaction model using the following model test results with constrained vessels.

a) SSPA [41] data for passing Panamax Bulk Carriers in a shallow canal.
b) SSPA [41] data for bank suction on a Panamax Bulk Carrier.
c) NSMB [38] data for the mooring forces on a tanker model as another ship passes by.
d) Fujino's [14] results for bank suction.
e) Moody's [29] data for bank suction on a cargo ship in a shallow, asymmetric canal

f) Calvano's [6] results for the interaction forces during replenishing type maneuver of Mariner Class ships.

g) Results for passing Barge-trains in a canal from the model testing facility at VBD, Duisburg, FRG [18].

2) Trajectory simulation of UNREP operations using data for two Mariner Class cargo ships. Results are compared with those from Alvestad and Brown [5].

3) Simulations of passing ships in a canal. Ship data used are again those for Mariner Class cargo vessels. Results are compared with those from Eda [12].

4) Simulations with the Container ship 'New York' and a barge-train, to study their behavior during some passing and overtaking situations.

7.1) Captive Model Test Results.

a) Passing Ships in a Canal:

At the ship model basin of SSPA in Sweden, a number of tests were carried out to determine interaction forces on identical passing Panamax bulk carrier models in a shallow canal. The test conditions and the model parameters used for comparisons are given below in Table-1. The canal was

750 feet wide and the center-line of Ship-2 was always 119.14 feet away from the canal center-line, except for Case-5 where ships were symmetrically placed with respect to the canal center-line. Computations were carried out for these test cases, with representative results for the interaction forces and moments acting on Ship-1 plotted and compared with the test results in Fig. 4(a-j). The results are also compared with the numerical results of Sankaranarayanan [39] which uses the center-plane source distribution method. The parameter η, measured in ship beams, represents the (fixed) lateral separation between the longitudinal center lines of each vessel. The lateral forces and yaw moments on a single ship (Ship-1) are plotted against the longitudinal separation distances (stagger) between the ship centers during passing (i.e., $x_2 - x_1$) in Fig. 4(a-j), where that separation distance is proportional to time.

TABLE-1
SSPA Ship Parameters

Length between perpendiculars	= 260.60 m
Breadth	= 32.233 m
Draft	= 12.191 m
Displacement (cu. m)	= 84,800
Block coefficient	= 0.828
Scale ratio	= 1:46.62

Test Conditions

No.	H/T	η	U_1 kt.	U_2, kt.
1	1.150	1.25	7.0	-7.0
2	1.150	1.50	7.0	-7.0
3	1.225	1.25	7.0	-7.0
4	1.225	1.50	7.0	-7.0
5	1.225	2.00	0	7.0

The time histories of the interaction forces and moments have their characteristic shape with regard to the occurrence of peak values of forces and moments. A discussion of the physical reasoning for these wavy patterns is given in Sankaranarayanan [39]. Solid lines in these plots are the computed results using the present model. The dash line represents computed results obtained using the theoretical model of Sankaranarayanan [39] and the stars indicate the experimantal measurements carried out at SSPA. Both the theoretical results are found to be in good agreement with the experimantal data. In most cases, present results show as good an agreement with the experimantal data as the results of Sankaranarayanan [39]. It may be noted here that the method of [39] require about twenty times more computational effort than the present model, and so was not adaptable for simulation purpose.

b)Passing a Moored Ship in Shallow Water

A number of tests were carried out to measure mooring forces induced by passing ships at the Netherlands Ship Model Basin [38], which are also used as a basis for validating the present results. In these tests forces were measured on a captive tanker model during the passage of another tanker model in shallow water, which was unrestricted in width. The water depth was 1.15 times the draft of the moored vessel, and measurements were made for different speeds and separation distances.

It was difficult to make a direct comparison of the present results with the NSMB experimental results because the hull geometry information on the models was not available. However it was decided to use the results for those tests with models which resemble Panamax type bulk carriers, selecting the case for the forces on a moored 100,000 dwt tanker model due to the passage of a 110,000 dwt tanker model since the gross features of the lines of these ships are likely to be similar to those of Panamax bulk carriers. For the computation, the main dimensions and offsets of the Panamax bulk carrier are scaled to those for the NSMB vessel. Since the block coefficients of these

ships are fairly close to that of the Panamax bulk carrier, the displacements of the ships for which computations are carried out are close to the displacements of the ships for which tests were conducted.

Table-2 below illustrates the NSMB test cases, the main particulars of the tankers, and those used for the computations. (Here η^* is the side-side separation distance).

TABLE-2
NSMB Test Cases

No.	H/T	η^*	U_1	U_2
1	1.15	30 m	0	7 kt.
2	1.15	60 m	0	7 kt.
3	1.15	120 m	0	7 kt.

Moored ship parameters	NSMB ship	Values used
Length B.P.(m)	= 257.0	257.0
Breadth (m)	= 36.8	36.8
Draft (m)	= 15.7	15.7
Displacement (m3)	= 118800	122950
Block coefficient	= 0.8	0.828

Passing ship parameters	NSMB ship	Values used
Length B.P.(m)	= 250.0	250.0
Breadth (m)	= 40.4	40.4
Draft (m)	= 15.1	15.1
Displacement (m3)	= 129600	126280
Block coefficient	= 0.85	0.828

The calculated results, together with the model test

data are shown plotted in Fig. 5(a-f). In these set of plots, solid lines represent the computed results using the present model, dash lines represent the calculated results using the method of Sankaranarayanan [39] and stars indicate the model test results of Remery [38]. The calculated results are found to be in very good agreement with the model test data. There is no significant difference between the theoretical results of the present model and those of Sankaranarayanan [39].

c) Bank Suction in a Canal:

The data used in this case is for a single Panamax bulk carrier in a canal of uniform depth, as obtained in the SSPA tests [41]. The computations were carried out with the ship center-line 1.82B from the canal center-line for different speeds and for different water depths, with the ship moving parallel to the canal walls. The calculated results are shown together with the test data in Fig. 7(a-d). Theoretical results show show good agreement with the experimental data for the forces as well as moments. (Forces and moments were found to be nearly quadratic functions of speed as one would expect if wave action is negligible)

Fig. 8(a-f) are comparisons of the present results for bank suction forces with the experimental data of Fujino [14]. These tests were conducted using Mariner Class Ship model in a shallow and narrow canal. Model particulars are given in Table-3 below.

Table-3

Mariner Class Ship Model Data

Length Between Perpendiculars	2500 mm.
Breadth	359.8 mm.
Mean Draft	116.0 mm.
Draft, Fore	106.5 mm.
Draft, Aft	125.5 mm
Block Coefficient	0.5888
Scale Ratio	1/64.37

Sectional area distribution of Mariner Class ships was approximated by the parabolic formula. Using this representation, the sectional area distribution is given by:

$$S(x) = S_m . X(x)$$

Where S_m is the mid-ship sectional area, and X is obtained from:

$$X(x) = 1 - (x/l)^n, \quad (n \geq 2, \; l = L/2)$$

$$n = \frac{C_w}{1 - C_w}$$

$$C_w = 0.20 + 0.93.C_B$$

Tests were conducted for H/T values of 1.3, 1.5, and 1.9 corresponding to 7 kn. full scale speed (Fn=0.0905). Width of the model canal was 1.0 m. Computed results are in good agreement with experimental data for H/T = 1.9. Results do not compare well with Fujino's data for very shallow water cases. The reason could be inadequate representation of the aft and forward regions of the ship with a parabolic area distribution. This would affect lift forces and moments significantly which are dominant, more so in very shallow water.

d) Bank Suction in an Asymmetric Canal

Data from the work of Moody [29] is used to check the computed results for the case of bank suction in an asymmetric canal. Moody's data is for a 500 ft. wide canal which has a shallow channel (300 ft. wide and 47 ft. deep) on one side, and a deep channel (200 ft. wide and 52 ft. deep) on the other. Only the gross features of the ship model tested are available in [29], so that the calculations

were carried out for a Panamax type hull with the same dimensions as the ship model tested in [29] (L=600.5 feet, B=100.6 feet, T=12.6 feet and C_B=0.60). Comparisons between Moody's data [29] and the theoretical results are presented in Fig. 9(a) and 9(b), where the ship was travelling at a speed of 5 kn. The agreement is very good between the present computed results for lateral forces and Moody's experimental data. Computed yaw moments are found to be higher than those of Moody's data. The yaw moments are more sensitive to bow shape of the ship than the lateral forces, with certain bulbous bows and spoon bows giving a moment turning the bow towards the near bank (usually moments are in a direction turning the bow away from the near bank). The lack of agreement for yaw moments may be due to the improper representation of ship geometry, especially at the ends of the ship.

For this case, as well as the case above in a uniform depth canal, the forces mainly arise from the lift force effects. The problem is that of a steady state condition, and the hydrodynamic interaction terms due to the singularity systems (Lagally steady state force terms) are relatively small compared to the lift force contribution.

e) Passing Barge-Tows in a Canal:

Model tests were carried out at VBD in Duisburg [18] for passing barge-tows in a shallow canal 675 feet wide in full scale. Main particulars of the barge and tug as well as the test conditions are given in Table-4 below.

Table-4a
Main Particulars of the Barge and the Tug

Length Overall	(single barge)	76.50 m.
Breadth	(single barge)	11.33 m
Length b.p.	(tug)	35.00 m.
Breadth	(tug)	14.00 m.
Draft	(tug)	1.75 m.

Table-4b
Test Conditions

Case	Water Depth(ft)	Draft (ft)	U_1 (kn.)	U_2 (kn.)	Side-Side Separation (ft)
1	16.4	9.19	5.94	5.94	86.12
2	16.4	9.19	6.48	5.40	86.12
3	16.4	9.19	5.94	5.94	137.8
4	16.4	9.19	5.94	5.94	34.45
5	16.4	12.47	4.32	5.4	34.45

The test configuration had two barge systems each comprising of four barges arranged two side by side, and a

tow-boat pushing from behind. The barge systems were towed along parallel course in the towing tank and the forces were measured at two points on the first barge-train (indicated by subscript 1) as the second barge configuration passed by. Results from these experiments were obtained from Prof. Heuser et al. [18].

Numerical computations using the present model was carried out for these test cases. Results for the forces and moments are presented along with experimental results in Fig. 10(a-o).

Theoretical results are found to be generally in good qualitative agreement with the experimental results. Quantitative comparisons are also satisfactory for simulation purposes in the cases of lateral force and yaw moment. Even though the trend of the longitudinal force is correctly predicted by the theory, the magnitude is higher than what was obtained experimentally. This may be attributed to the highly concentrated source strengths at the two ends of the barge-tows as given by the δ-function representation. Fortunately this is not very critical for the cases cases considered here as the effect of longitudinal forces on the motions of barges are negligible. It should also be mentioned here that the above set of model

test results had too much noise in the data making these comparisons difficult. Some of these results show a phase shift which does not show a consistent pattern. Results also show large fluctuations and scatter which is not expected in real maneuvers.

e) Overtaking ships in shallow water:

Model test results for the interaction forces on two Mariner class merchant ships overtaking (similar to the UNREP operation) at different lateral separation distances are given in Alvestad and Brown [5]. The characteristics of the Mariner class ship model as used by Brown is given in Table-5 below. Computations were carried out with these parameters using the present computer program and the results for the interaction forces and moments are compared with the experimental results. Numerical results for side to side separation distances of 50 feet and 100 feet in deep unrestricted water is presented in Fig. 6(a-f). Experimental data for longitudinal forces were not available for comparison. It can be seen that the present results for the side forces and yaw moments are in good agreement with the experimental results.

Table-5
Main Particulars of the Mariner Class Ship

Length Overall (ft)	527.8
Breadth (ft)	76.0
Draft (ft)	29.75
Displacement (tons)	20,400
Block Coefficient C_b	0.60

During these maneuvers, longitudinal force acting on the ships are affected by their proximity to each other, like lateral force and yaw moment. Ships experience an increase or decrease in resistance depending on whether the flow field is accelerating or decelerating. Generally the overtaking ship experiences a reduction in resistance as it pulls up along the after shoulder of the leading ship. As it reaches the forward shoulder of the leading ship it experiences an increase in resistance due to accelerating flow field. This would hold back the overtaking ship if power is maintained constant.

7.2) Simulations of Replenishment Operations:

Replenishment operations at sea are carried out with two ships moving side by side along parallel paths.

This is a common practice in Navy's Underway Replenishment (UNREP) Operations. Ship-ship interaction forces make it extremely difficult to maintain course as the ships sail close to each other. Several accidents have occurred in the past during such maneuvers causing significant damages to the ships.

Results of computer simulations of ship maneuvering during UNREP operations, using captive model test results are presented in Alvestad and Brown [5]. The characteristics of the Mariner class ship model as used by Alvestad and Brown is given in Table-5 above. Its hydrodynamic coefficients are provided in Appendix-B. Computations were carried out for deep water using these parameters with the present computer program and the resulting trajectory predictions are compared in this section with those of Alvestad and Brown [5].

Simulations were carried out in Alvestad and Brown [5] using captive model model test results, which were interpolated for instantaneous values of lateral separation, without accounting for the influence of instantaneous heading angle, drift angle and velocities of the ships. In order to perform these simulations here we have used the set

of linear stability derivative coefficients presented in Alvestad and Brown [5]. This also requires the use of the same maneuvering model used in Alvestad and Brown [5], which is represented by the following set of linear equations.

$$(X'_{\dot{u}} - m')\dot{u} + X'_u \Delta u' + X'_n \Delta n' + X' = 0 \tag{7.1}$$

$$(Y'_{\dot{v}} - m')\dot{v}' + Y'_v v' + (Y'_{\dot{r}} - mx'_G)\dot{r}' + (Y'_r - mu')r' + Y'_\delta \delta + Y'_n \Delta n' + Y' = 0 \tag{7.2}$$

$$(N'_{\dot{v}} - mx'_G)\dot{v}' + N'_v v' + (N'_{\dot{r}} - I'_Z)\dot{r}' + (N'_r - mx'_G u')r' + N'_\delta \delta + N'_n \Delta n + N' = 0 \tag{7.3}$$

where X', Y' and N' are the interaction force and moment, respectively and Δn is the change in propeller revolutions.

Trajectory simulations under these circumstances were carried out using the present interaction force model and the above referred dynamics model. Results are presented for zero rudder angle in Fig. 11 (a-f) and for a case with an automatic pilot control in Fig. 11 (g-j).

As the present force model is in good agreement with the experimentally obtained time histories of interaction force under the constrained conditions, one would expect good agreement between the simulated

trajectories herein and those presented in Alvestad and Brown [5]. However the comparisons were not quite satisfactory for several cases with constant rudder angle control, with the better results obtained for the cases with zero rudder angle and for a case using an auto-pilot. Ships are unstable in the first case with zero rudder angle and the simulation does not last for a long time. In the case of constant rudder control, time duration of the simulation is so long that even small differences in forces and moments can generate quite different trajectories. This is even aggravated by the fact that the ships move at constant speed, always maintaining the same relative longitudinal positions (stagger), putting them always operating at the same point in the interaction time-history curve, resulting in the application of a disturbance in force or moment , constantly. Moreover Alvestad and Brown [5] used interaction forces obtained from captive model test results which do not account for the instantaneous headings and relative velocities of the ships.

Fig. 11(a-f) show the results of UNREP simulations with no rudder control compared with the simulations of Alvestad and Brown [5]. The first case examined had the bow of the tracking ship alongside the stern of the leading ship (A=-524). The tracking ship is

made to run along a straight course and the trajectory of the leading ship was studied. Both ships are moving at a forward speed of 15 knots at the beginning of the run. Simulation started with 75 feet side to side separation between the two ships and was terminated when the separation becomes 100 feet or 50 feet. There is a negative moment acting on the leading ship because of the high pressure at the stern due to the tracking ship on its port side. The net force acting on the leading ship is positive trying to push it away from the tracking ship. This produces a positive lateral velocity and a negative yaw angle on the leading ship. As they move along, the leading ship is turning into the path of the tracking ship which could turn into a dangerous situation.

In the second case [Fig. 11(d-f)] both ships are abreast of each other at the beginning of the simulation and no rudder control was applied. The leading ship will be subjected to a negative force and a positive moment. The resulting lateral velocity is negative, pulling the ships together. However, the trajectory is dictated by the positive yaw angle which makes the leading ship turn away from the tracking ship. This is similar to the bank rejection phenomena, and if not anticipated can cause violent turns which may result in stern collisions.

The third simulation in this series had an automatic pilot control. The auto pilot used was the same one described in Chapter-6, Eq. (6-10) with $a = b' = 4$ and $c' = d' = 0$. As before, simulations started with 75 feet side to side separation between the ships and the tracking ship approaching from behind. Tracking ship was given slightly higher speed in order to pass the leading ship. The auto pilot tries to maintain course at 75 feet lateral separation and zero yaw angle. The results are presented in Fig. 11(g-j) along with the results from Alvestad and Brown [5]. Results from Alvestad and Brown are for manual control of the leading ship as the tracking ship passes by. Comparisons show reasonably good agreement between present results and those from Alvestad and Brown [5]. This is not unexpected because this maneuver is close to that of a captive model test as far as the interaction forces are concerned, as there is no appreciable yaw angle to deal with. That may be the reason for the better agreement with Alvestad and Brown's results which use captive model test results, and the present free running simulation results.

Adequate control was achieved with less than 10 degree rudder deflection. As the tracking ship approaches along the port side of the leading ship, rudder is deflected

away from the tracking ship to counteract a bow-in (negative) yaw moment. As the tracking ship is abreast of the leading ship, it has maximum rudder angle towards the tracking ship to counteract the bow-out (positive) yaw moment. This pattern repeats as the tracking ship pulls away.

The inadequacy of using captive model test results is apparent especially as the ships move closer or they swing toward each other. As the ships can yaw, maintaining constant side to side separation at the mid-ships, interaction forces based only on the side to side separation (as in the case of captive model test results) can be grossly in error.

7.3) Simulations of Passing Ships in a Canal:

The nature of interaction between passing ships is quite different from that of overtaking ships. Passing is a highly unsteady phenomenon where forces are dominated by added mass type inertial contributions. Steady Lagally type forces are very small when compared to the unsteady terms. However there still can be significant contributions arising from the lift force and Munk moment terms. The time duration

of interaction while passing is too short to significantly affect the trajectories of the ships. However the disturbance which occurred during passing, if not corrected, could produce drift angles which in turn generate large yaw moments, and will result in significant heading changes. Such situations could lead to a loss of control and collision with a third ship or grounding.

Trajectories of two Series-60 ships, passing in a shallow canal are presented in Eda [12]. Particulars of these ships are given in table-6 below. In this section, maneuvering simulations with the present model will be compared with those from Eda [12].

Table-6
Main Particulars of Cargo Ships

	Ship-A	Ship-B	Series-60
Length b.p. (ft)	624.10	602.51	600.00
Beam (ft)	89.2	87.10	80.00
Draft (ft)	31.70	34.24	35.00
Trim	00.00	00.00	00.00
Block Coefficient	0.767	0.621	0.60
Prismatic Coefficient	0.778	0.632	0.614
Rudder Area/(LT) (%)	1.56	1.70	1.60

Simulations of Eda [12] use captive model test results of Moody [29] for interaction forces and moments.

Bank suction forces and moments are obtained in a polynomial form based on experimental data of Fujino [14]. The equations of motion used in Eda [12] has the following form.

$$X' = X'_{vr}v'r' + X'_{vv}v'^2 + X'_{\delta\delta}\delta'^2 + X'_{\dot{u}}\dot{u}' + X'_0 + X'_p + X_{int.} \quad (7.4)$$

$$Y' = Y'_v v' + Y'_\eta y'_0 + Y'_\delta \delta + Y'_{vvv}v'^3 + Y'_{\eta\eta\eta}y'^3_0 + Y'_{\delta\delta\delta}\delta^3 +$$

$$Y'_r r' + Y'_{rrr}r'^3 + Y'_{\dot{r}}\dot{r}' + Y'_{\dot{v}}\dot{v}' + Y_{int.} \quad (7.5)$$

$$N' = N'_v v' + N'_\eta y'_0 + N'_\delta \delta + N'_{vvv}v'^3 + N'_{\eta\eta\eta}y'^3_0 + N'_{\delta\delta\delta}\delta^3 +$$

$$N'_r r' + N'_{rrr}r'^3 + N'_{\dot{r}}\dot{r}' + N'_{\dot{v}}\dot{v}' + N_{int.} \quad (7.6)$$

In the surge equation X_0 is the drag and X_p is the propeller thrust which cancel each other at the self propulsion point. It may be noted that in these equations the wall effect is modeled by a third order polynomial representation. Along with these, auto-pilot equation is also added which is the same as the one given in Eq.(6.10).

Before attempting trajectory simulations, the interaction force obtained from the present model was

compared to the captive model test results of Moody [29]. These calculations were run with the ships in a shallow canal described in the later part of this section. It can be seen from the respective comparisons in Fig. 12(a) and 12(b) that present results are in general agreement with Moody's experimental data.

Hydrodynamic data for the above maneuvering model for a Series-60 cargo ship are presented in the Appendix-C. (from Eda [12]). The main particulars of the cargo ships tested by Eda (those of Ship-A and Ship-B) are given in Table-6. Present simulations are carried out using the above maneuvering model and hydrodynamic data, with the ships considered to be at their self propulsion points.

In his simulations Eda used a canal 5.7B wide and 1.5T deep where B and T are the beam and draught of the ships considered. Ship-A was moving at 4 kn. speed, 1.24B away from the center line of the canal on one side and Ship-B was moving at 4 kn. speed, 0.94B away from the center line of the canal on the other side, (or they were passing at a lateral separation of 2.18B). Trajectories of Ship-B were analyzed due to the passage of Ship-A, which was made to run in a straight course. Ship-B was initially given its pre-determined equilibrium conditions to maintain a steady

off-center line course. Then the time history of interaction force was given to it and the ensuing motions were studied. The interaction force and moment time history used by Eda [12] were determined from captive model tests of Moody [29].

Simulations were carried out for these conditions using the present interaction model. Initially Ship-B was given equilibrium rudder angle -7.465 deg. and drift angle -0.1303 deg., as determined by Eda [12]. Then it is allowed to run freely, subject to the interaction and bank-suction forces and moments. Three different conditions were studied, varying rudder control system parameters, viz:

$a = b' = c' = d' = 0$

$a = b' = 4,\ c' = d' = 0$

$a = b' = 6,\ c' = d' = 0$

The first case has no control system, which means that the Ship-B had a constant rudder angle. The rudder angle is maintained at the initial equilibrium value during the entire simulation. The second case has an auto pilot as described in Chapter-6, with mild responsiveness and the last case has an auto pilot with high responsiveness.

Results for the trajectory of Ship-B, heading change, drift angle, and rudder activity during passing are presented in Fig. 12(c-m), along with corresponding results from Eda [12]. As the ships meet each other and start passing, there is a developing force of repulsion between the ships and a moment turning the bow outwards. This repelling lateral force generates a positive lateral velocity. The resulting negative drift angle, even though small, produces a large negative hydrodynamic yaw moment from $N_v v$ term in the equation. This drift angle reaches its negative peak when the separation distance is -L/4. At this point Ship-B has a drift angle -2 deg. which results in a yaw moment $N'_{v'}v' = -0.0005$, which is comparable to the interaction moment itself, which has a value of -0.0007. As the ships continue passing, maximum positive drift angle is produced at the point when the separation is L/4. At this point, the moment due to the drift angle is 0.00025 while the hydrodynamic interaction moment is 0.0005. It can be seen that the effect of drift angle complements that of the interaction moment resulting in large heading changes, which dictates the path of Ship-B.

The present results for the trajectories and other parameters do not compare well with Eda's results, especially after the ships pass each other. This is despite

the fact that the interaction forces used in both the simulations match reasonably well when running in the captive mode. The dynamic models used in both the simulations are also identical, except for the way bank-suction forces are treated. Bank suction terms in Eda's model is represented as cubic polynomials as functions of off-center distance, without any regard to the ship's angular orientation. Essentially this means that $X_{\psi} = Y_{\psi} = N_{\psi} = 0$. As the simulation shows yaw angles of about 5 deg. this would have major influence in lateral force and in yaw moment. In the simulations of Eda [12], especially in the case without any rudder control, yaw angle increases after the ships pass each other, without showing any bank rejection phenomena. At the end of the simulation presented in Fig. [27], and Fig [29] of Eda [12], Ship-B center line is 130 feet off the center line of the canal and it has a heading angle of +4 deg. Even at such extreme off center position, ψ is positive, which is contrary to the observed and physically anticipated phenomenon of bank rejection. Eda also uses captive model test results for interaction force and moment time-history and imposes this on Ship-B during the simulation. This completely obscures the influence of heading and changes in relative velocities on the interaction forces and moments. The effect due to the neglect of these is more so in the case without any rudder

control, where Ship-B trajectory deviates far from a straight course. For these reasons, it is believed that the present results represent the real phenomenon in a more satisfactory manner.

7.4) COLLISION ANALYSIS

We have discussed the nature of hydrodynamic interaction between ships and shallow bottom and canal walls in detail in the previous sections. These are situations where there is evidence of increasing occurrence of collisions and grounding of large vessels. A recent Cost Guard accident analysis shows that twice as many collisions involving vessels of over 500 tons occur in narrow canals as occur in harbors and open sea combined (Bradden [3]). Situations leading to such collisions can now be studied with the aid of a maneuvering simulator incorporating the hydrodynamic model developed herein.

To illustrate general features of collision situations, several simulations were carried out using a container ship hull (NEW YORK) and a barge-tow. Main particulars of the container ship and the barge-tow are

given in Table-7 and their hydrodynamic coefficients in deep water are given in Appendix-E.

Table-7(a)
Main Particulars of 'New York'

Length Overall (ft)	915.0
Breadth (ft)	106.0
Draft (ft)	36.0
Displacement (tons)	79,350

Table-7(b)
Main Particulars of 'Barge-Tow'

Length Overall (ft)	1130.0
Breadth (ft)	105.0
Draft (ft)	9.0
Displacement (tons)	27,000

Results of these simulations are presented in Fig. 13 (a-h). These plots show snapshots of the ships taken at several instants of time as they pass by. Results are presented in this form of plots, in order to give a better feel for the interaction phenomena than is possible by plots of lateral velocity, heading angle or sideslip angle against time. It may well be noted here that in these simulations, both the ships are not constrained to move in any

predetermined manner. The ships respond to the relative hydrodynamic interaction forces and moments as well as to any control forces applied by the rudder. This is in contrast to all the previous simulations presented herein, where one of the two ships was constrained to move in a straight course. Results of these free-running simulations are obtained using the hydrodynamic coefficients appropriate for deep water case. This would have caused differences in the simulated trajectory from what one would get in a realistic full scale maneuver. These are presented here to illustrate the qualitative nature of the interaction phenomena in common maneuvering situations.

The first case analyzed was that of overtaking ships in shallow water. Ship-A travelling at 7 kn. speed is overtaking Ship-B travelling at 5 kn. (Both ships are models of the container ship 'New York'). Ships are operating in a sea of depth 54 feet (H/T = 1.5). At the beginning of the simulation Ship-B is about half the ship-length ahead of Ship-A, and they are twice their beam apart laterally, moving along parallel course. The result of this simulation without any rudder controlling action is shown in Fig. (13a). It can be seen that the leading ship-B turns inwards into the path of the overtaking ship-A, resulting in a broad side collision.

Similar phenomena is known to occur whenever the leading ship is just ahead of the forward shoulder of the trailing ship (as pointed out by Dand [10]), at which point the leading ship is subjected to strong bow-in moment resulting from the accelerated flow between them. The situation can be worse if the leading ship is much smaller than the other. An interesting situation of this type occurs when a tug is handling the bow line of a large ship. The ship and the tug may be free running along parallel paths with the tug near the forebody of the ship. If the tug moves ahead, it will be subjected to strong bow-in moment and can be easily sucked into the path of the ship it is tending to. Just before this happens, the tug is likely to experience bow-out moment (when the tug is aft of the foreward shoulder of the ship) at which time the correcting helm is towards the ship. If this helm is not reversed, anticipating strong bow-in moment, situation will get aggravated and go out of control.

The previous case (case-1) is repeated after adding an auto-pilot with gain constants $a = b' = 4$ and $c' = 2$. In all the cases using an auto-pilot the gain constant d' will be taken as zero for simplicity. At the beginning ships are subjected to bow-in moment due to the

accelerated flow between their bows. Correcting helms are 35 degrees maximum for Ship-B and 15 degrees maximum for Ship-A, away from each other. The moments change sign as Ship-A catches up with and get abreast of Ship-B. At this point the correction rudder deflection is towards the other ship. The resulting trajectory is shown in Fig. 13(b). Even though the ships went far off their original straight line path, they passed without a collision.

In the third case illustrated in Fig. 13(c), ships are abreast of each other at the beginning of the maneuver. Ship-B was traveling at 7 kn. and Ship-A at 5 kn at the beginning. Water depth was 54 feet with H/T = 1.5. This maneuver is similar to UNREP operation and is known to produce strong bow-out moment on both the ships, forcing them away from each other. This can be clearly observed in Fig. 13(c), where the bow rejection is so violent almost resulting in a stern to stern collision.

Case-3 was repeated with the addition of an auto-pilot using gain constants a =b'= 4 and c'= 2. At the beginning, to counteract strong bow-out moment, both ships have their rudders laid hard over towards the other ship. As Ship-B reaches the forward shoulder of Ship-A the interaction yaw moments change sign. At this time Ship-A has

its rudder laid away from Ship-B. However Ship-B maintains a negative rudder angle (towards Ship-A). The explanation for this behavior is that the slower Ship-A is subjected to stronger interaction forces and so its motion is more dominated by interaction forces. Motions of faster Ship-B is more dominated by the negative drift angle generated by the initial attractive force which produce a negative turning moment. The resulting trajectory is plotted in Fig. 13(d) where it can be seen that the ships pass without collision.

The fifth case is that of passing ships in a shallow canal. The canal is 500 feet wide (W/B=5) and 45 feet deep (H/T=1.25). Ship-B is 32 feet off the center line of the canal to the left side and Ship-A is 100 feet off the center line of the canal to the right side, lateral separation between the ships being 132 feet (1.25B). At the beginning of the simulation, the ships are more than one ship-length apart longitudinally, and are travelling toward each other along parallel paths at 7 kn speed. No controls are applied on either ship. The resulting trajectories are plotted in Fig. 13(e). As they meet, the ships are rejected from each other by strong bow-out moments. As they start overlapping, the moments change sign, trying to turn the ships towards each other. At this point, while turning towards the center of the canal, Ship-A rear ended its near

bank, ending the simulation. This clearly illustrates that even though there is little danger of collision between passing ships themselves, the resulting disturbance could lead to grounding or loss of control leading to a collision with a third object.

The previous case of passing ships in a canal was repeated after adding an auto-pilot. This resulted in the same type of collision of ship-A on the near bank. Therefore a slightly 'milder' case was run with a 700 feet wide (W/B=7), and 54 feet deep (H/T=1.5) canal. An auto-pilot was included in the model with gain constants a=b'=6 and c'=4. Ships were positioned in the canal at the beginning of the simulation as in the previous case. The resulting trajectory is presented in Fig. 13(f). The rudder activity followed the pattern of the turning moment acting on the respective ship. As the ships meet, to counter the bow-out moment, rudder is laid hard over towards the center of the canal. As their forward shoulders pass each other, the interaction moments change sign and become bow-in. At this point rudder is laid hard over away from the center of the canal. This pattern is repeated in the case of Ship-B as it pulls away. However, Ship-A has its rudder laid towards its near bank for the rest of the maneuver because of the dominating influence of its near bank. This was not observed in the case of Ship-B

as it was closer to the center of the canal than Ship-A.

Case-7 was a simulation of a single ship moving off-center in a shallow canal, without applying any control. This situation is well known to produce bow rejection and result in unstable motions. The container ship 'NEW YORK' was run in a 600 feet wide, 54 feet deep canal (W/B=6, H/T=1.5). The ship was initially travelling at 7 kn. speed, 100 feet from the center line of the canal. The resulting trajectory is shown if Fig.13(g). Within 3 minutes after the simulation started or by the time the ship travelled 2000 feet, its bow hit the far bank.

The previous case was repeated after adding an auto-pilot using gain constants a=b'=4 and c'=2. the resulting trajectory is shown in Fig.13(h). The ship maintained course with a constant rudder angle of 18 degrees towards the near bank, and a drift angle less than 2 degrees. Rudder forces and moments can counteract the interaction forces and moments due to the bank suction, with little or no drift angle. This illustrates the common knowledge among river and canal pilots that ships need to lay their helm towards near bank to transit off-center in a river or canal.

Case-9 was similar to the case 3 of overtaking ships in a shallow water, except that the vessels are now two barge-tows moving in parallel courses at the same speed of 5 kn. The behavior of the barge tows were similar to those of the container ships, as can be seen from the plot 13(i), where strong bow rejection caused a stern-stern collision. Case-13 was a replica of Case-9 with the inclusion of an auto-pilot with $a = b' = 4$, $c' = 2$ and $d' = 0$. Resulting trajectories are shown in Fig. 13(j). In general barges behave similar to ships in these and other maneuvers predicted by the present formulation.

CONCLUSIONS

A computationally simple method has been implemented for maneuvering simulation of ships in shallow and asymmetric canals. The computations mainly involve simple evaluation of numerical quadrature, in contrast to other analyses that involve solutions of coupled integral equations, etc. The computed results show good qualitative agreement with experimental results as well as good quantitative agreement in a number of cases. The simplified modeling of the singularity distribution used here still provides a good prediction of the interaction forces, while also reducing the computation time appreciably.

For the case of passing ships, the major forces arise from the inertial effects while the lift forces in the after hull region and viscous cross-flow drag forces are generally small compared to the inertial forces. In the case of a single ship moving parallel to the canal walls, or two ships moving in tandem at the same speed, the problem becomes steady and the dominant contribution is from the lift forces. Based on the illustrated results, it can be seen that lift forces are satisfactorily modeled using the

concepts of slender body and low aspect ratio wing theories.

The computer program for determining these hydrodynamic interaction forces is developed as a module and combined with a ship motion trajectory code enabling free running maneuvering simulation of passing ships in shallow channels. The present analysis and program will allow the ships to have arbitrary orientation in the canal, and to approach the canal walls at an angle. All associated dynamic effects due to their motions are considered in calculating the interaction forces. This generalized model will also be applicable to other cases such as overtaking, a single ship in a canal, etc. with the computation module in a form readily adaptable for use in any simulator.

A major benefit obtained by these simplified hydrdynamic modelling procedures is in regard to computation time, which decreased by about a factor of 20 compared to that in [24] and [39]. The computation time for determining the longitudinal and lateral forces, as well as the yaw moment, due to interactions, with these hydrodynamic forces found for both ships, is 3 sec. for each time instant at which the computation is made (in an IBM 3090 Mainframe Computer). The requirement to calculate the longitudinal force essentially doubles the required time, so that

obtaining only the lateral force and yaw moment for both ships will take about 1.5 sec. at each instant of time.

For the time of passing (where the ships move from bow-to-bow to the stern-to-stern condition), which is about 72 sec. in real time for the Panamax vessels at 7 kn. speed for each, a total of 20 time instants would be adequate for use in representing the time histories of the interaction forces. This would certainly be adequate if only the lateral force and yaw moment due to interaction were being considered in a simulation study. While the real time for this ship passing case was about 72 sec., it must be mentioned that the computation times given above were for a large mainframe IBM 3090 computer which is not the type of machine used in ship simulators. However there are some relatively fast minicomputers presently in use, or planned for use, in some simulators that have sufficient computational speed and capacity that can incorporate the generalized hydrodynamic interaction force calculation within their operation when considering real time simulation. It is apparent that the computation requirements for use in the real time simulation mode would allow direct utility of this force calculation, while special considerations would have to apply to fast time simulation and/or the inclusion of longitudinal force

evaluation. For barge-tows, fast simulation is now possible with the special formulation for box forms.

The prospect of more realistic modeling of ship interaction forces, and their use in simulator studies, provides an opportunity for enhancing the simulation fidelity and accuracy for many problems of interest in simulator applications for restricted waterway design and analysis studies.

List of References

1) Abkowitz, M.A., Ash, G.M., and Forston, R.M., "Interaction effects on ships operating in proximity in in shallow and deep water", Eleventh Symposium on Naval Hydrdynamics, March 1976.

2) Beck, R.F., "Forces and moments on a ship moving in a shallow channel", Trans. RINA, 1976.

3) Bradden, F.D., Discussion to Eda [12]

4) Brard, R., Capt., "Maneuvering of ships in deep water, in shallow water, and in canals", Summer meeting SNAME, 1951, Washington, D.C.

5) Brown, S.H., and Alvestad, R., "Hybrid computer simulation of maneuvering during underway replenishment", International Shipbuilding Progress, September 1974.

6) Calvano, C.N. : "An investigation of the stability of a system of two ships employing automatic control while on parallel courses in close proximity," M.S. Thesis, Dept. of Naval Architecture and Marine Engineering, M.I.T, 1970.

7) Clarke, D.: "The application of maneuvering criteria in hull design using linear theory," Trans. RINA, Vol 125, 1983.

8) Collatz, G., "Potential theoretische Untersuchung der hydrodynamischen wechselwirk zweier Schiffskorper", Jahrbuch Schiffbautechnischen Gesellschaft, 57, 1963.

9) Cummins, W.E., "The force and moment on a body in time-varying potential flow", Journal of Ship Research, April 1957.

10) Dand, I.W., "Hydrodynamic aspects of shallow water collisions", Trans. RINA 1976.

11) Dand, I.W., "Some aspects of maneuvering in collision situations in shallow water", Tenth Symposium on Naval Hydrdynamics, June 1974.

12) Eda, H., " Directional stability and control of ships in restricted channels", SNAME Transactions 1971.

13) Flagg, C.N., and Newman, J.N., "Sway added mass coefficients for rectangular profiles in shallow water", Journal of Ship Research, December 1971.

14) Fujino, M., "Experimental studies of ship maneuverability in restricted water, Part 1 and 2",International Shipbuilding Progress, no. 168, 1968 and no.186, 1970.

15) Goodman., A. et al : "Experimental techniques and methods of analysis used at hydronautics for surface-ship maneuvering predictions," Hydraunautics Inc. Technical Report.7600-1, June 1976.

16) Gurevich, M.I.: "Added Mass of a lattice consisting of rectangles" (in Russian), Prokl. Mat. i. Mech., Vol 4, no 2, 1940, pp 95-100.

17) Hess, F.: "Lateral forces on a ship approaching a vertical wall: A theoretical model,"
Journal of Ship Research, December 1979.

18) Heuser, H. et al: VBD Report-1052, June 1984.

19) Jacobs, W.R.: "Estimation of stability derivatives and indices of various ships forms, and comparisons with experimental results,"
Journal of Ship Research, September 1966.

20) Kaplan, P. and Sankaranarayanan, K.: "Development of a generalized hydrodynamic force module for interacting ships in a shallow asymmetric canal, " Report No. MA-RD, Maritime Administration, June 1988.

21) Kaplan, P. et al: "The dynamics and hydrodynamics of Surface Effect Ships," Trans SNAME, 1981.

22) Kaplan, P. et al: "Hydrodynamic analysis of Barge platform systems in waves," Spring meeting RINA 1982.

23) Kaplan, P.: "A generalized hydrodynamic interaction force module and its use in simulation of ship interactions in shallow channels." Proc. MARSIM-87 Conf., Trondheim, Norway, June 1987.

24) Kaplan, P. and Sankaranarayanan, K.: "Hydrodynamic interaction of ships in shallow channels, Including effects of asymmetry," Proc. RINA Int. Conf. on Ship Maneuverability, London, May 1986.

25) Landweber, L., and Yih, C.S.: "Forces, moments and added masses for Rankine bodies,"
Journal of Fluid Mechanics, Vol-1, Part-3, Sept. 1956.

26) Lighthill, M.J.: :Note on the swimming of slender fish,"
Journal of Fluid Mechanics, Vol-9, 1960.

27) Lunde, J.K.: "On the linearized theory of wave resistance for displacement ships in steady and accelerated motion," Advance copy of paper to be presented at SNAME summer meeting Sept. 1951.

28) Miller, E.R. : "The prediction of river tow maneuvering performance," Coast Guard Report No. CG-D-32-78, May 78.

29) Moody, C.G.: "The handling of ships through a widwned and asymmetrically deepened section of Gaillard Cut in the Panama Canal," DTMB report 1705, Aug. 1964.

30) Muga, B. and Steve, F.: "Passing ship effects from theory and experiment," Offshore Technology Conference, Vol-111, 1975.

31) Newman, J.N.: "Some theories for ship maneuvering,"
Journal of Mechanical Engineering Science, Vol-14, 1972.

32) Newman, J.N.: "Lateral motion of a slender body between two parallel walls,"
Journal of Fluid Mechanics, Vol-39, 1969.

33) Newman, J.N.: "Marine Hydrodynamics,"
The MIT press, Cambridge, MA.

34) Newton, R.N.: "Some notes on interaction effects between ships close aboard in deep water," Proc. First Symposium on ship maneuverability, DTMB report 1461, 1960.

35) Oltman, P.: "Experimentelle Untersuchung der hydrodynamischen Wechselwirkung Schiffsahuicher Korper,"
Schiff und Hafen, 22, 1970.

36) Pond, H.L.: "The pitching moment acting on a body of revolution moving under a free surface," Navy Department, The DTMB Report 819, May 1952.

37) Raff, A.I.: "Program SCORES - Ship structural response in waves," Ship Structure Comm. Rpt. SSC-230, 1972.

38) Remery, G.F.M.: "Mooring forces induced by passing ships," Offshore Technology Conference, No:2066, 1974.

39) Sankaranarayanan, K.: "Hydrodynamic interaction of passing ships in a shallow asymmetric canal," M.S. Thesis, VPI&SU AOE Dept., May 1986.

40) Shen Wang: "Dicussion of reference [44]"

41) SSPA results: Model test results at SSPA for CAORF Panama Canal Project, 1985.

42) Taylor, G.I.: "The energy of a body moving in an infinite fluid, with an application to airships," Proc. Royal Soc. A, Vol. 120, 1928.

43) Thwaites, B.: Incompressible Aerodynamics, Oxford at Clarendon Press, 1960.

44) Tin-Woo Yung: "Hydrodynamic interactions between ships in shallow water," University of Michigan, Report.201, June 1978.

45) Tuck, E.O. and Newman, J.N.: "Hydrodynamic interactions between ships," Tewnth Symposium on Naval Hydrodynamics, June 1974.

46) Wells, J.L.: "Effect of angular orientation on the hydrodynamic forces acting on a body in a restricted waterway" M.S. Thesis, VPI&SU AOE Dept. December 1985.

47) Willwm B. Van Berlekom and Thomas A. Goddard: "Maneuvering of large tankers," SNAME Transactions 1972.

48) Gertler, Morton and Hagen, Grant R., "Standard equations of motion for submarine simulation." NSRDC Report 2510, June 1967.

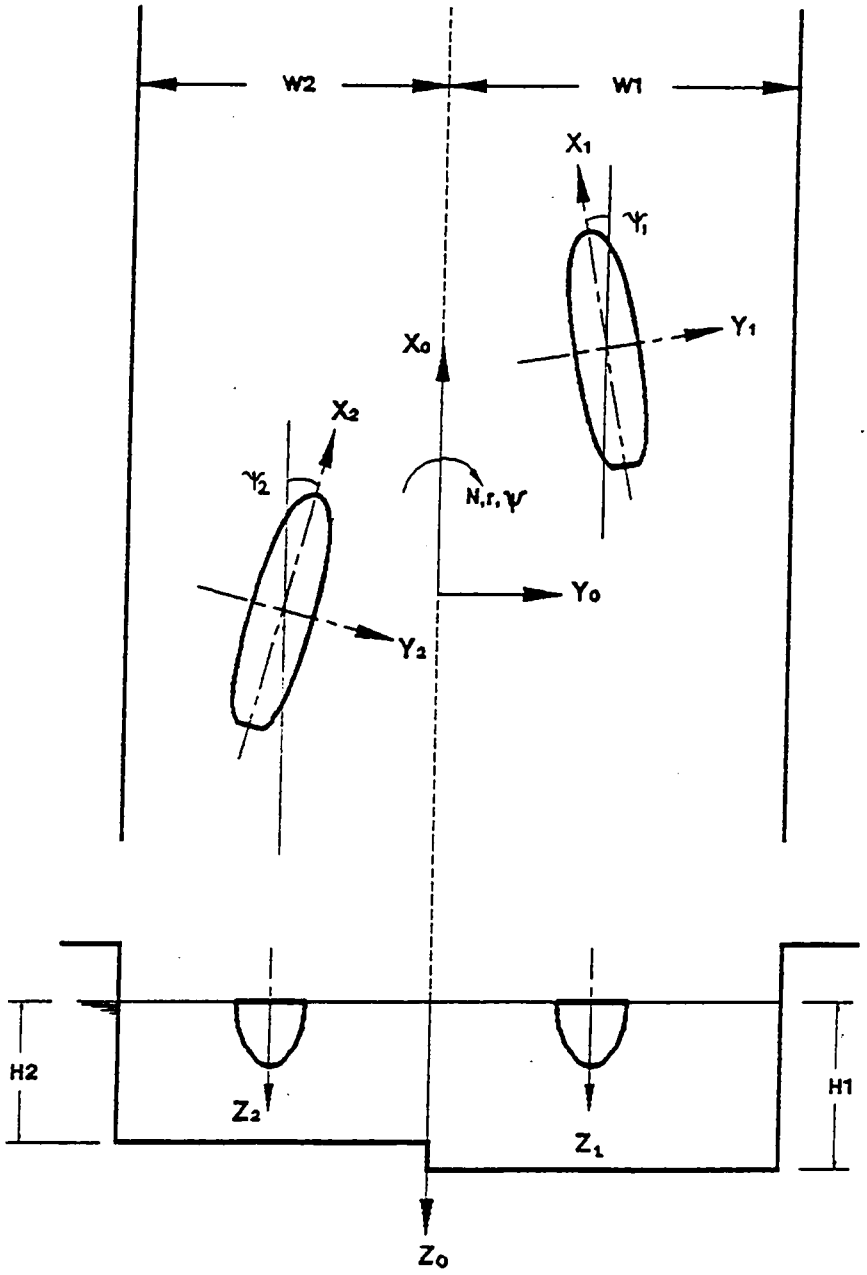

Figure 1. Definition Diagram with Coordinate Systems

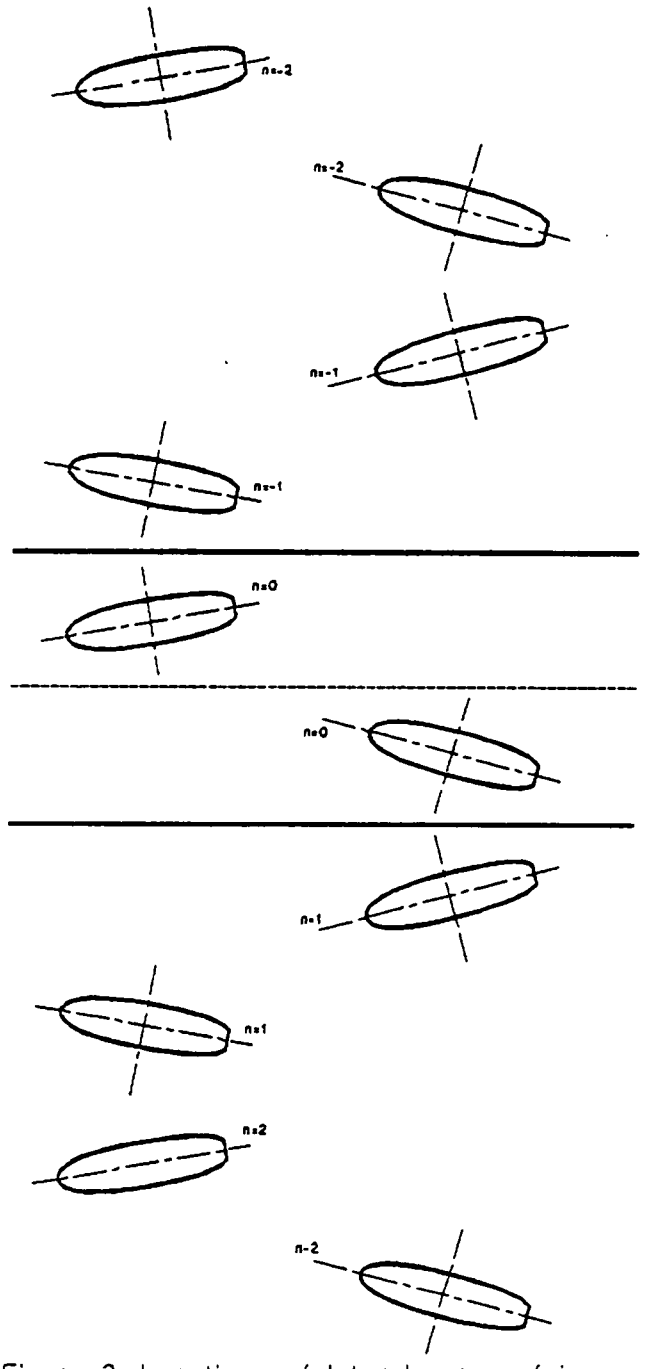

Figure 3. Locations of lateral array of images

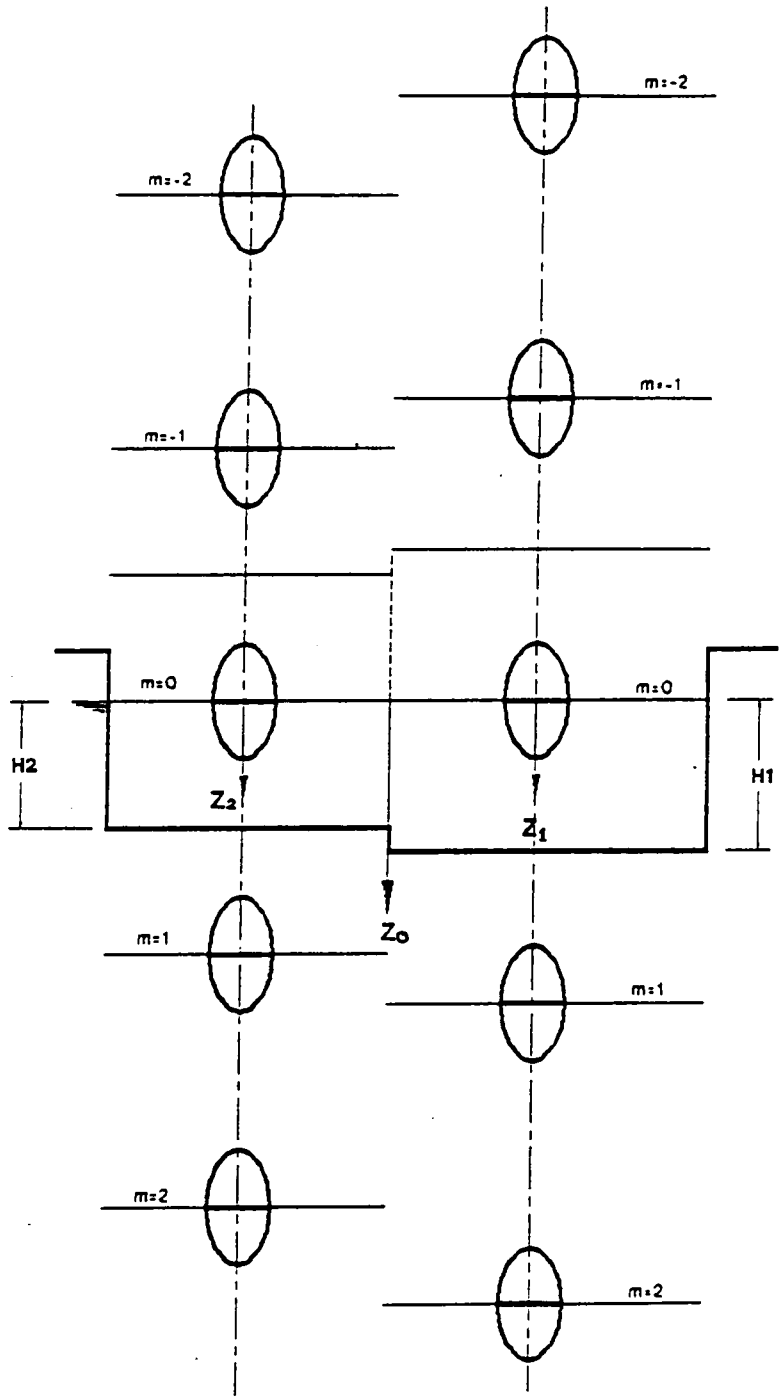

Figure 2. Location of vertical array of images

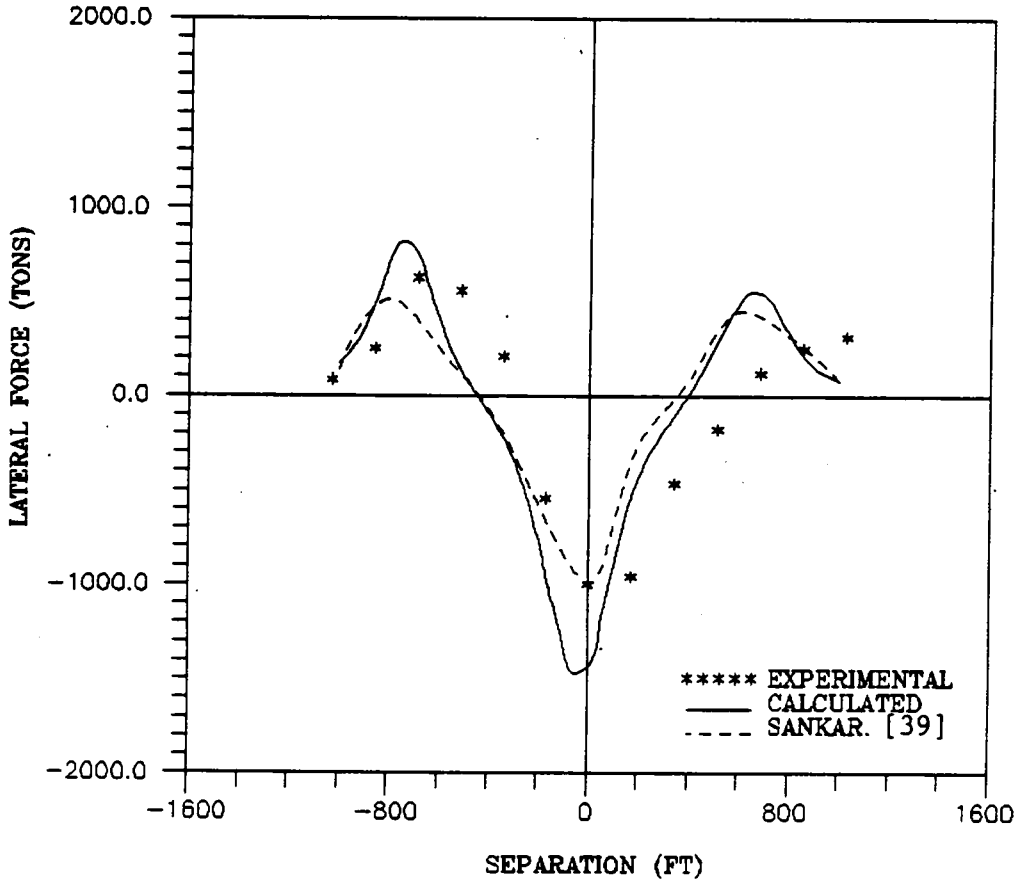

Fig-4(a): Lateral Force - SSPA Case-1

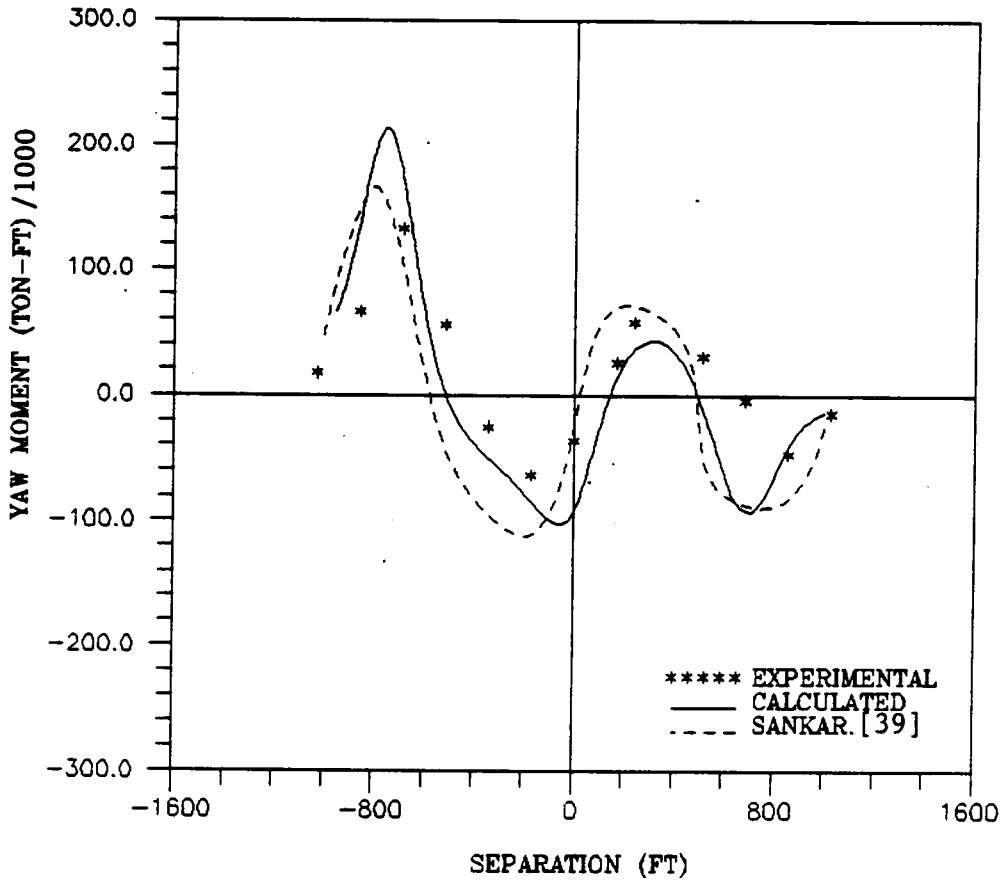

Fig-4(b): Yaw Moment - SSPA Case-1

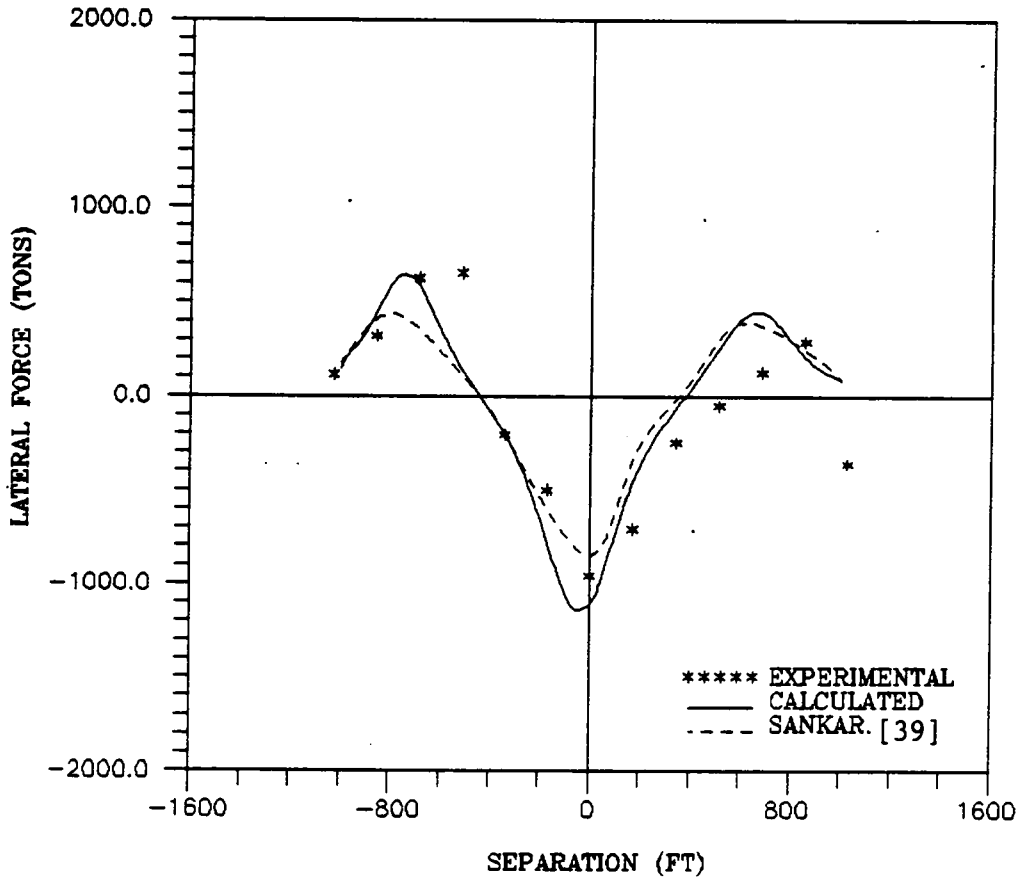

Fig-4(c): Lateral Force - SSPA Case-2

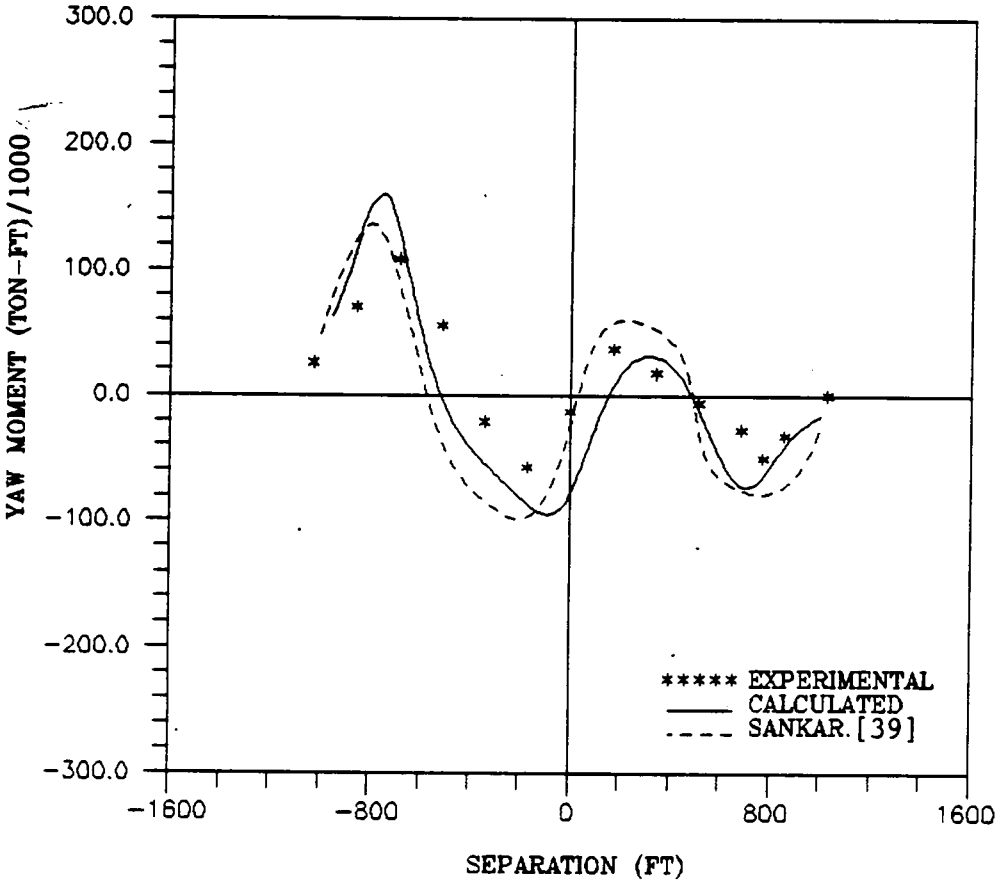

Fig-4(d): Yaw Moment - SSPA Case-2

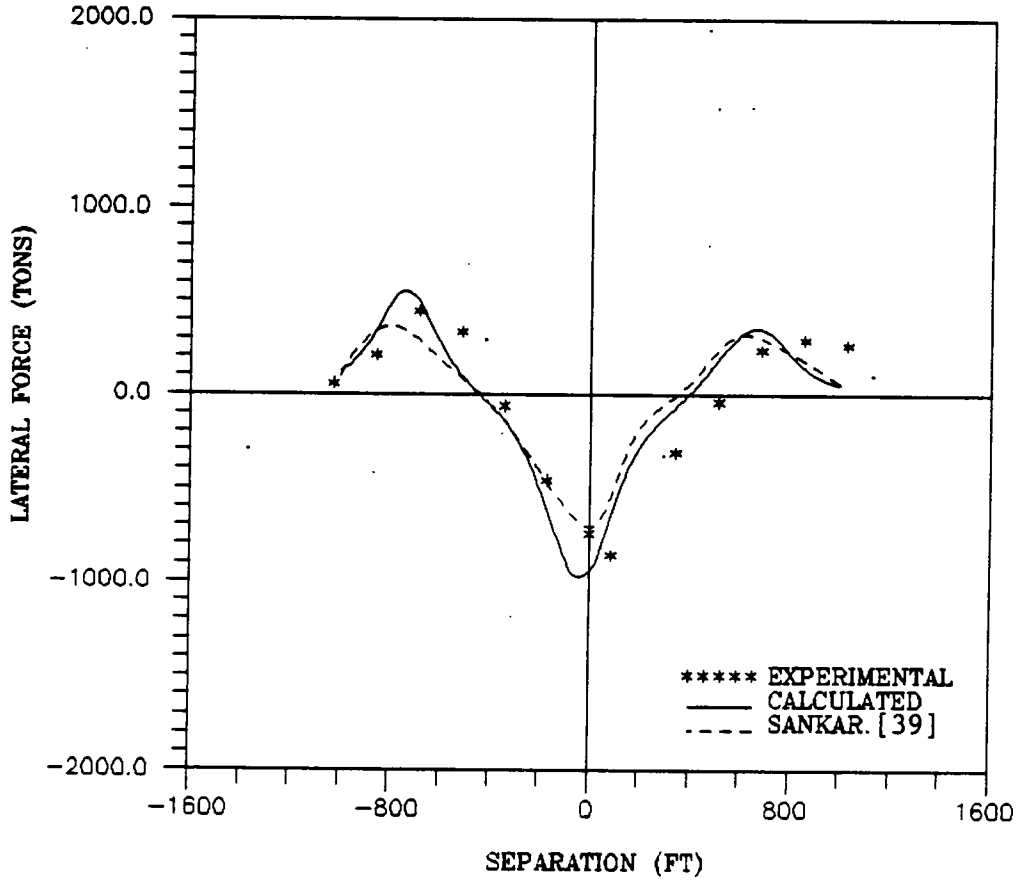

Fig-4(e): Lateral Force - SSPA Case-3

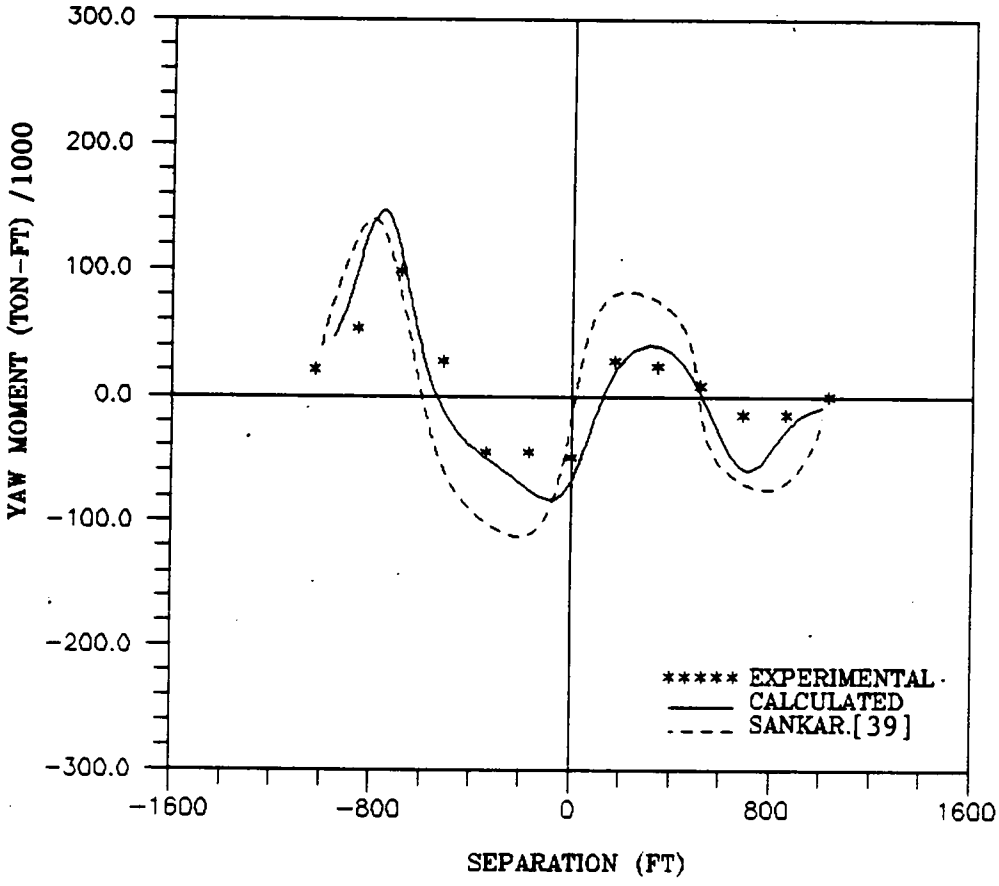

Fig-4(f): Yaw Moment - SSPA Case-3

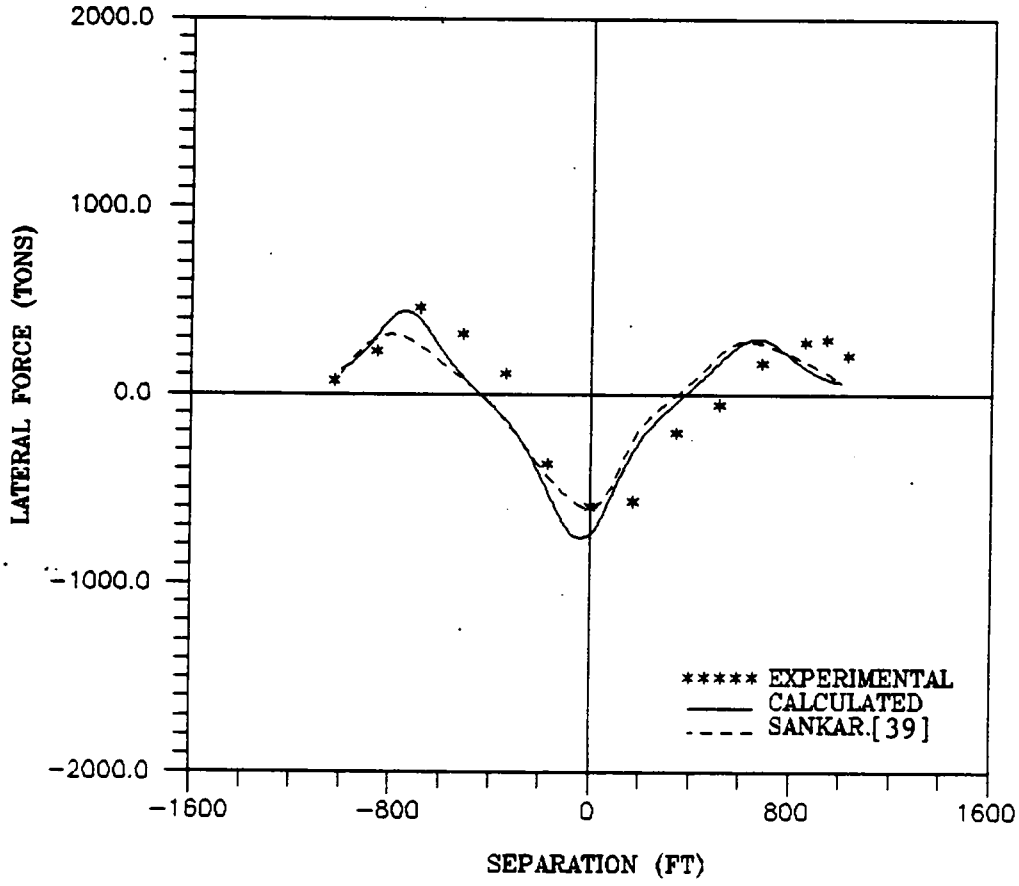

Fig-4(g): Lateral Force - SSPA Case-4

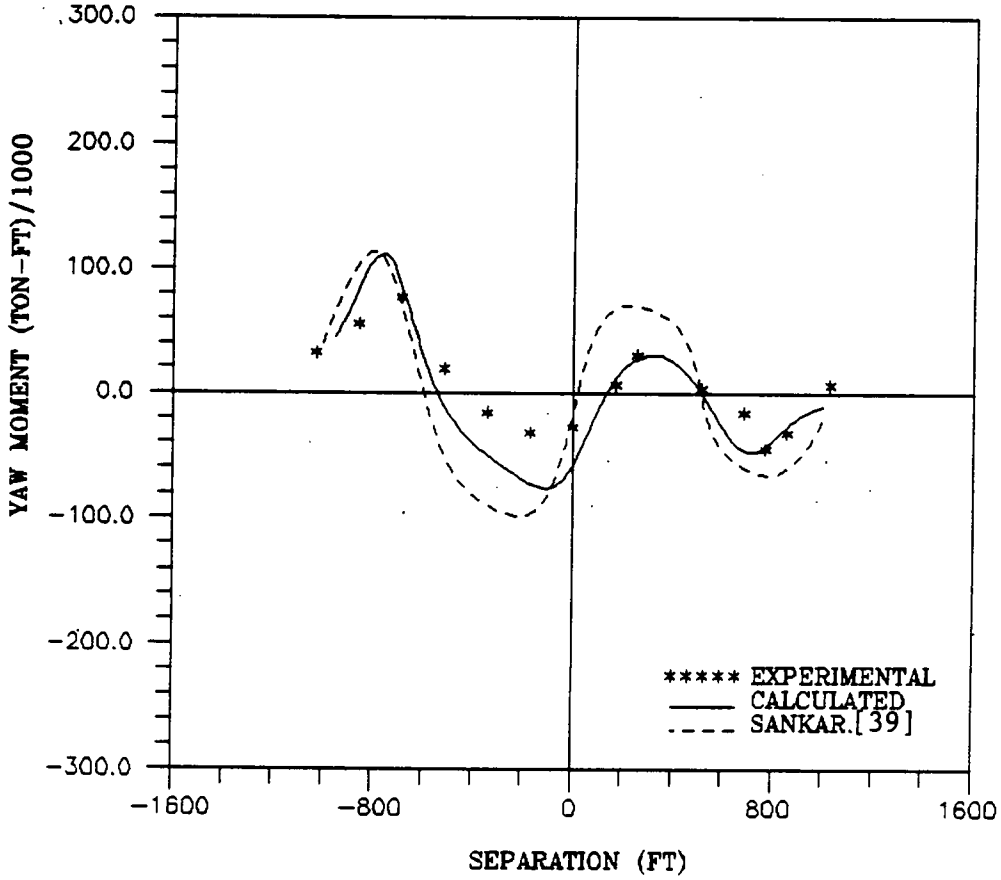

Fig-4(h): Yaw Moment - SSPA Case-4

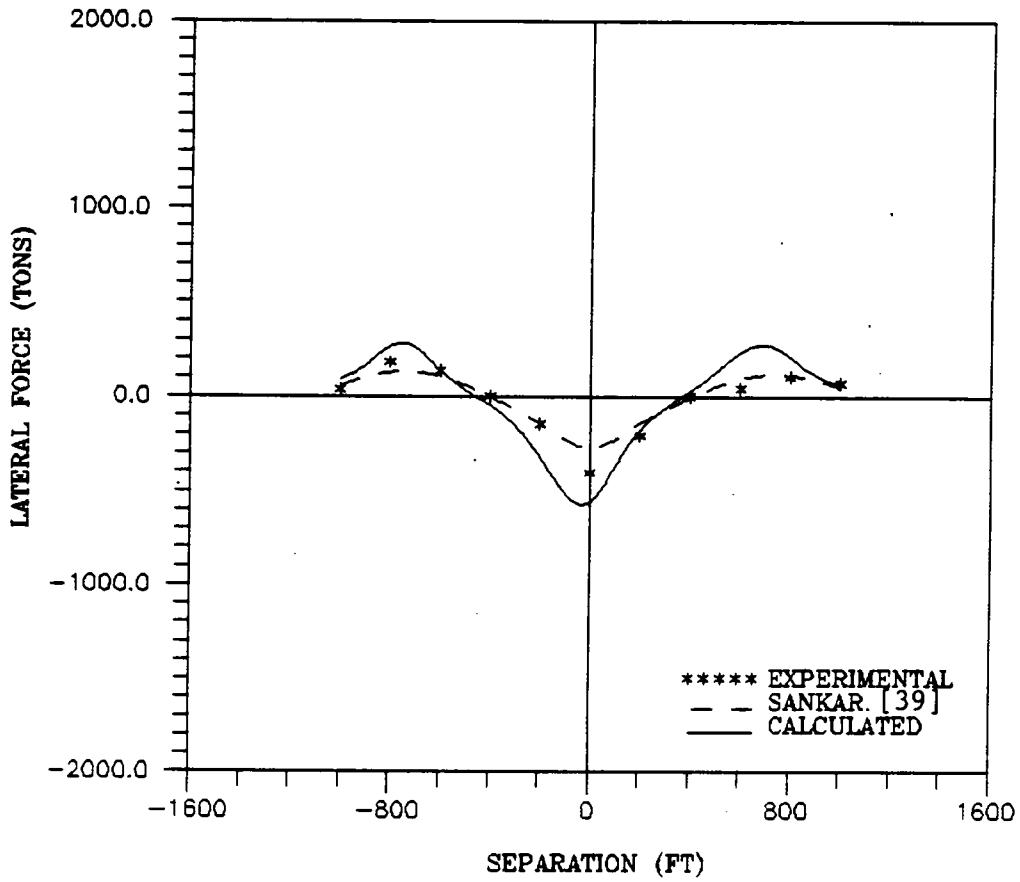

Fig-4(i): Lateral Force - SSPA Case-5

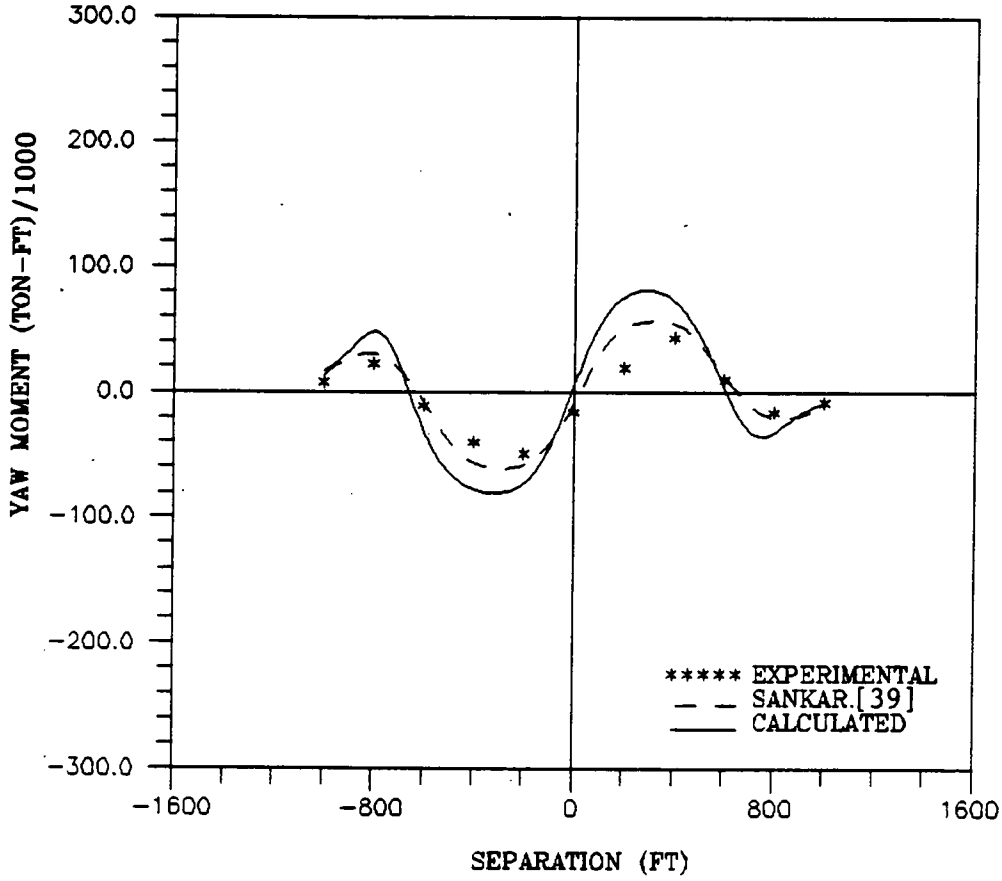

Fig-4(j): Yaw Moment - SSPA Case-5

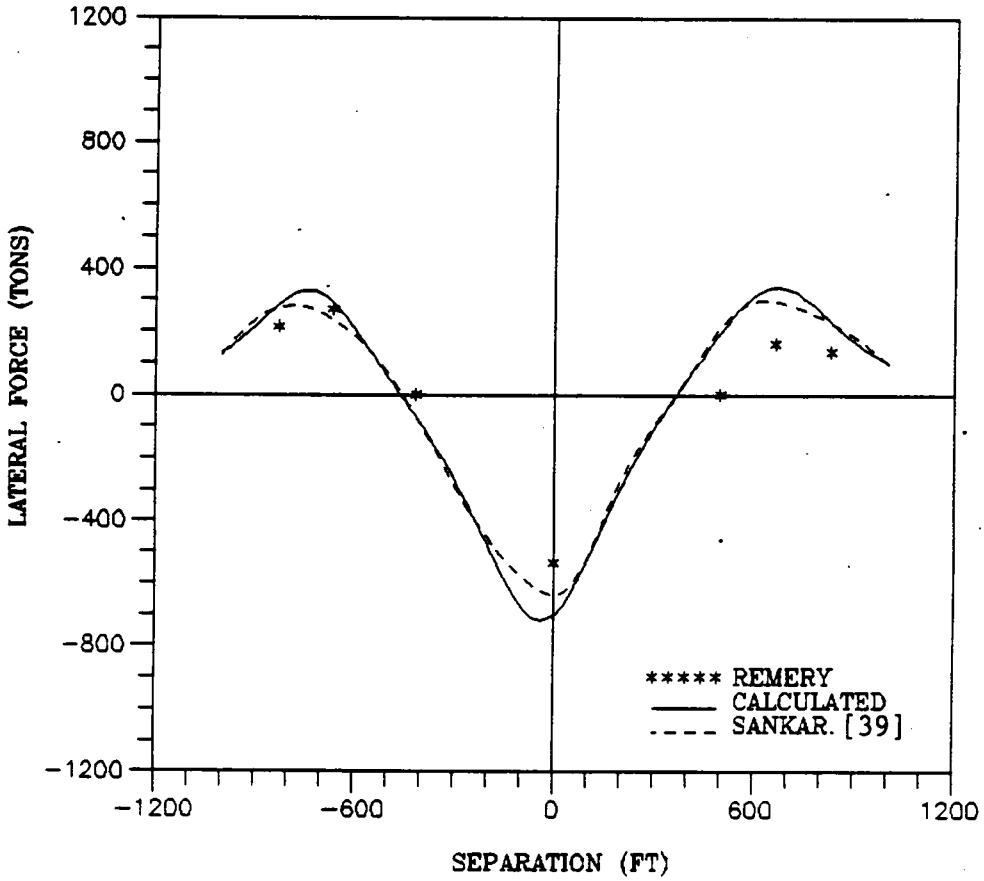

Fig-5(a): Lateral Force - NSMB Case-1

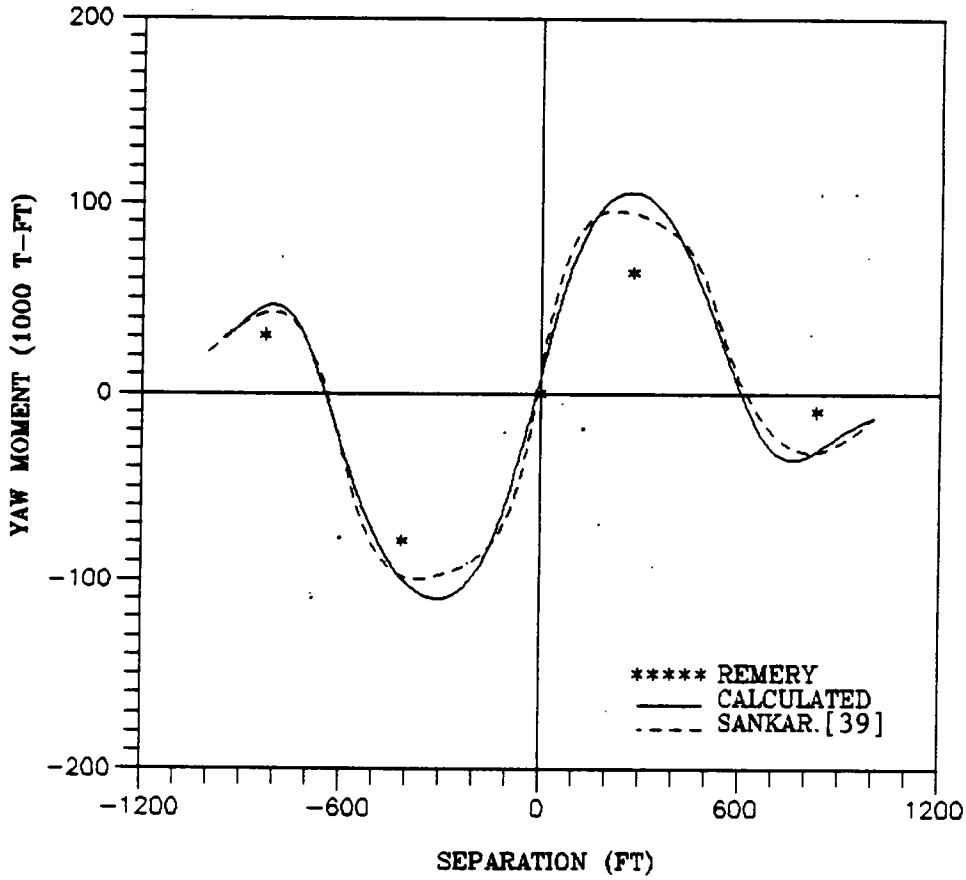

Fig-5(b): Yaw Moment - NSMB Case-1

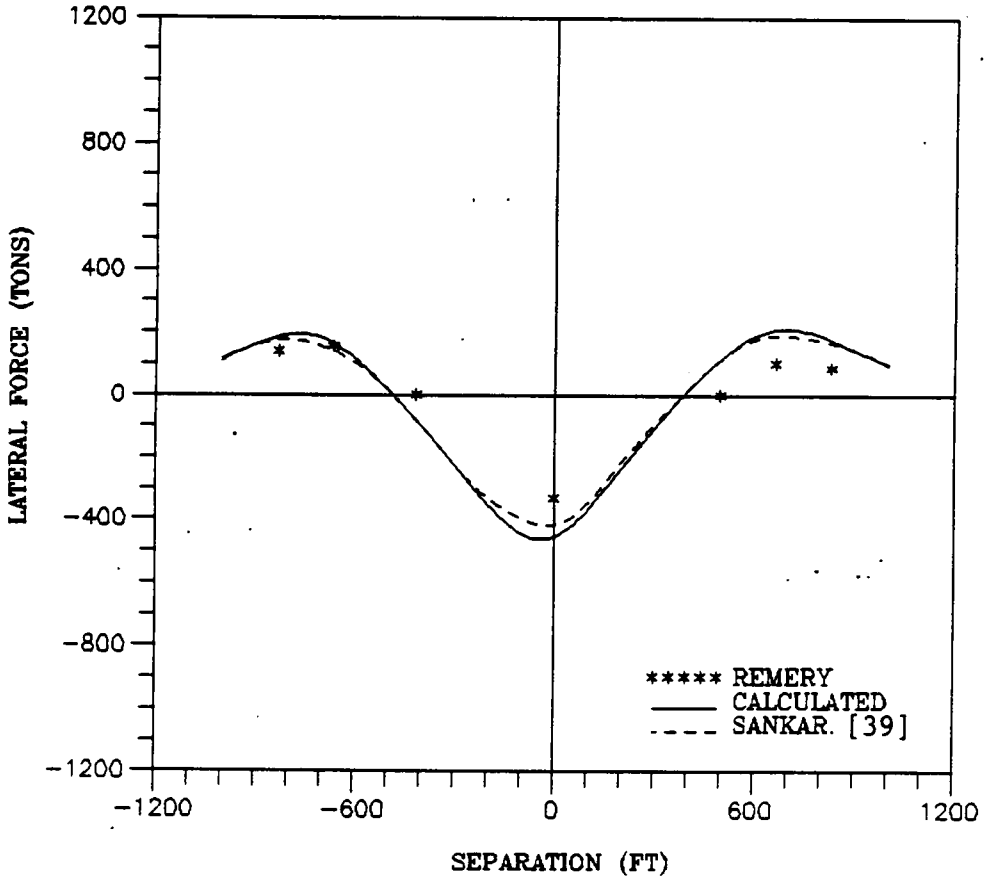

Fig-5(c): Lateral Force - NSMB Case-2

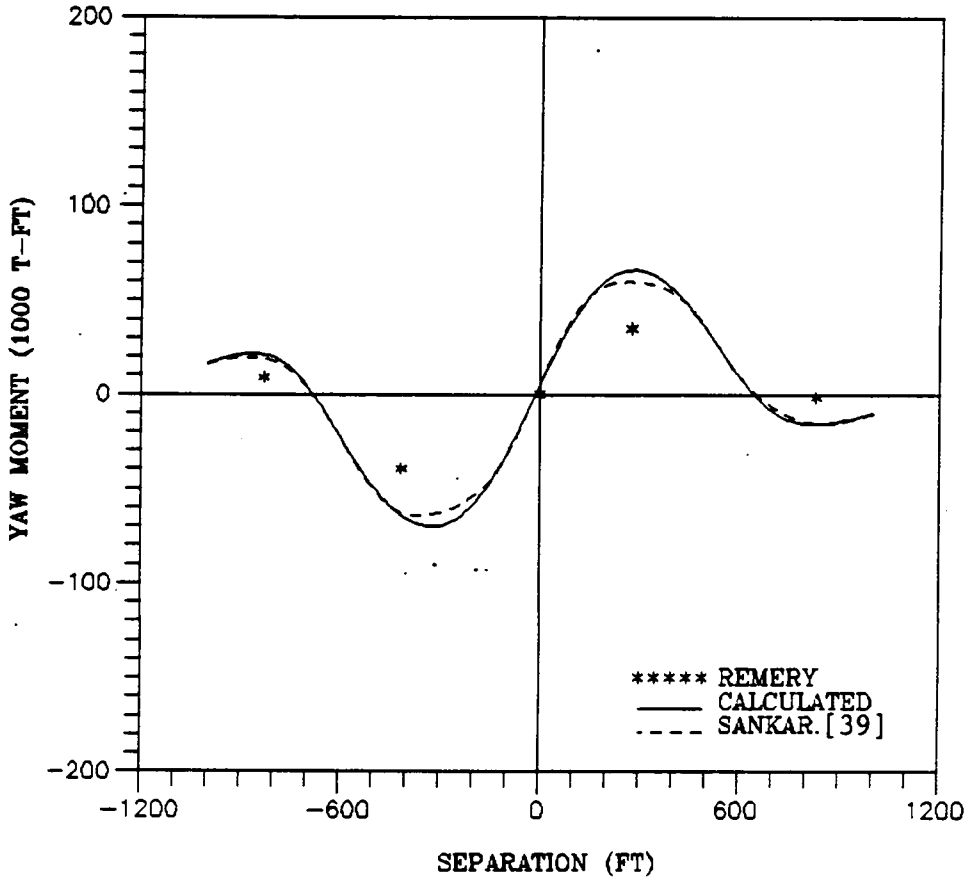

Fig-5(d): Yaw Moment - NSMB Case-2

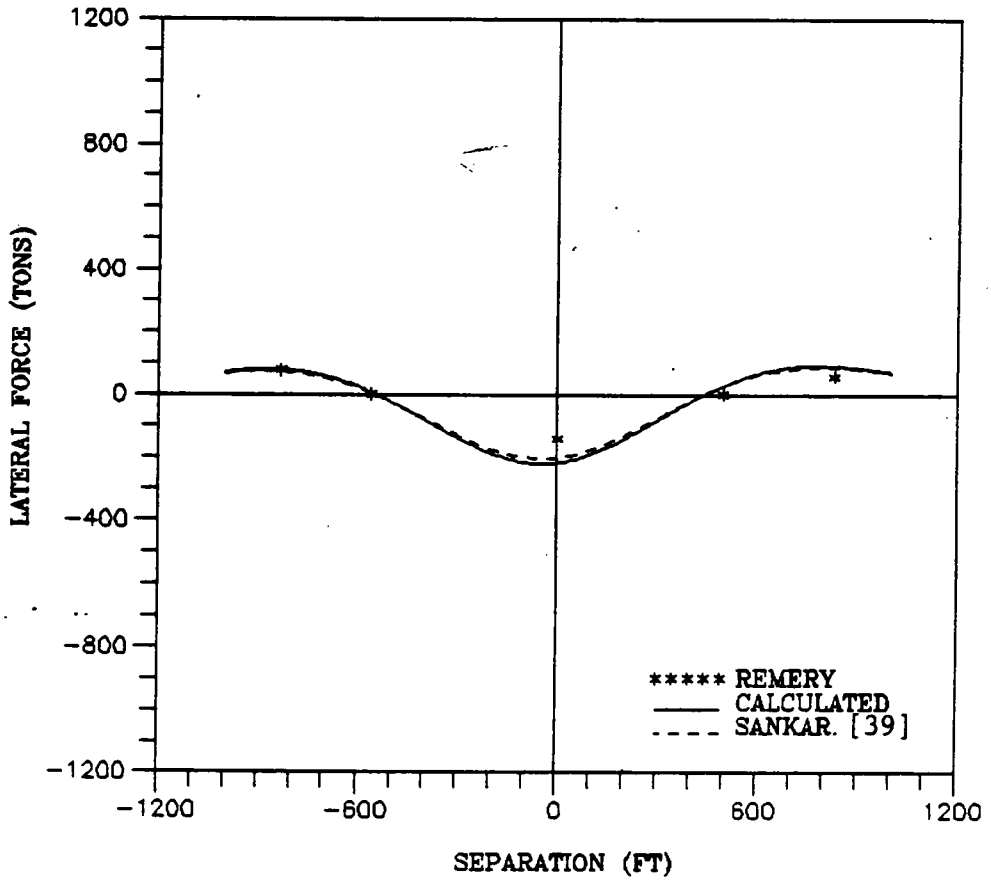

Fig-5(e): Lateral Force - NSMB Case-3

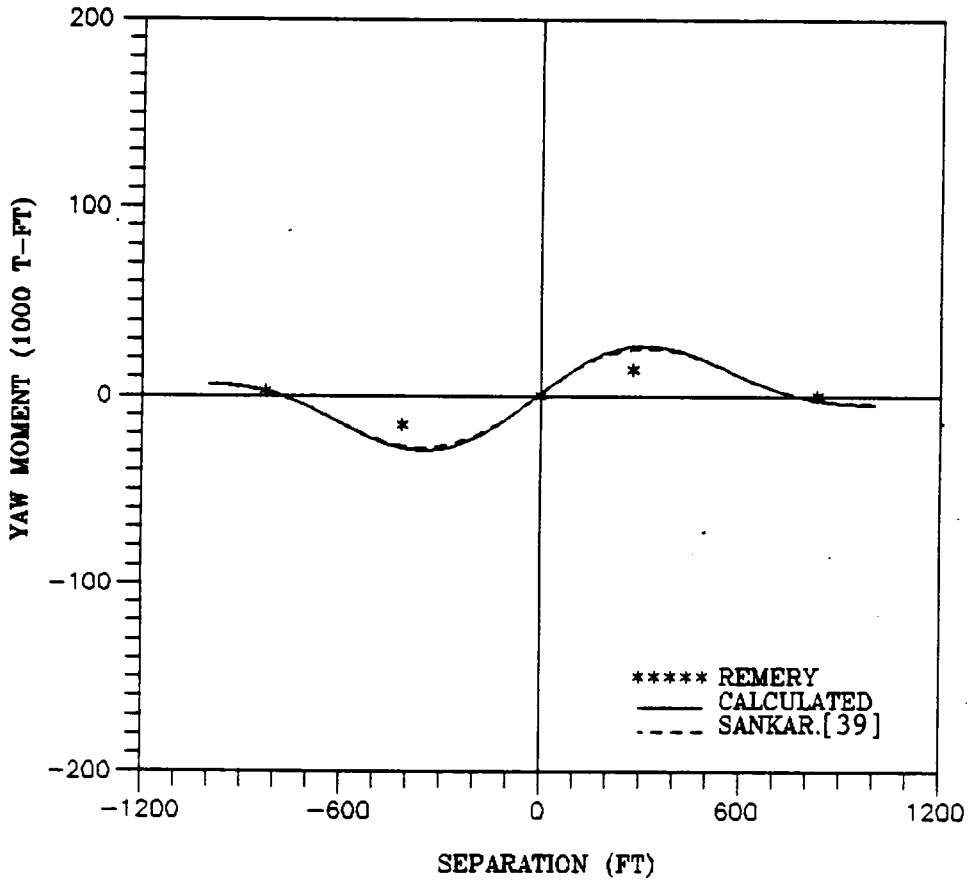

Fig-5(f): Yaw Moment - NSMB Case-3

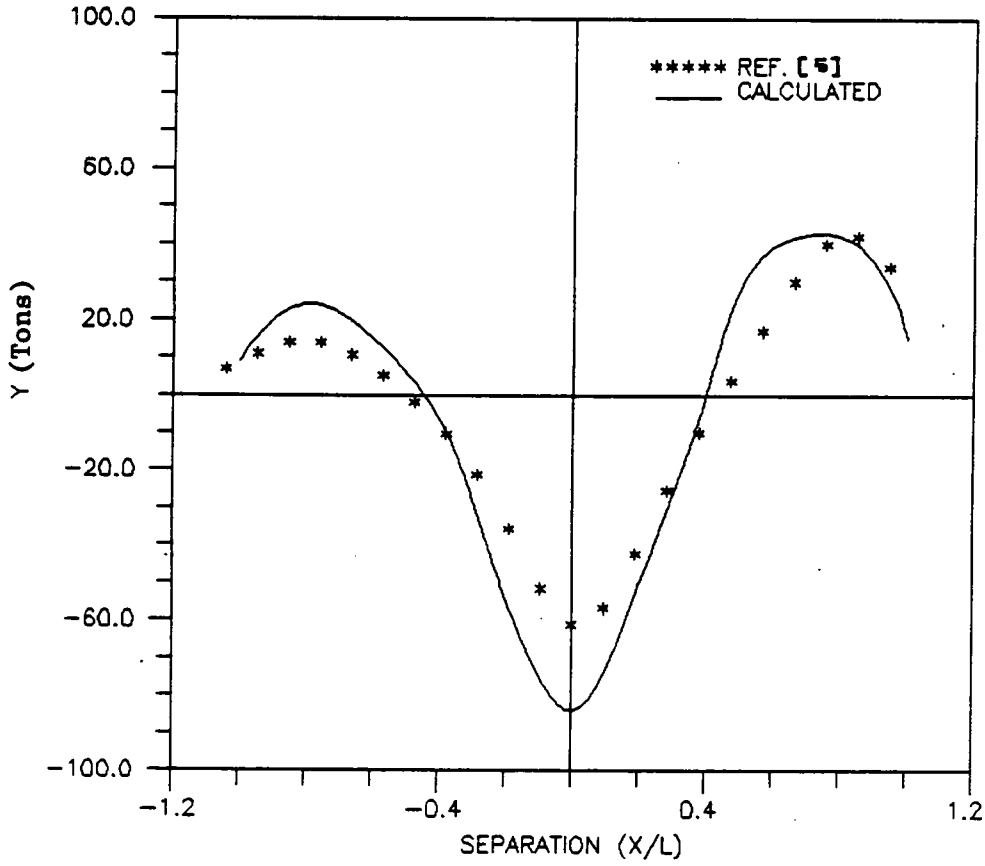

Fig-6(a): Lateral Force - Mariner - 50' Separation

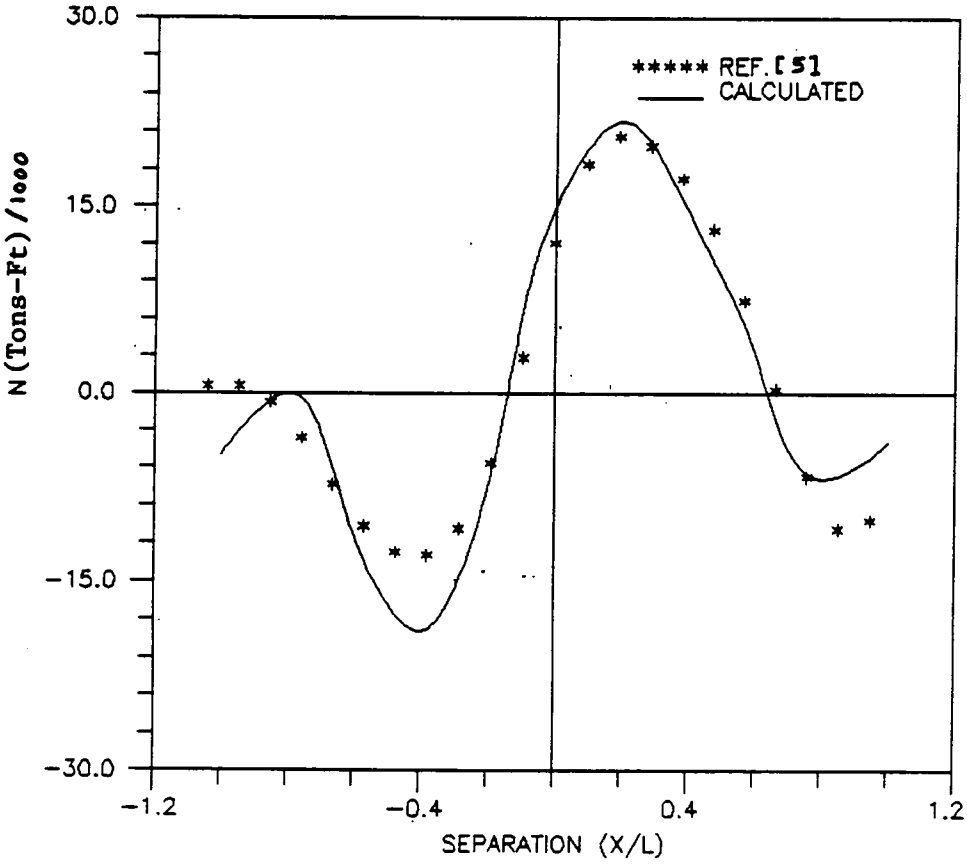

Fig-6(b): Yaw Moment - Mariner - 50' Separation

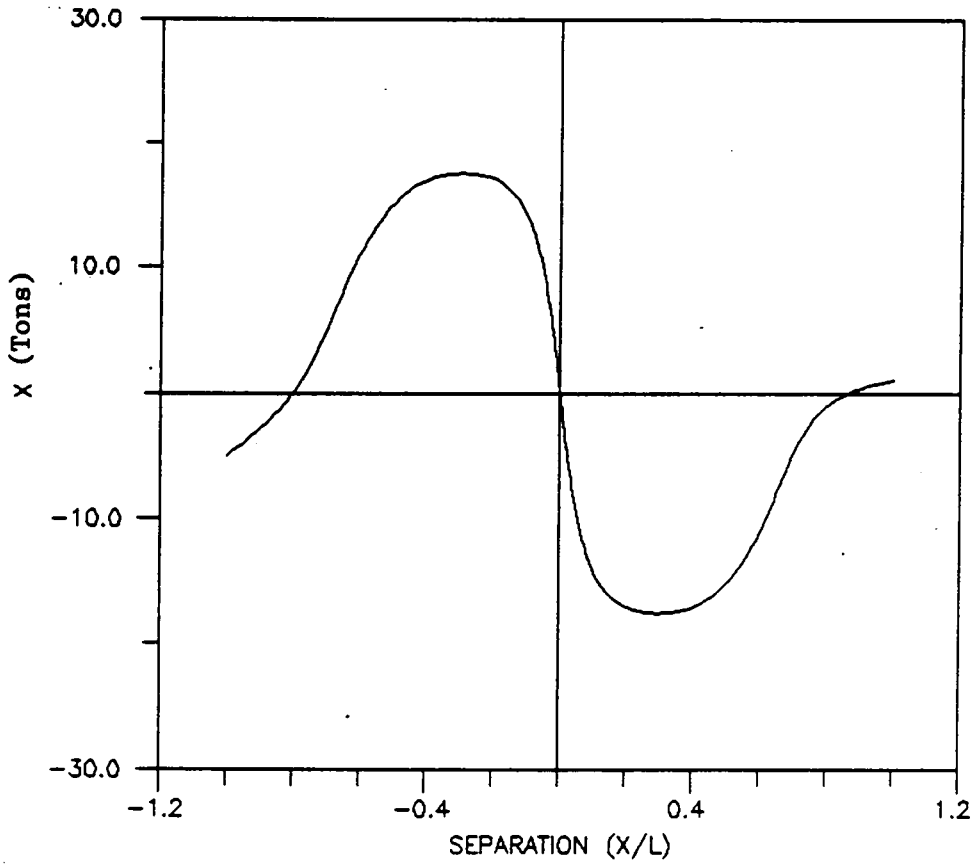

Fig-6(c): Long. Force - Mariner - 50' Separation

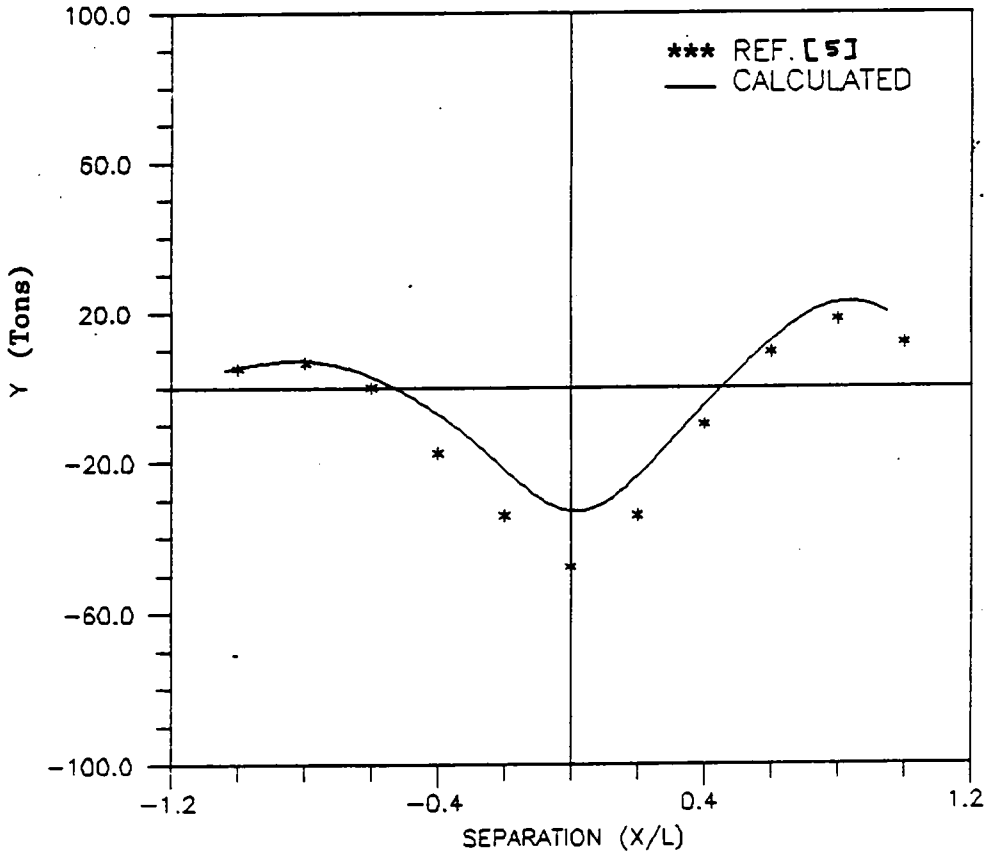

Fig-6(d): Lateral Force - Mariner - 100' Separation

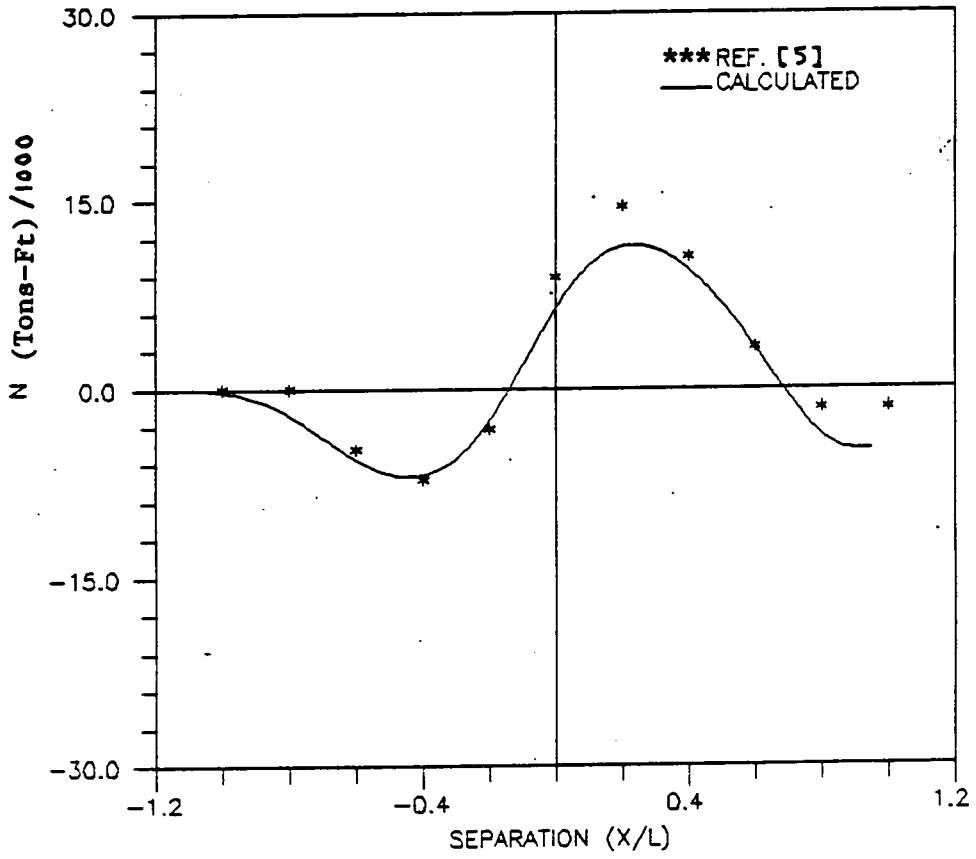

Fig-6(e): Yaw Moment - Mariner - 100' Separation

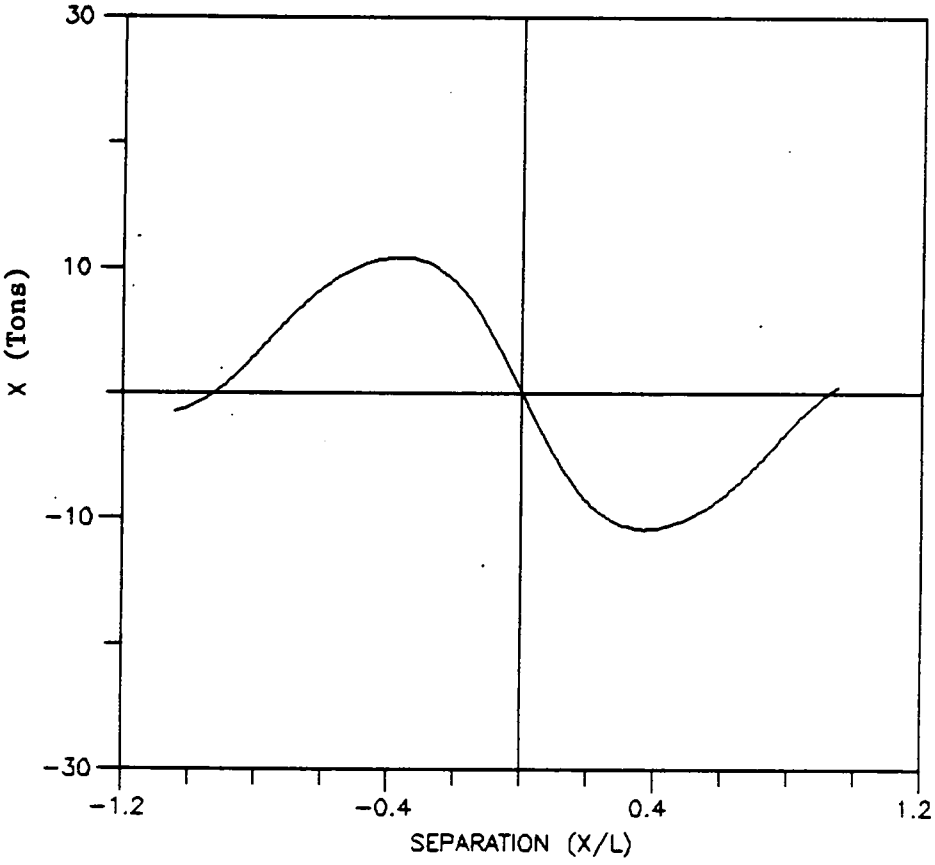

Fig-6(f): Long.Force - Mariner - 100' Separation

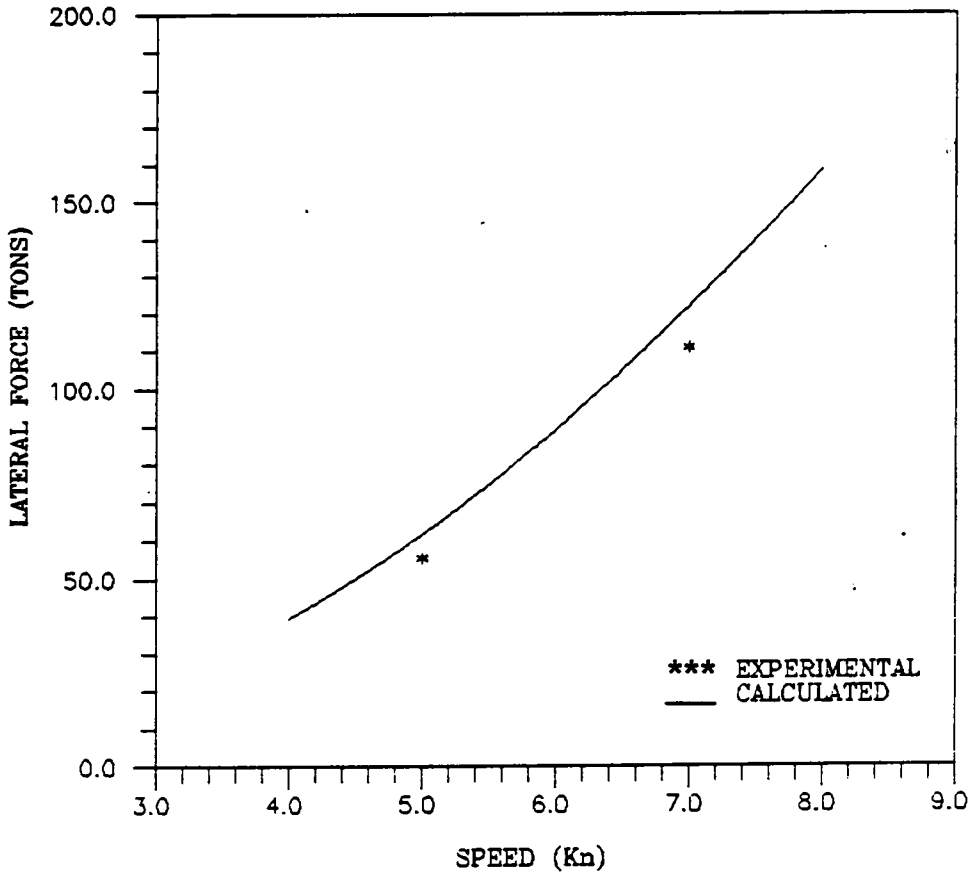

Fig-7(a): Bank Suction Force: SSPA - H/T = 1.15

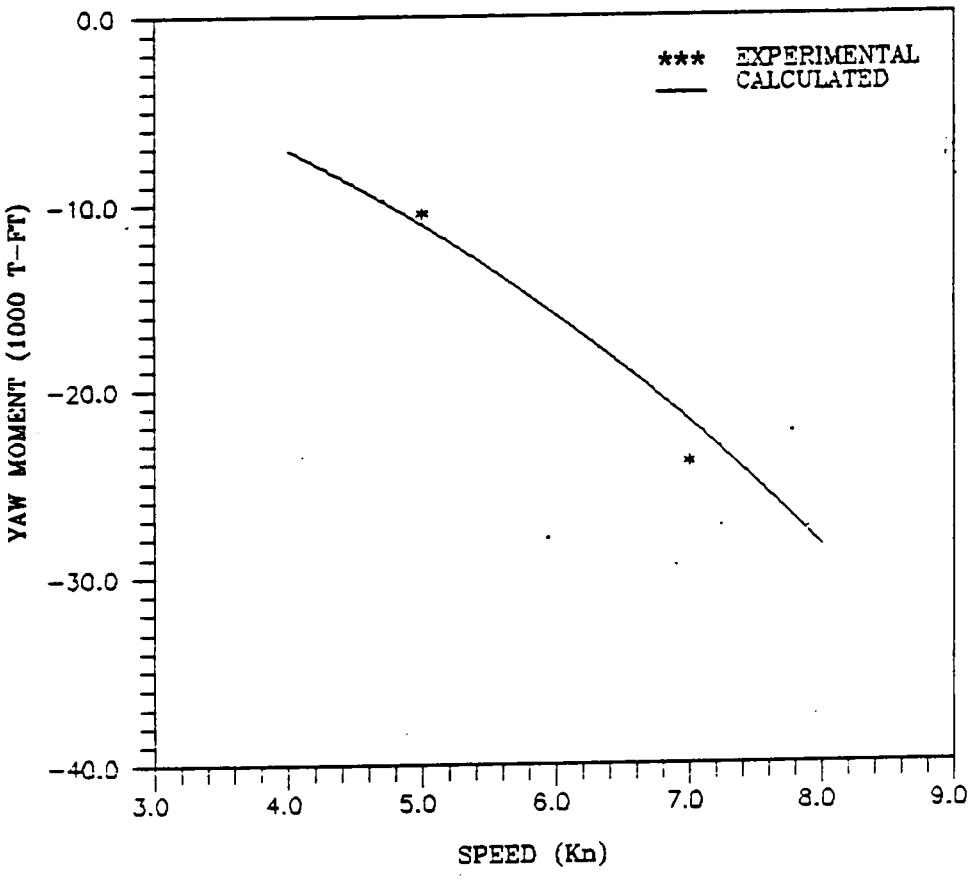

Fig-7(b): Bank Suction Moment: SSPA - H/T = 1.15

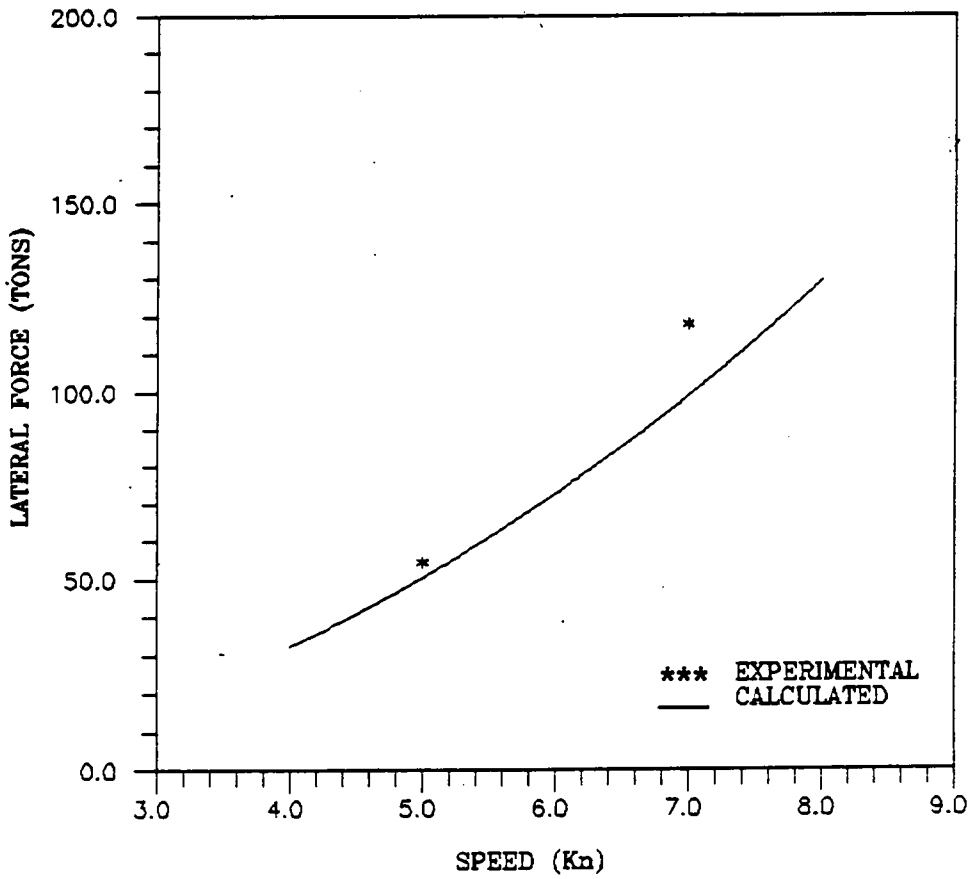

Fig-7(c): Bank Suction Force: SSPA - H/T = 1.25

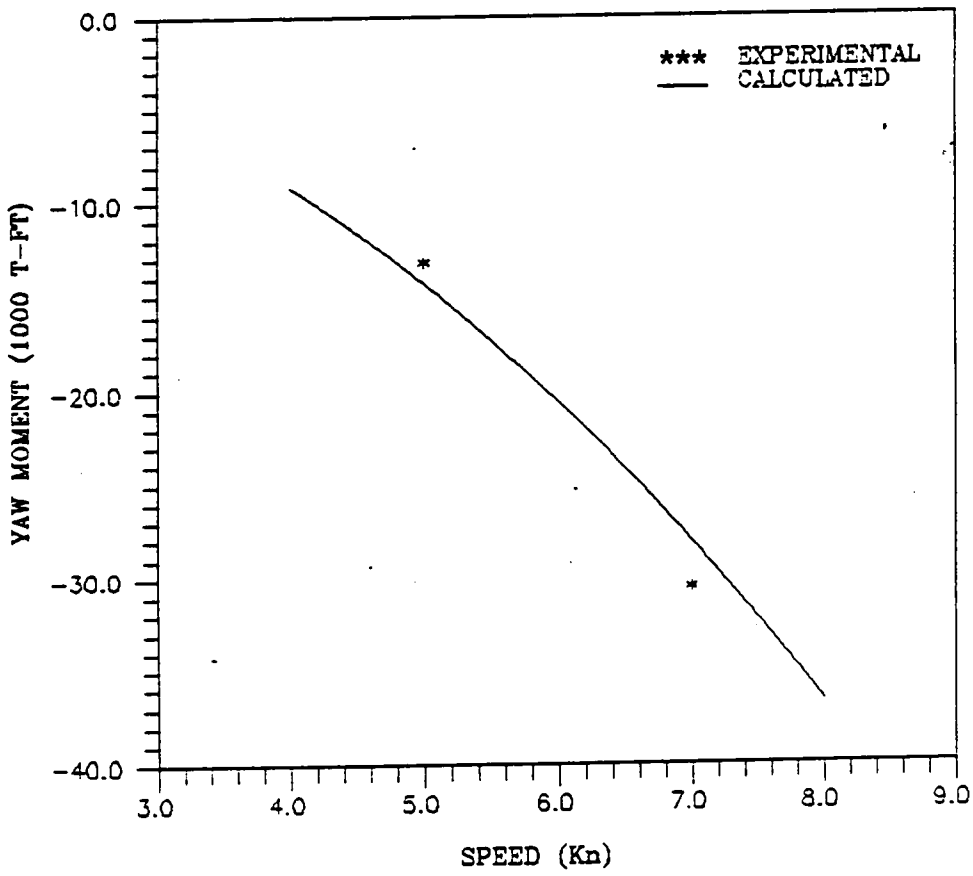

Fig-7(d): Bank Suction Moment: SSPA - H/T = 1.25

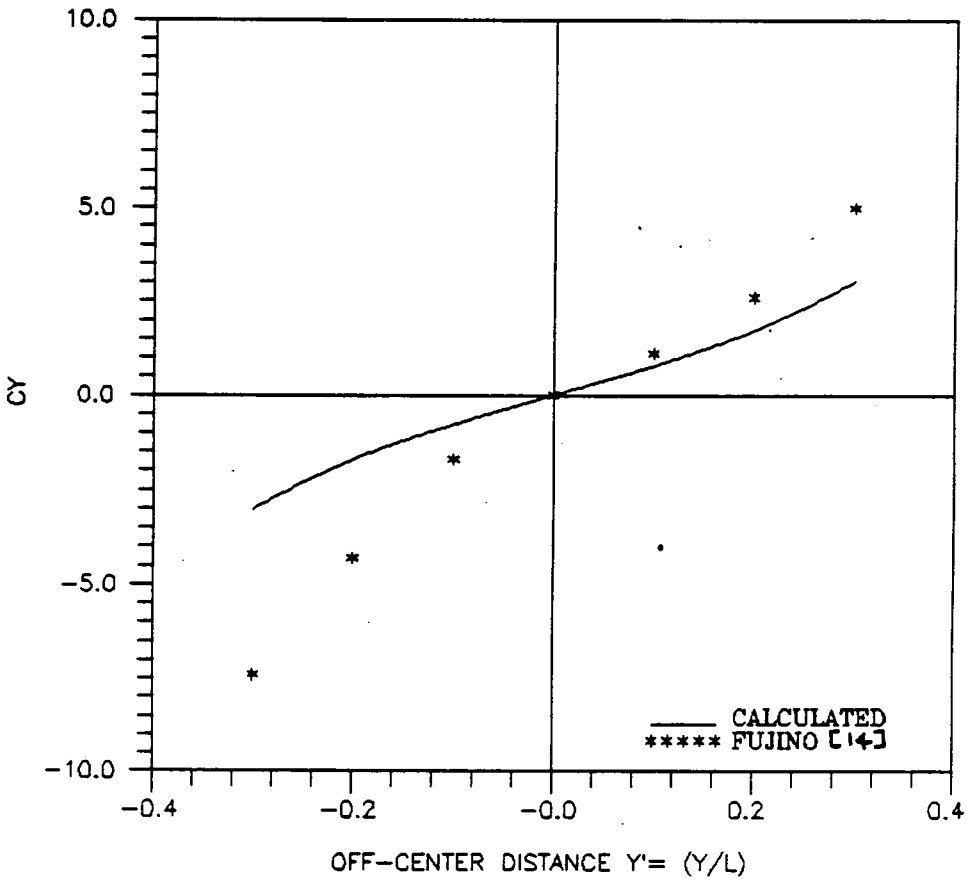

Fig-8(a): Bank Suction Force: Fujino - H/T = 1.3

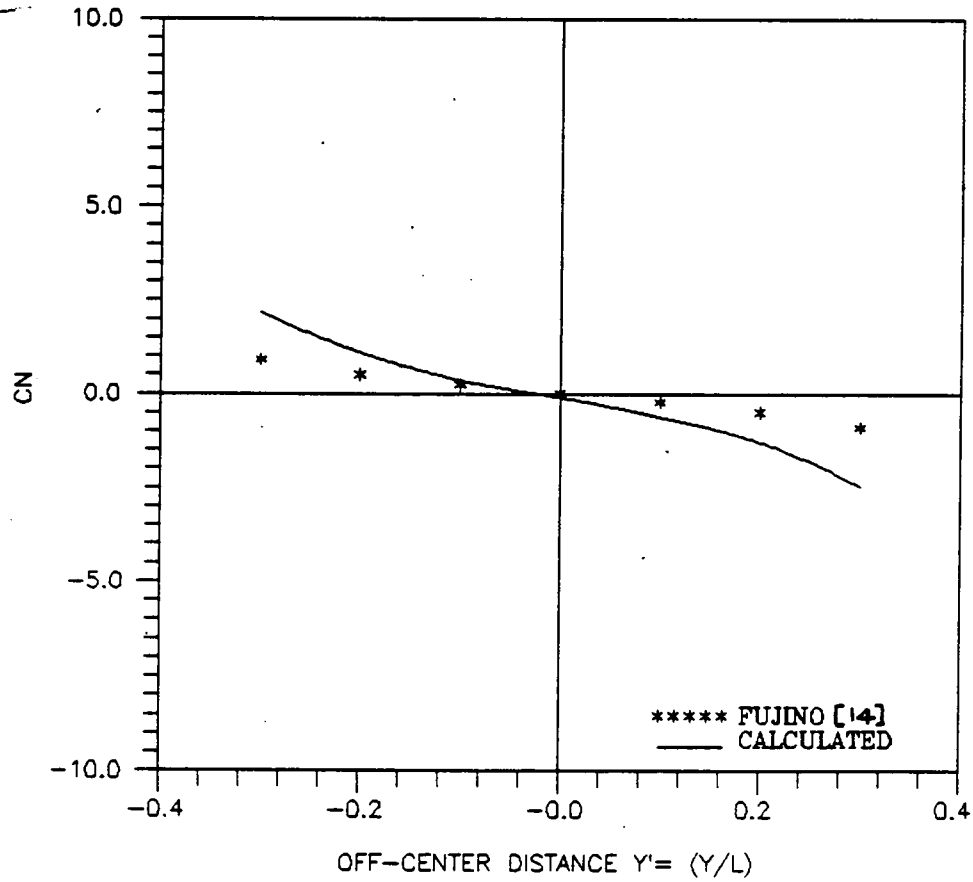

Fig-8(b): Bank Suction Moment: Fujino - H/T = 1.3

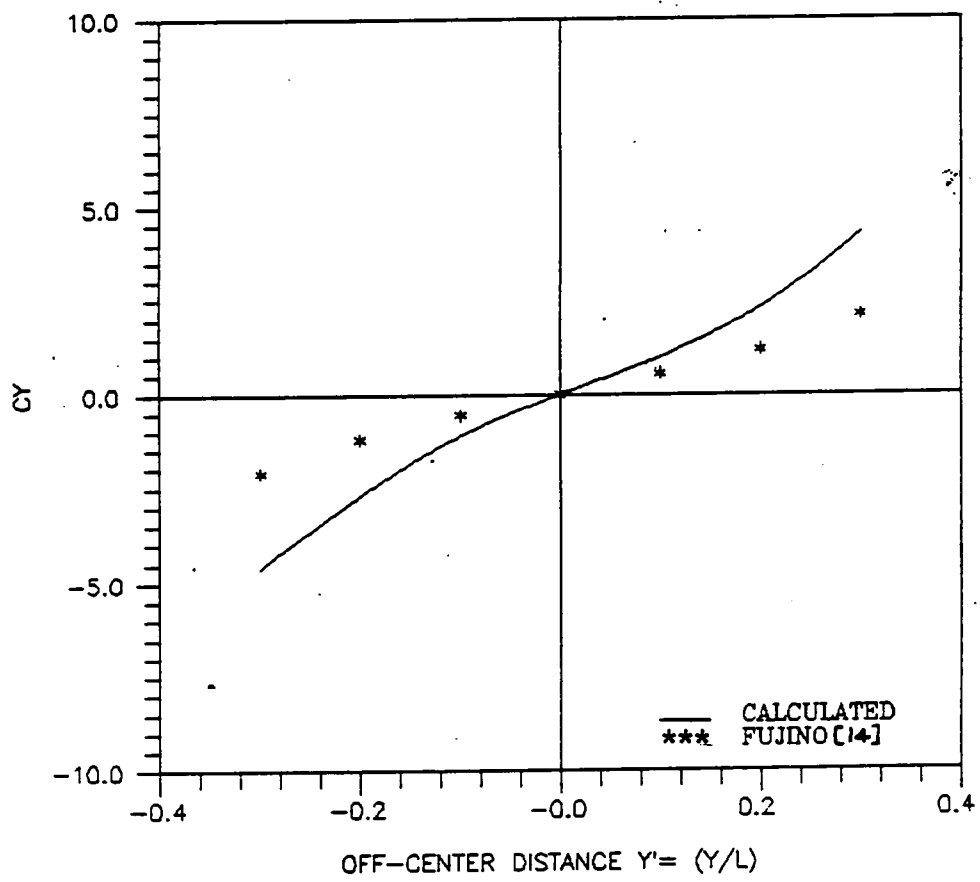

Fig-8(c): Bank Suction Force: Fujino - H/T = 1.5

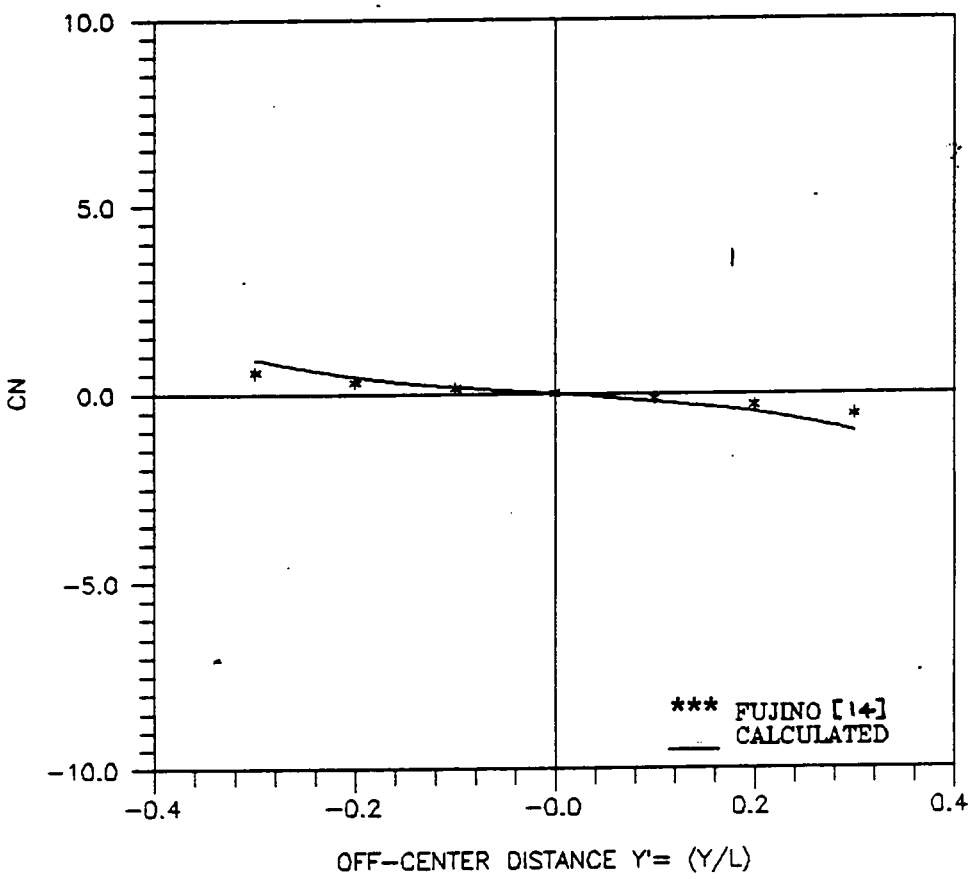

Fig−8(d): Bank Suction Moment: Fujino − H/T = 1.5

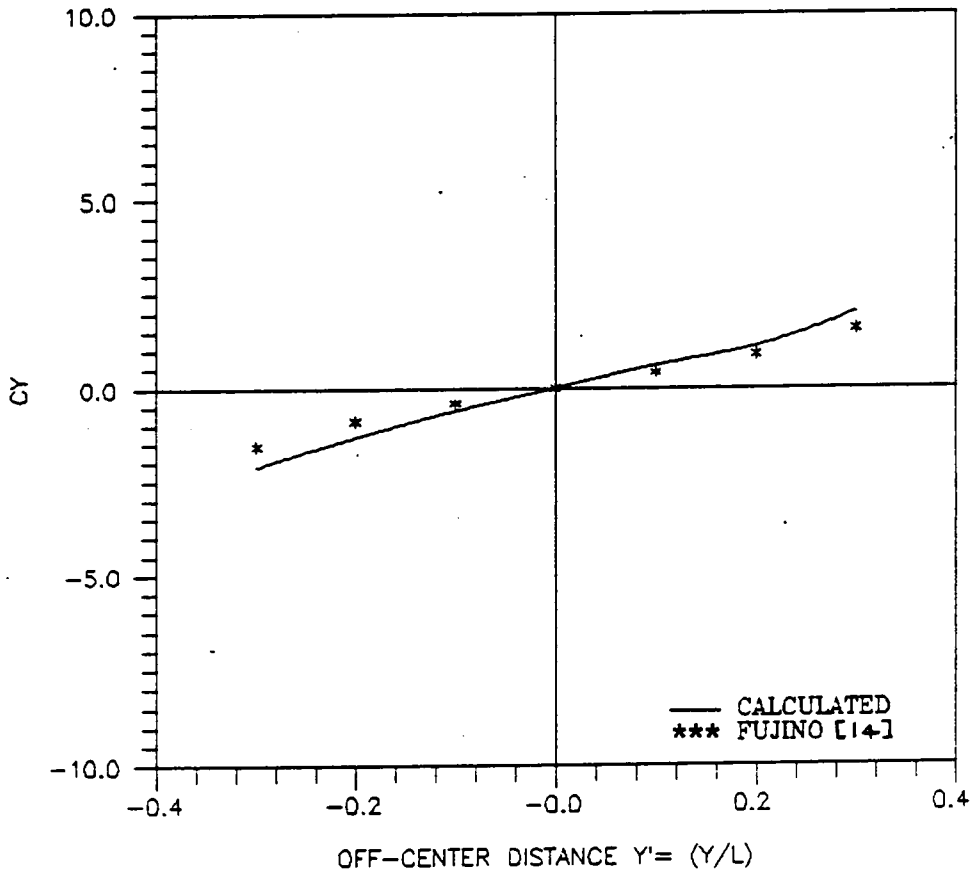

Fig-8(e): Bank Suction Force: Fujino - H/T = 1.9

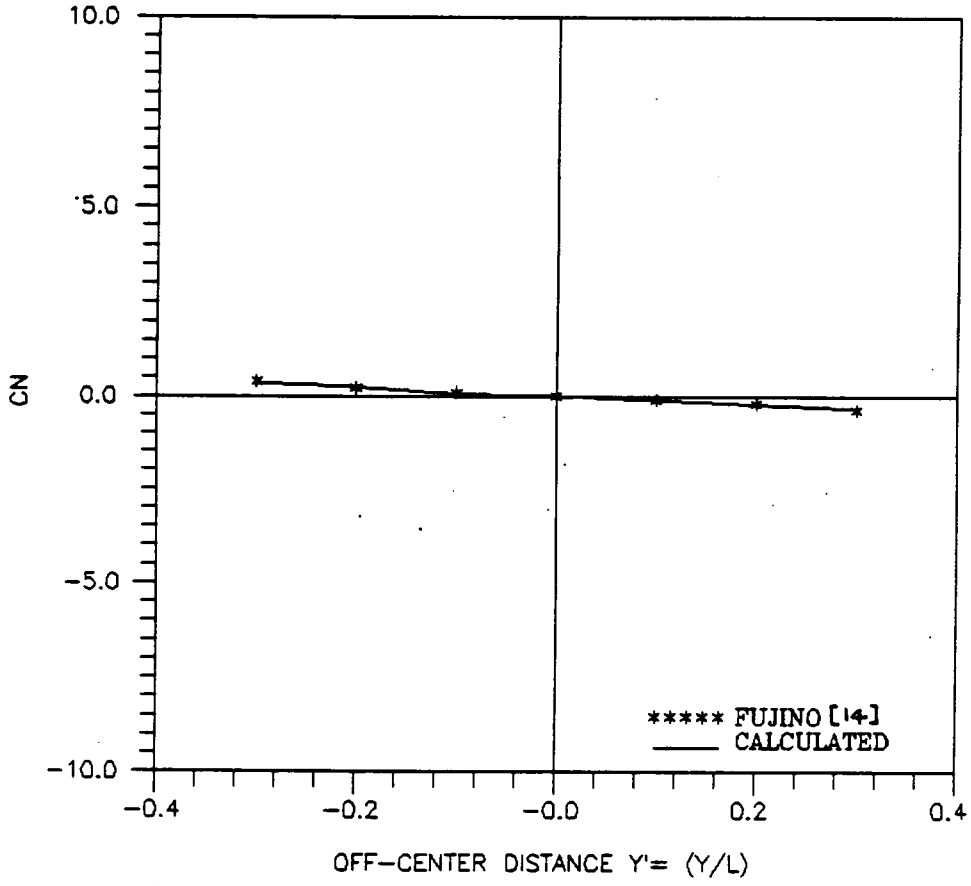

Fig-8(f): Bank Suction Moment: Fujino - H/T = 1.9

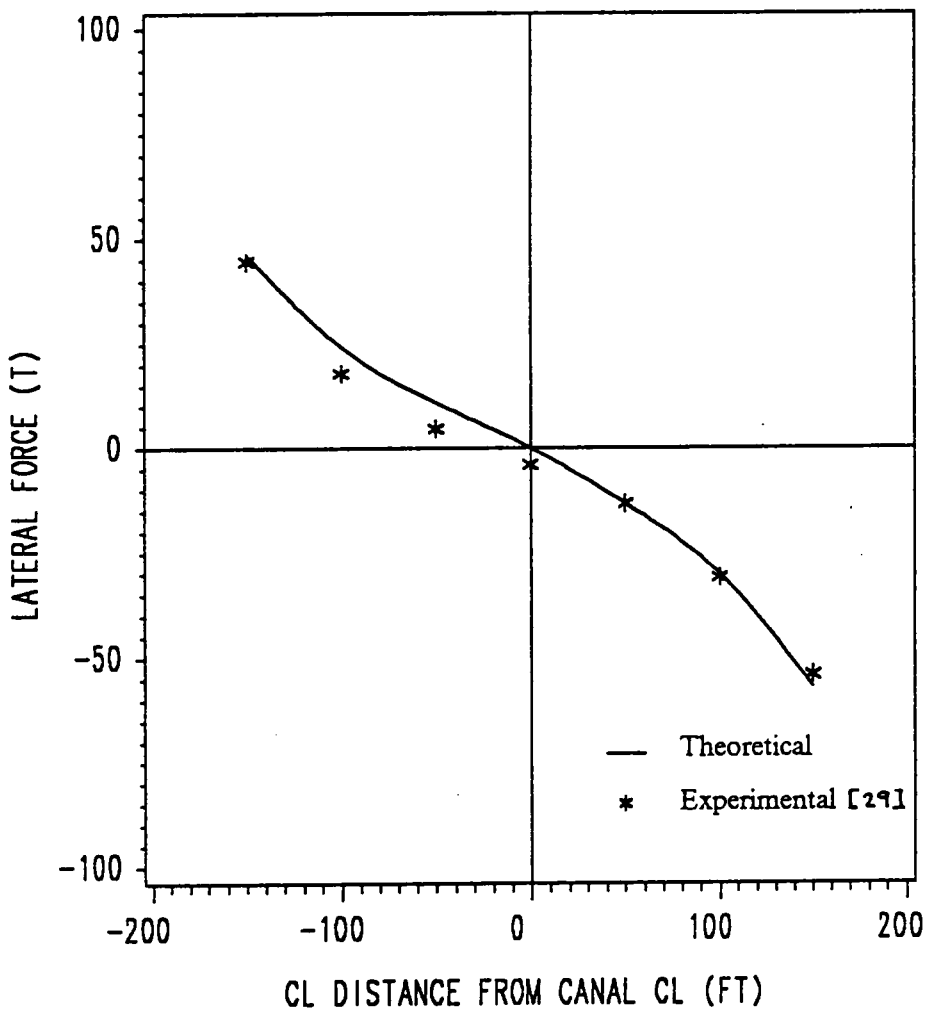

Fig.9(a): Bank Suction Forces
Comparison with Moody's Data

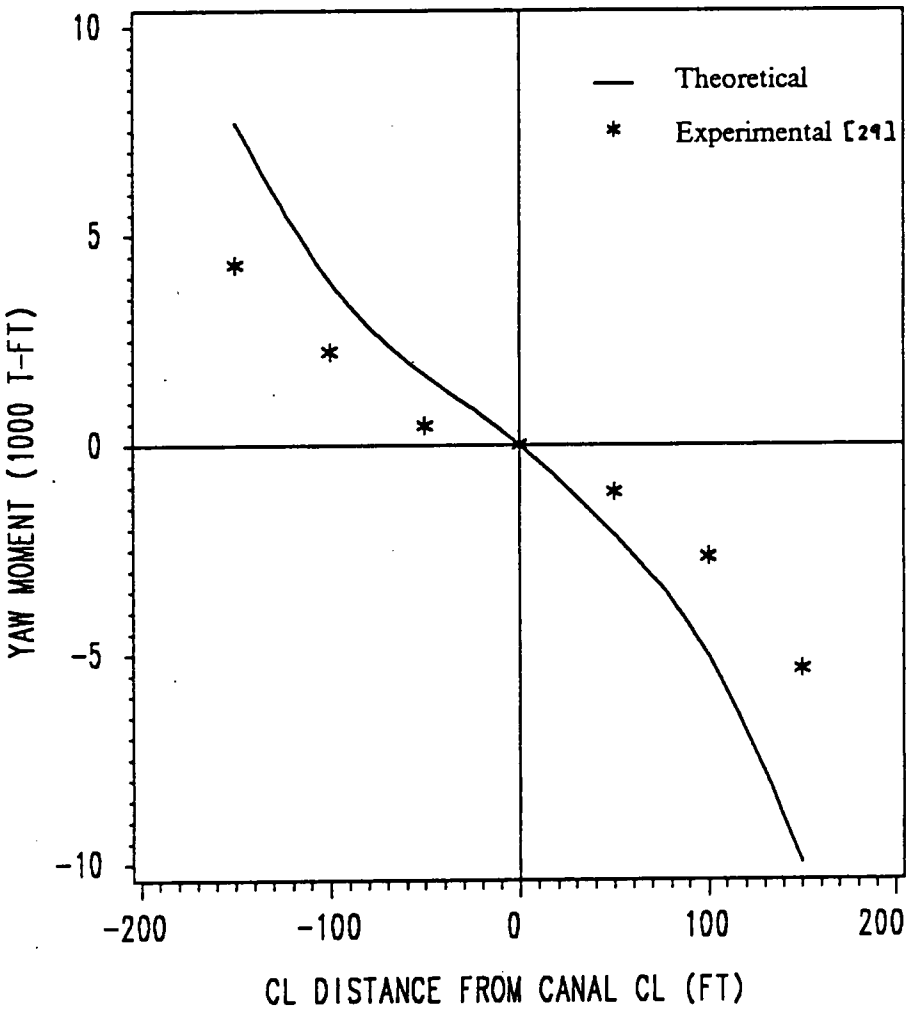

Fig.9(b): Bank Suction Moments
Comparison with Moody's Data

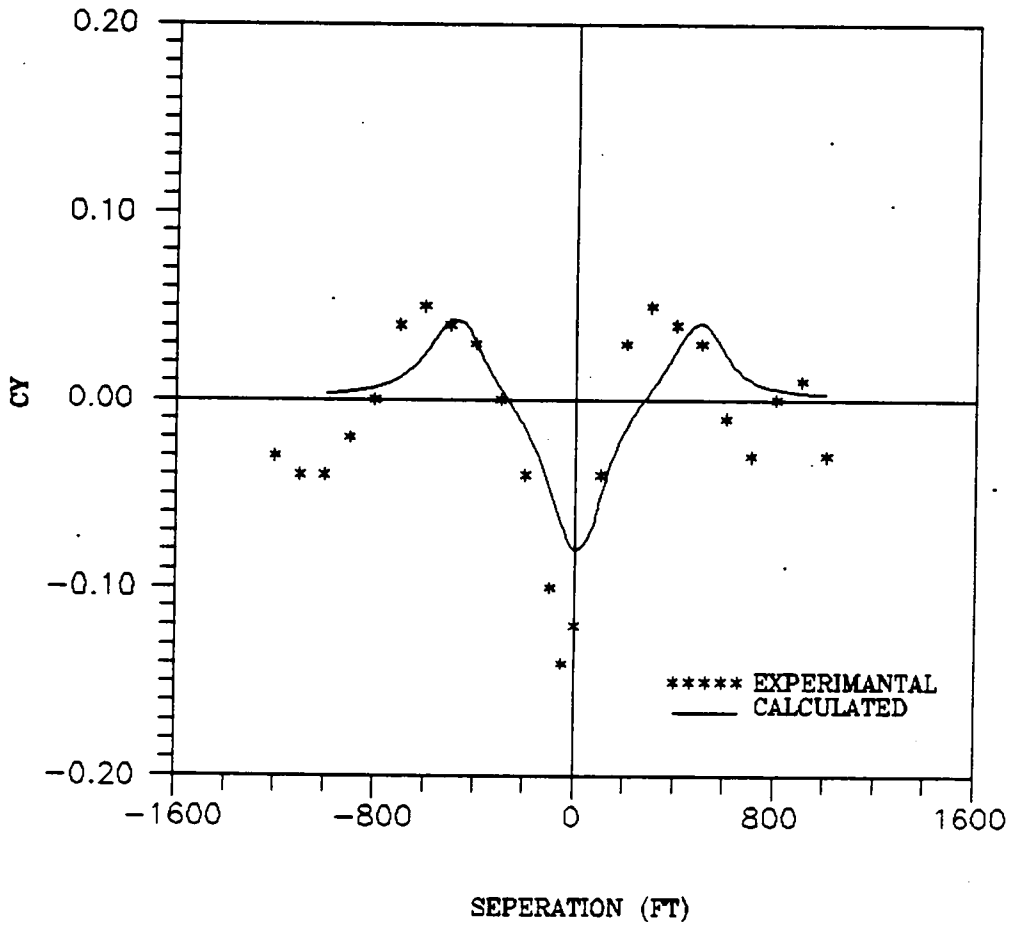

Fig-10(a): Lateral Force - Barge-Tows - VBD Case-1

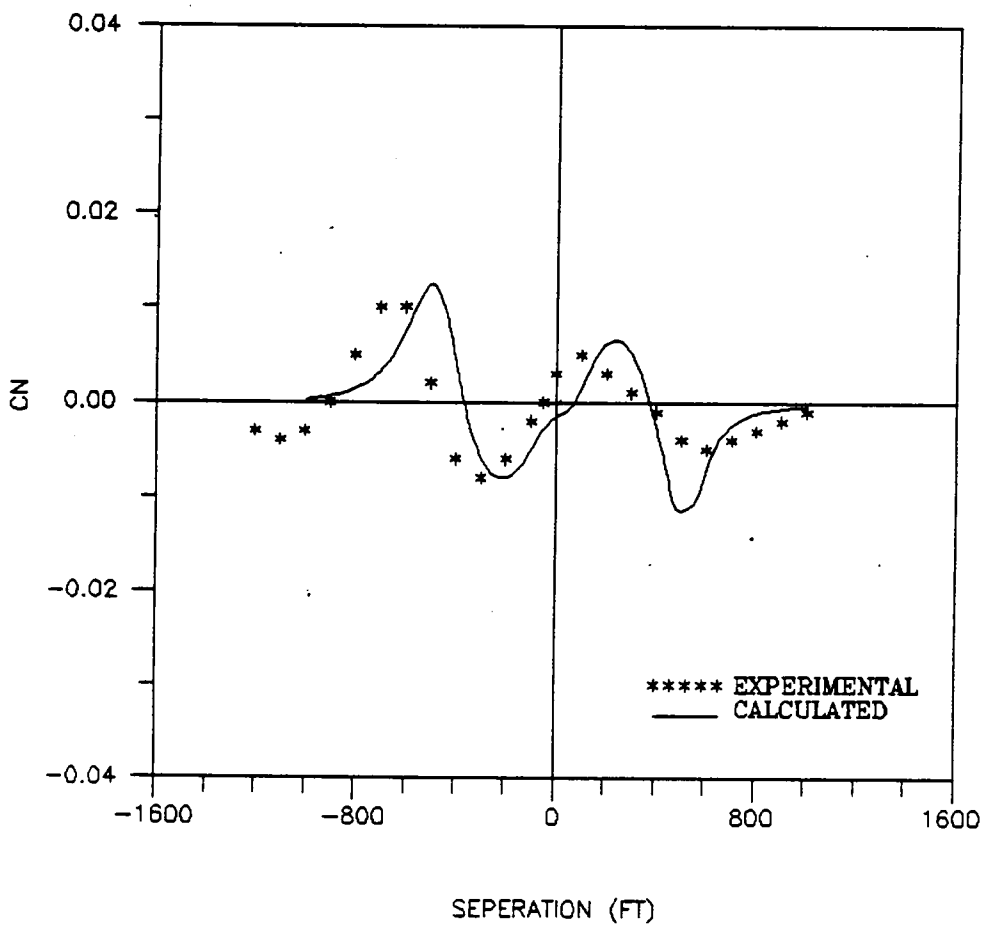

Fig-10(b): Yaw Moment - Barge-Tows - VBD Case-1

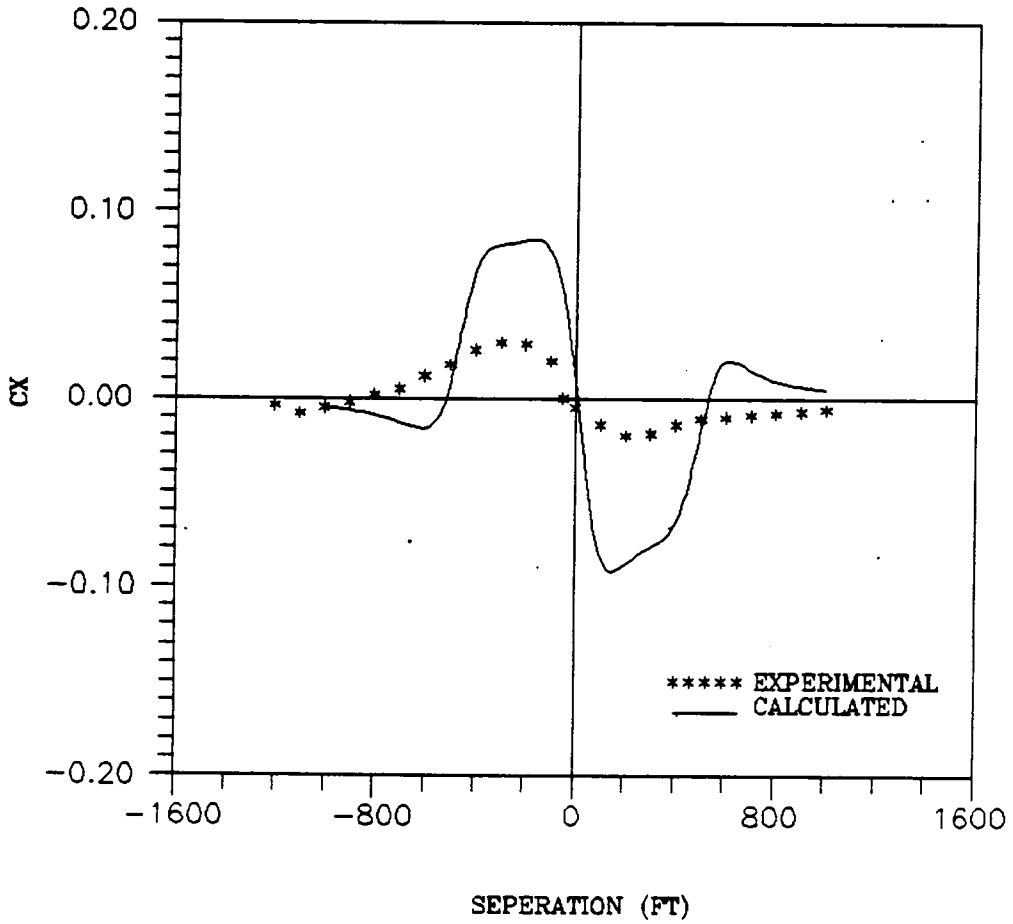

Fig−10(c): Long. Force − Barge−Tows − VBD Case−1

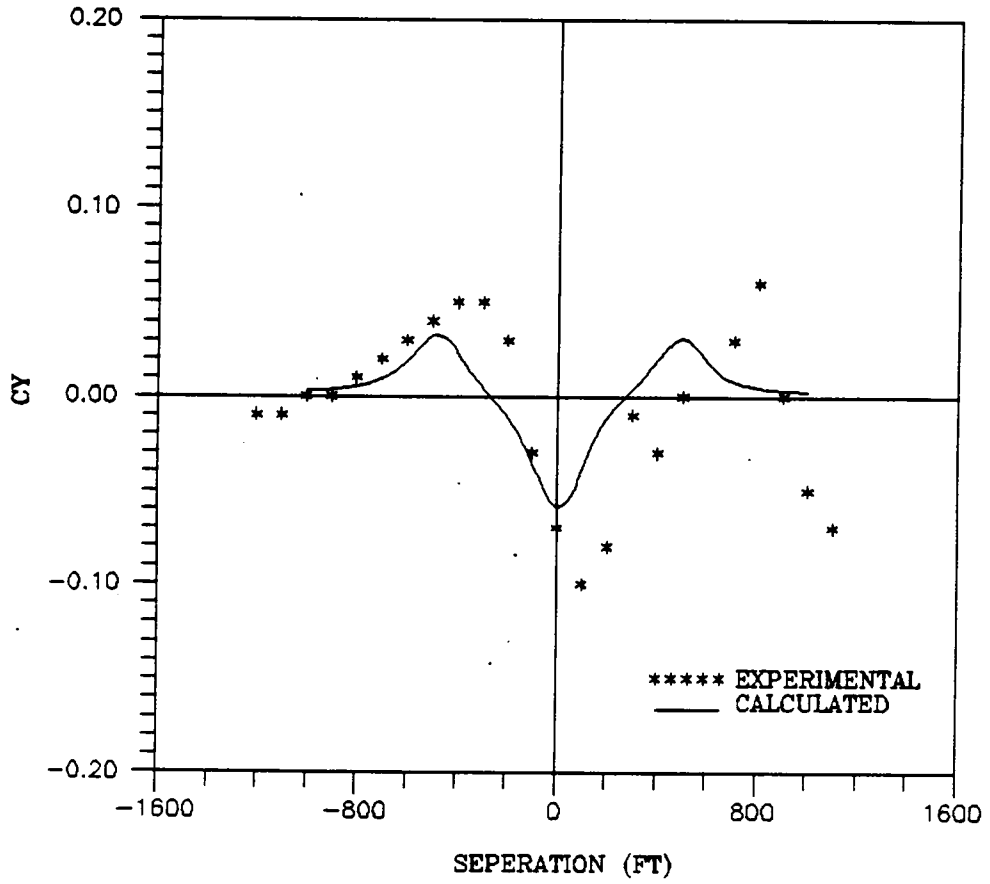

Fig-10(d): Lateral Force - Barge-Tows - VBD Case-2

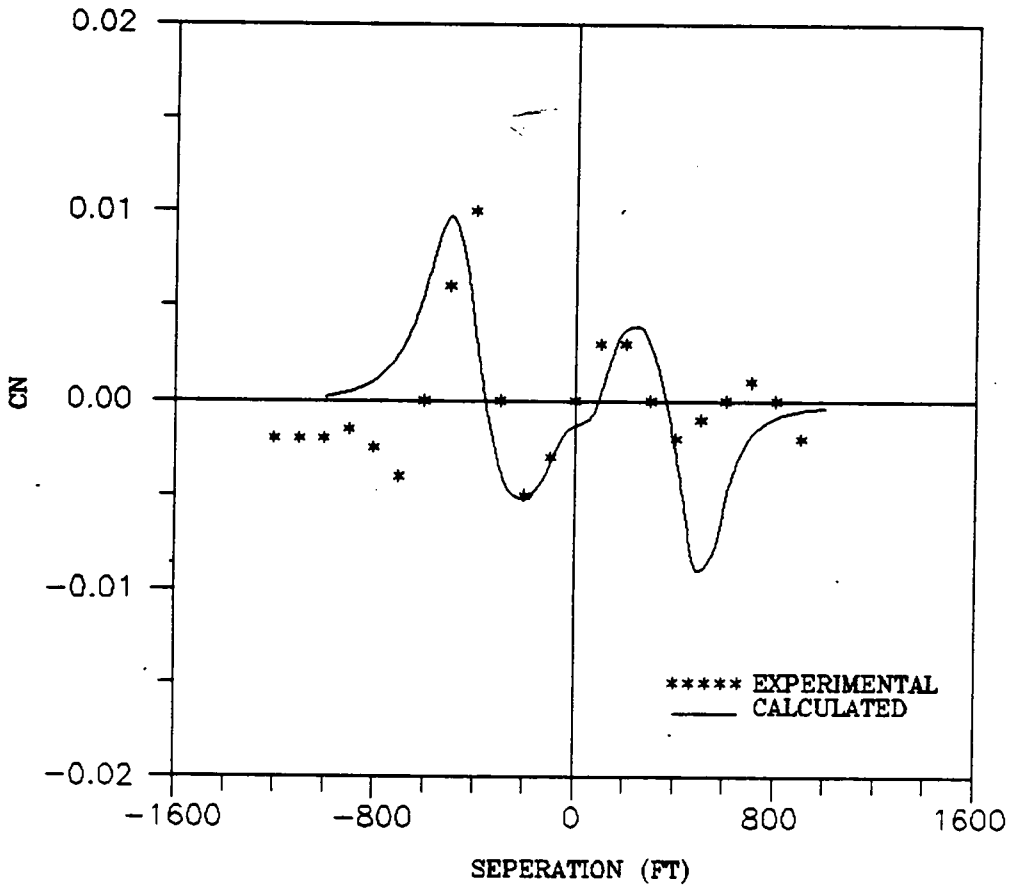

Fig-10(e): Yaw Moment - Barge-Tows - VBD Case-2

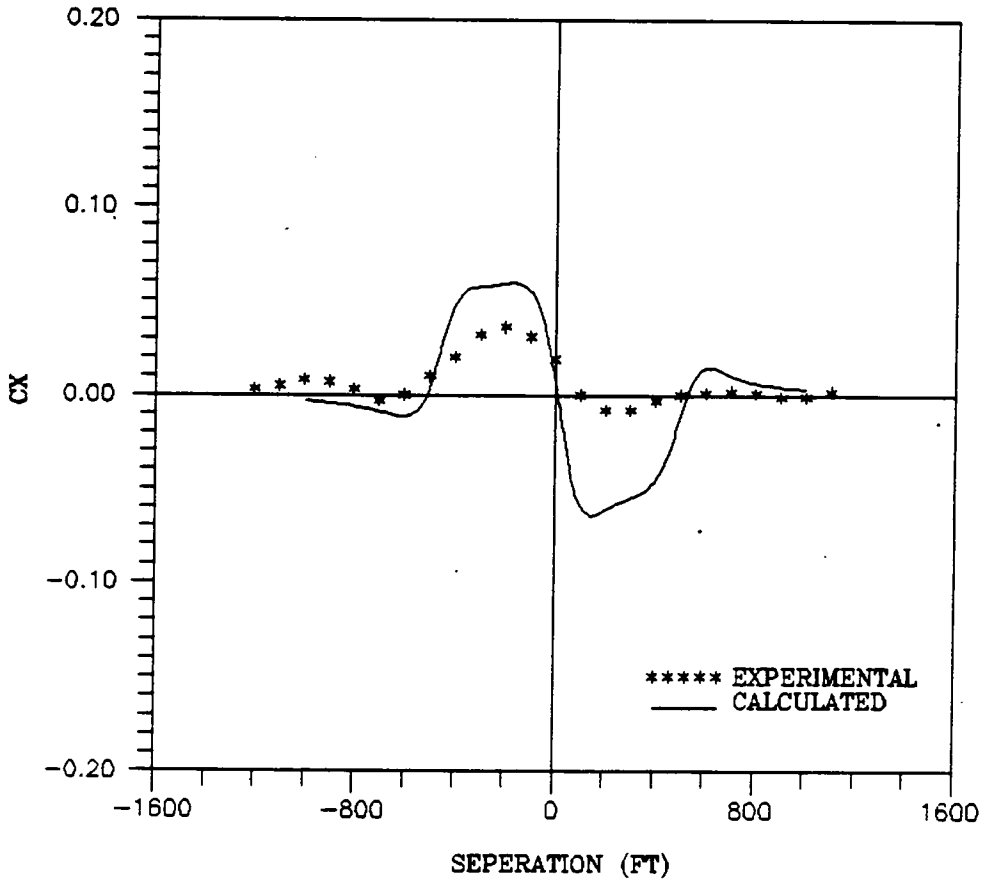

Fig-10(f): Long. Force - Barge-Tows - VBD Case-2

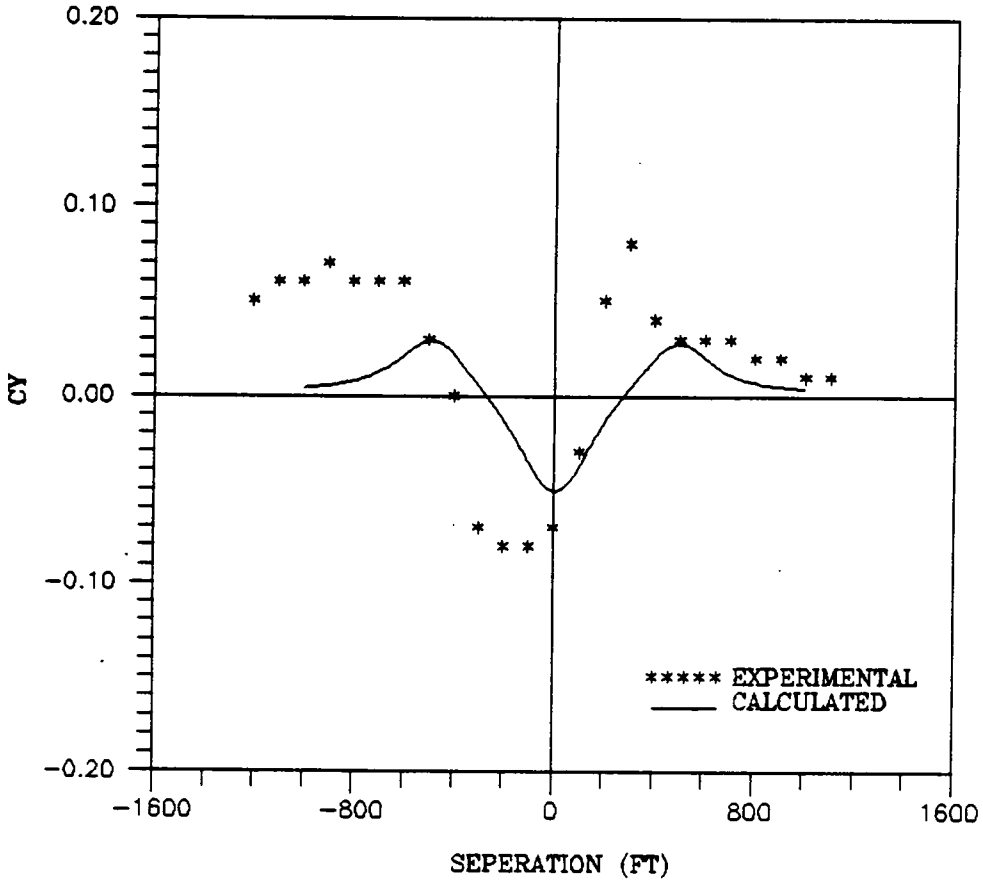

Fig-10(g): Lateral Force - Barge-Tows - VBD Case-3

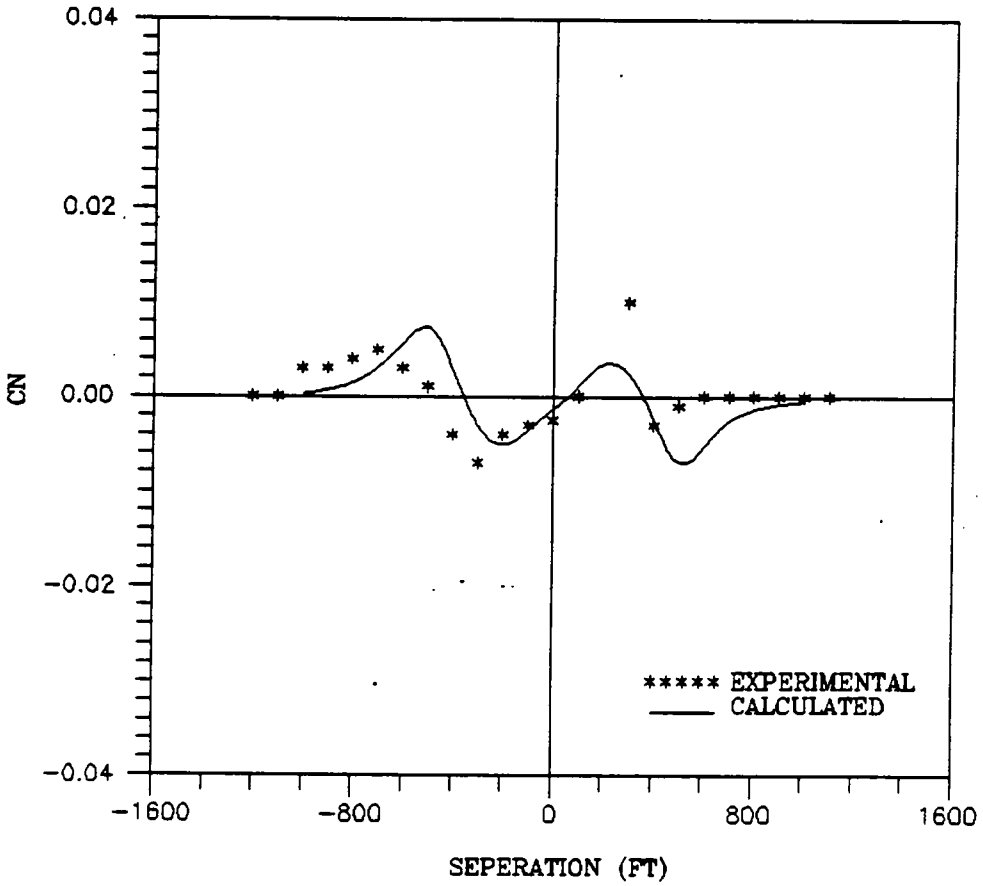

Fig-10(h): Yaw Moment - Barge-Tows - VBD Case-3

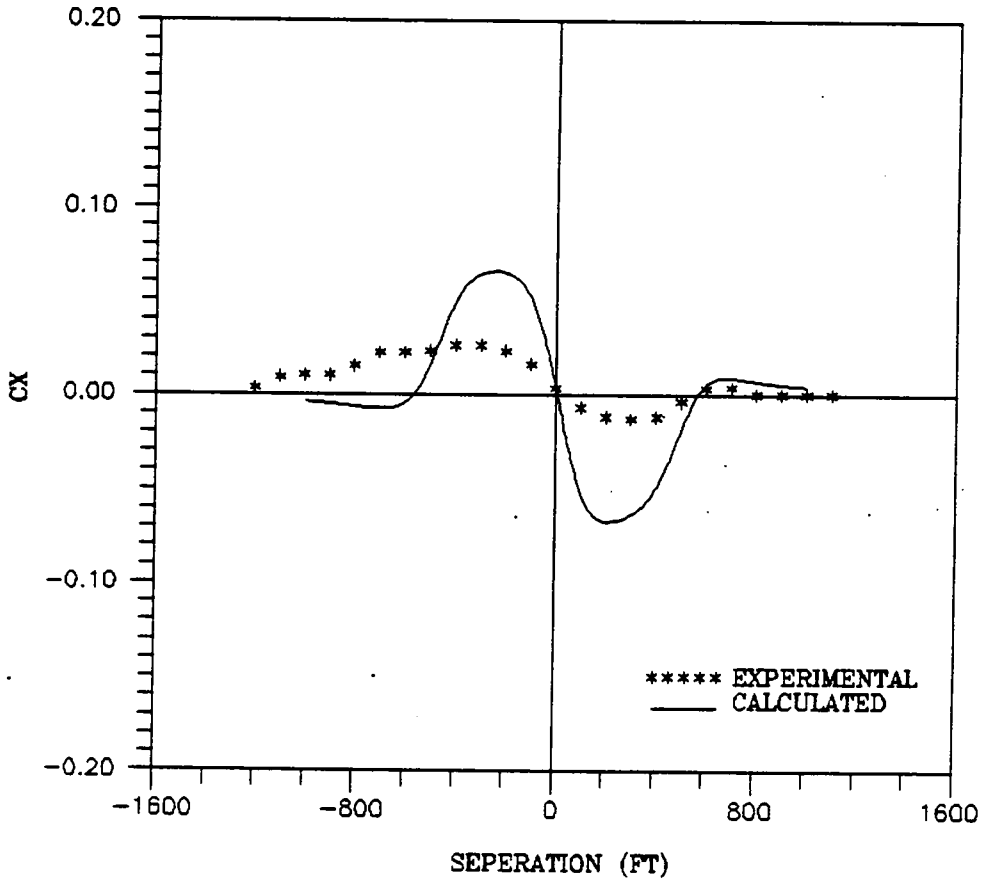

Fig-10(i): Long. Force - Barge-Tows - VBD Case-3

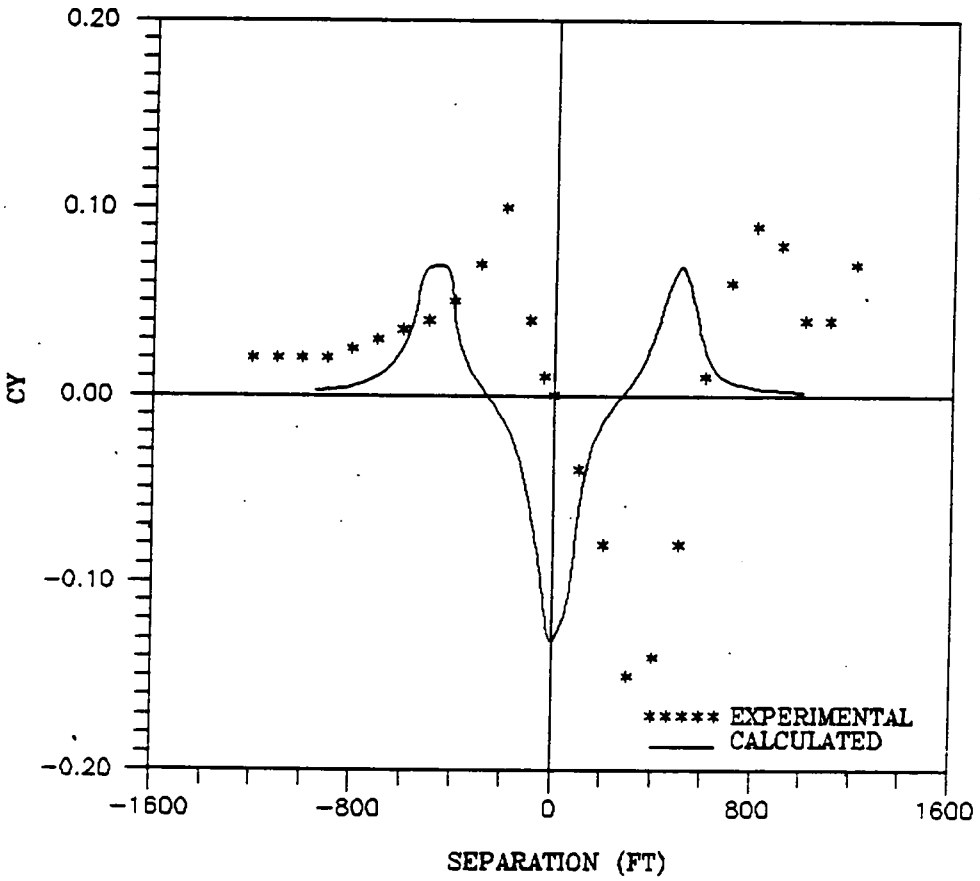

Fig-10(j): Lateral Force - Barge-Tows - VBD Case-4

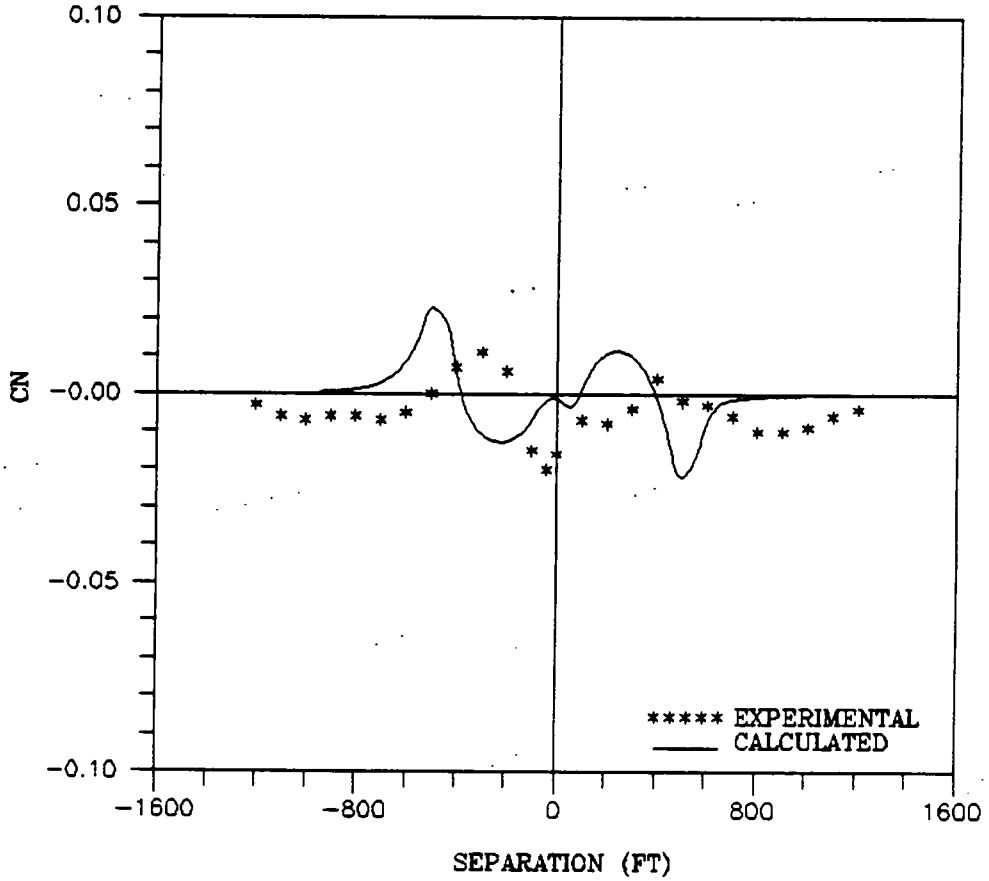

Fig-10(k): Yaw Moment - Barge-Tows - VBD Case-4

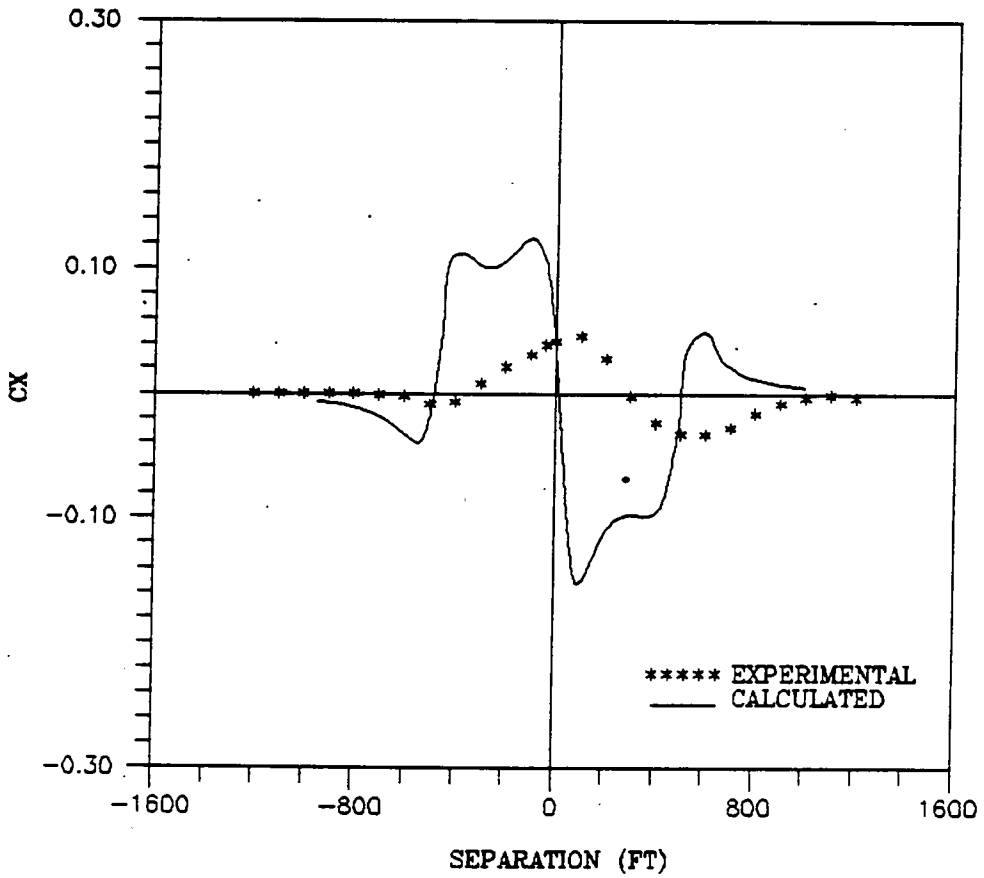

Fig-10(ℓ): Long. Force - Barge-Tows - VBD Case-4

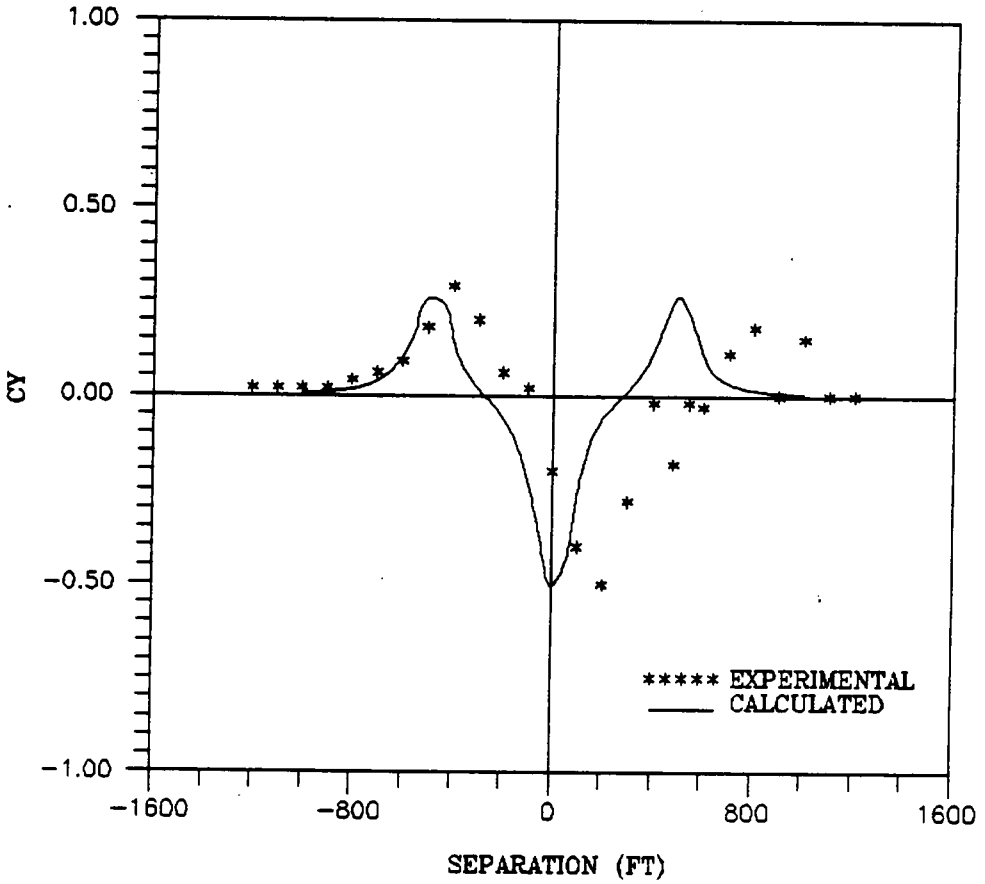

Fig-10(m): Lateral Force - Barge-Tows - VBD Case-5

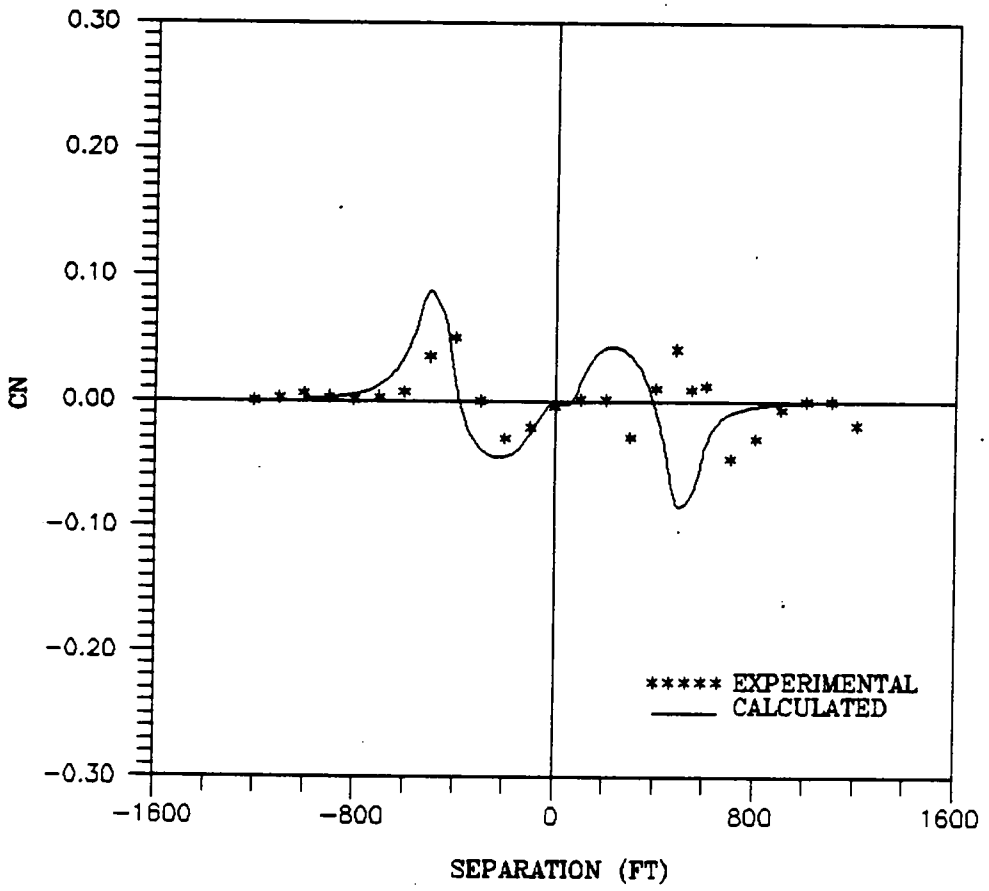

Fig−10(n): Yaw Moment − Barge−Tows − VBD Case−5

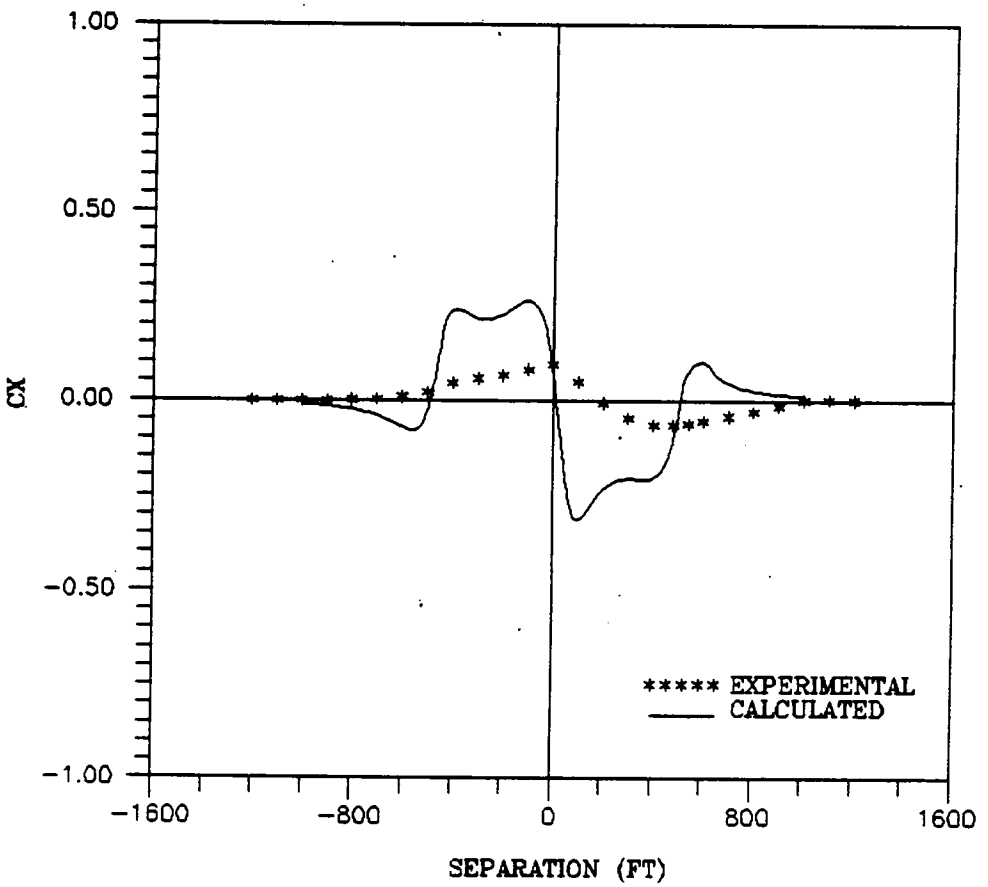

Fig-10(o): Long. Force - Barge-Tows - VBD Case-5

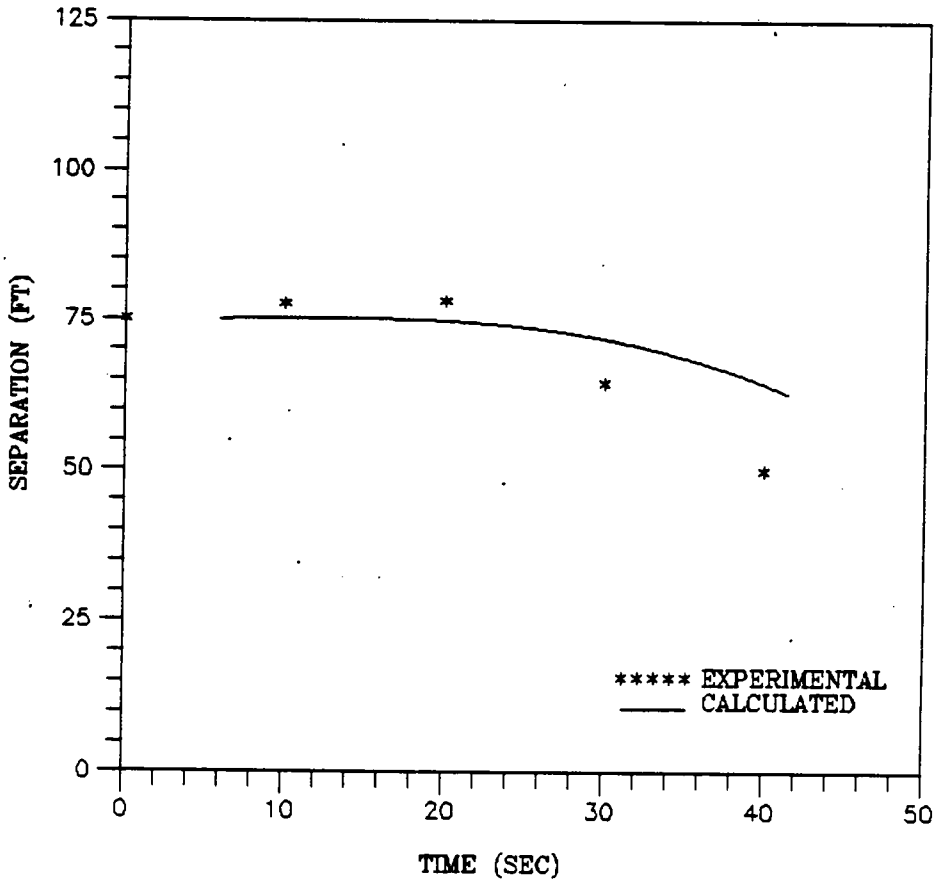

Fig-11(a): Lateral Position - UNREP Simulation - 1

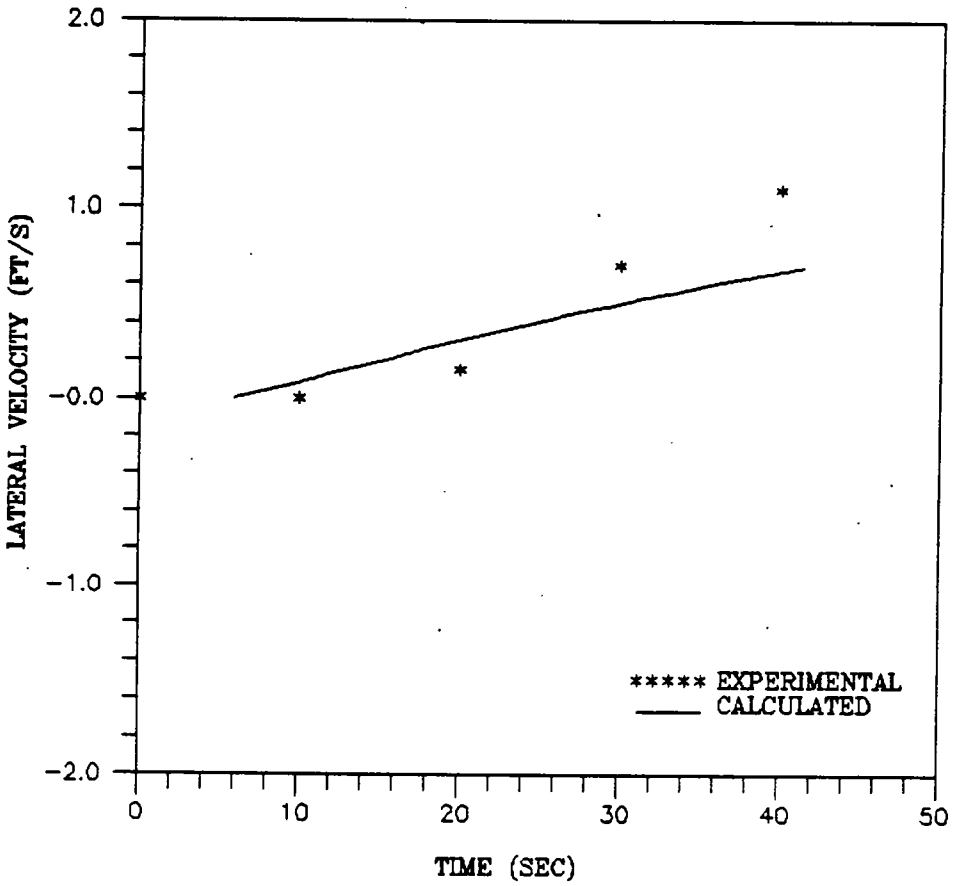

Fig-11(b): Lateral Velocity - UNREP Simulation - 1

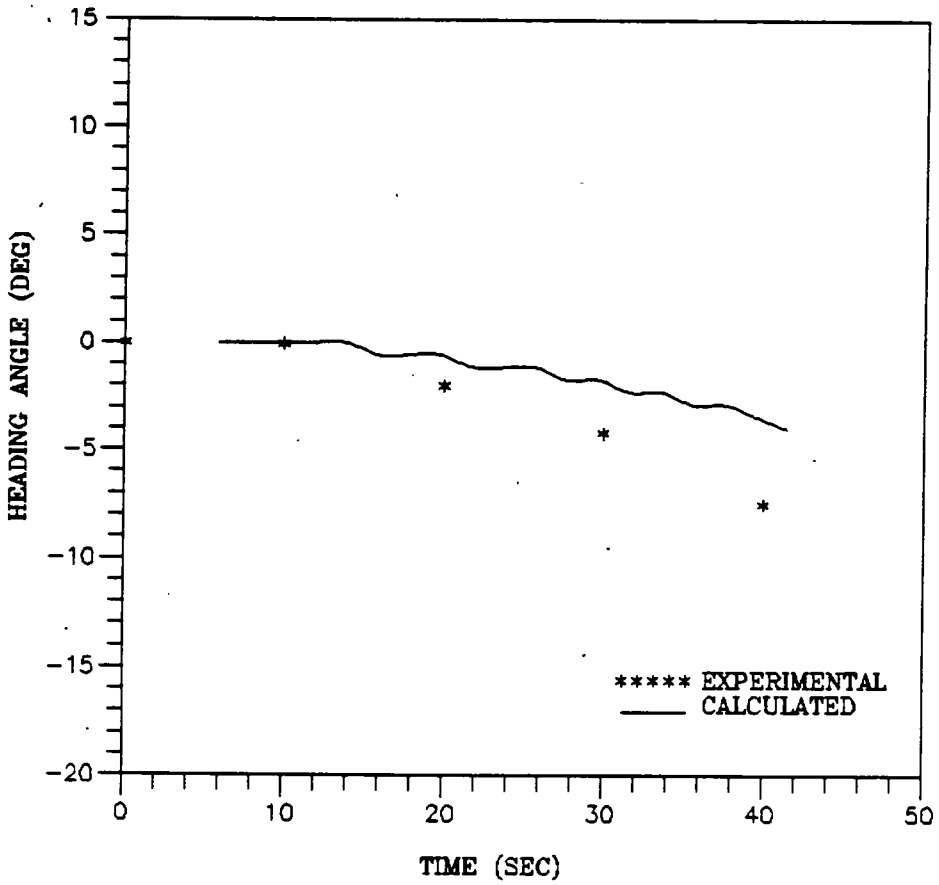

Fig-11(c): Heading Angle - UNREP Simulation - 1

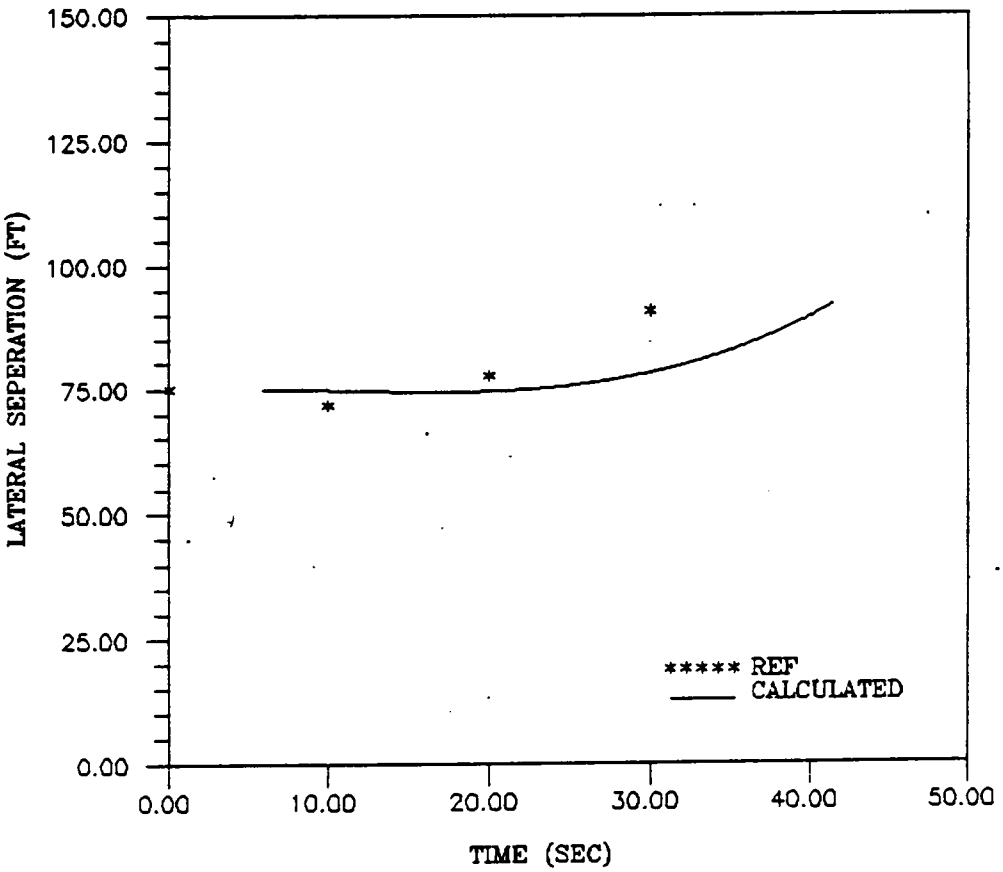

Fig-11(d): Lateral Position - UNREP Simulation - 2

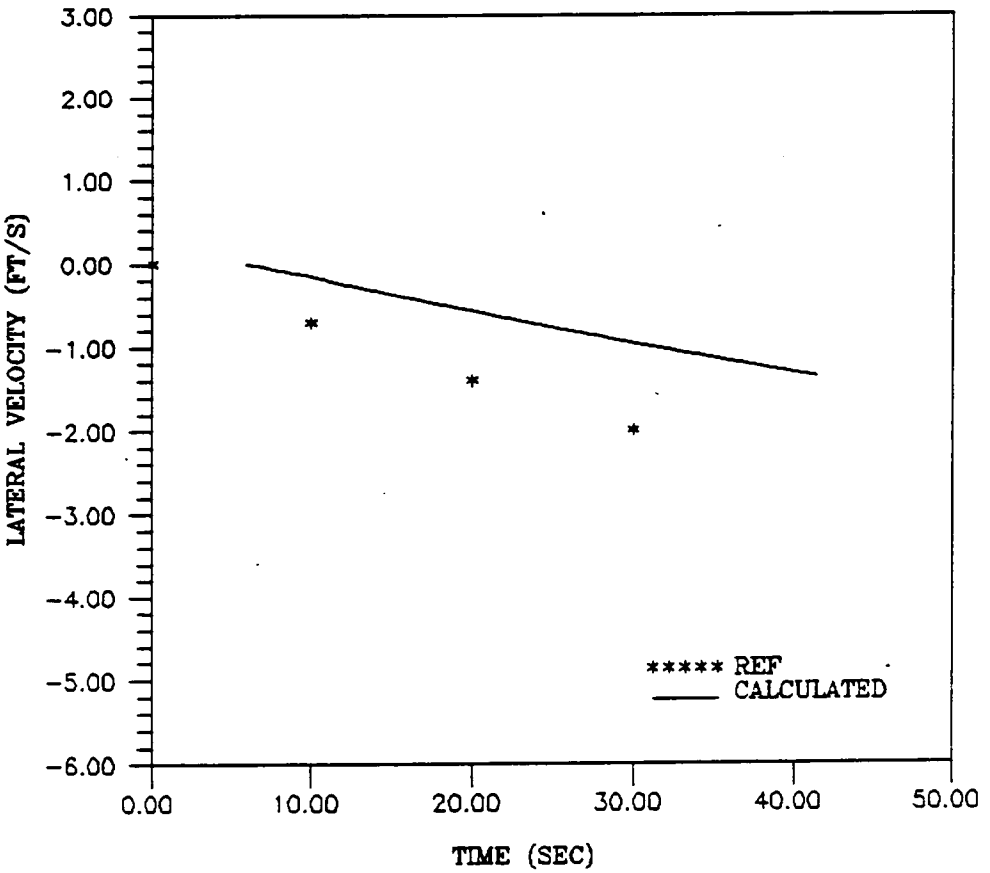

Fig-11(e): Lateral Velocity - UNREP Simulation - 2

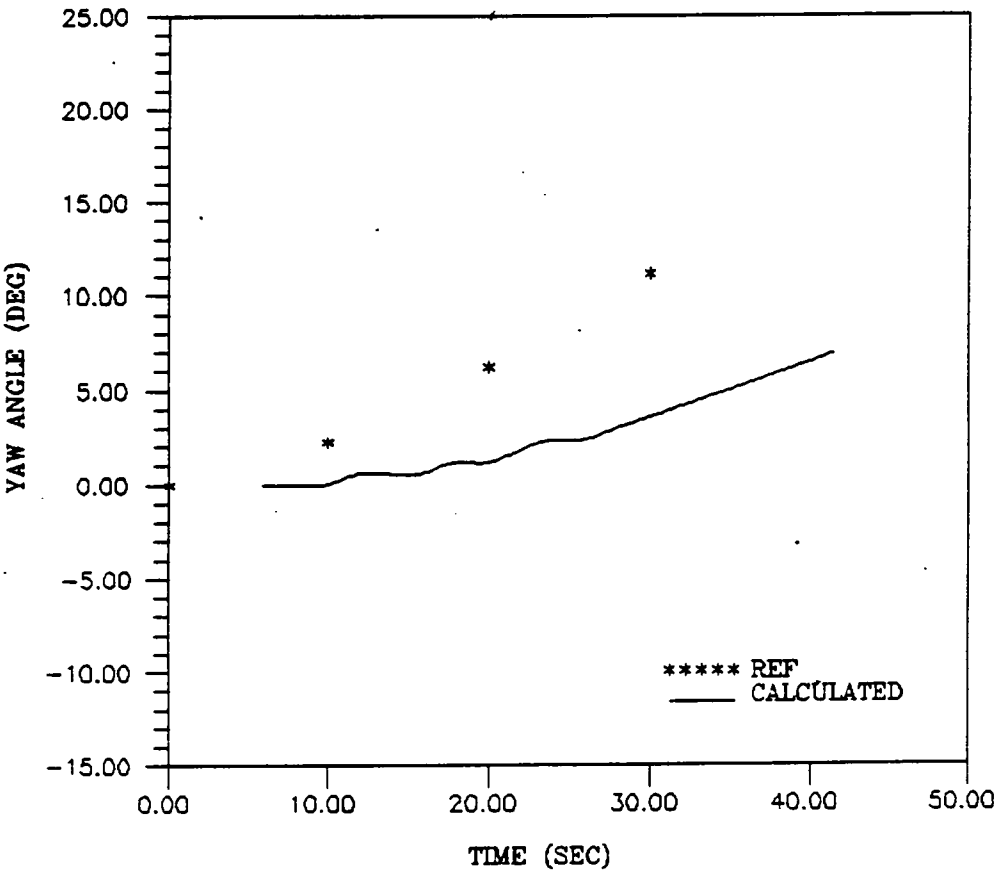

Fig-11(f): Heading Angle - UNREP Simulation - 2

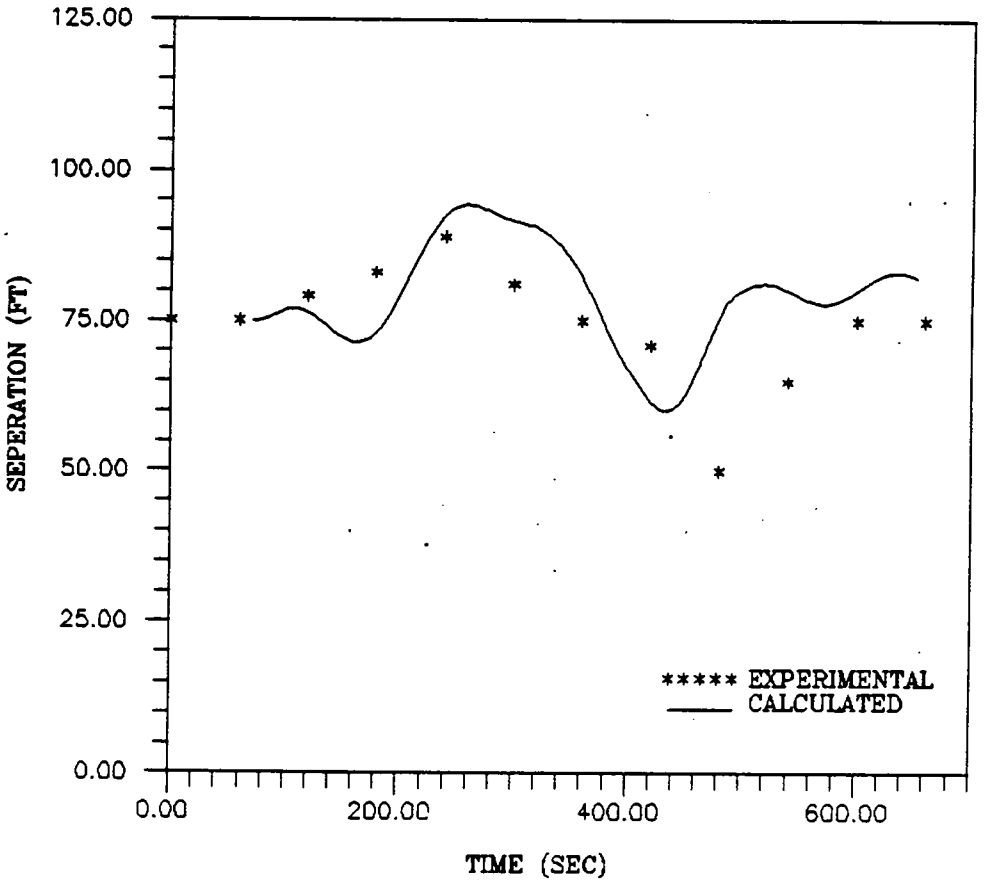

Fig-11(g): Lateral Position - UNREP Simulation - 3

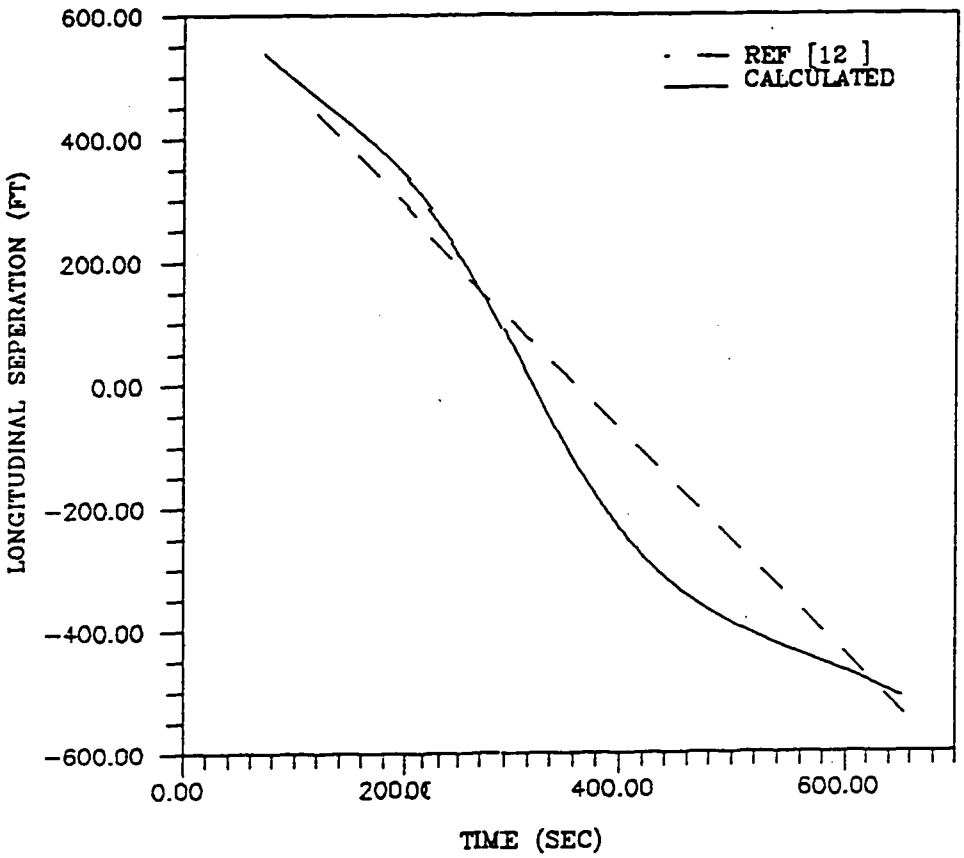

Fig-11h: Longit. Position - UNREP Simulation - 3

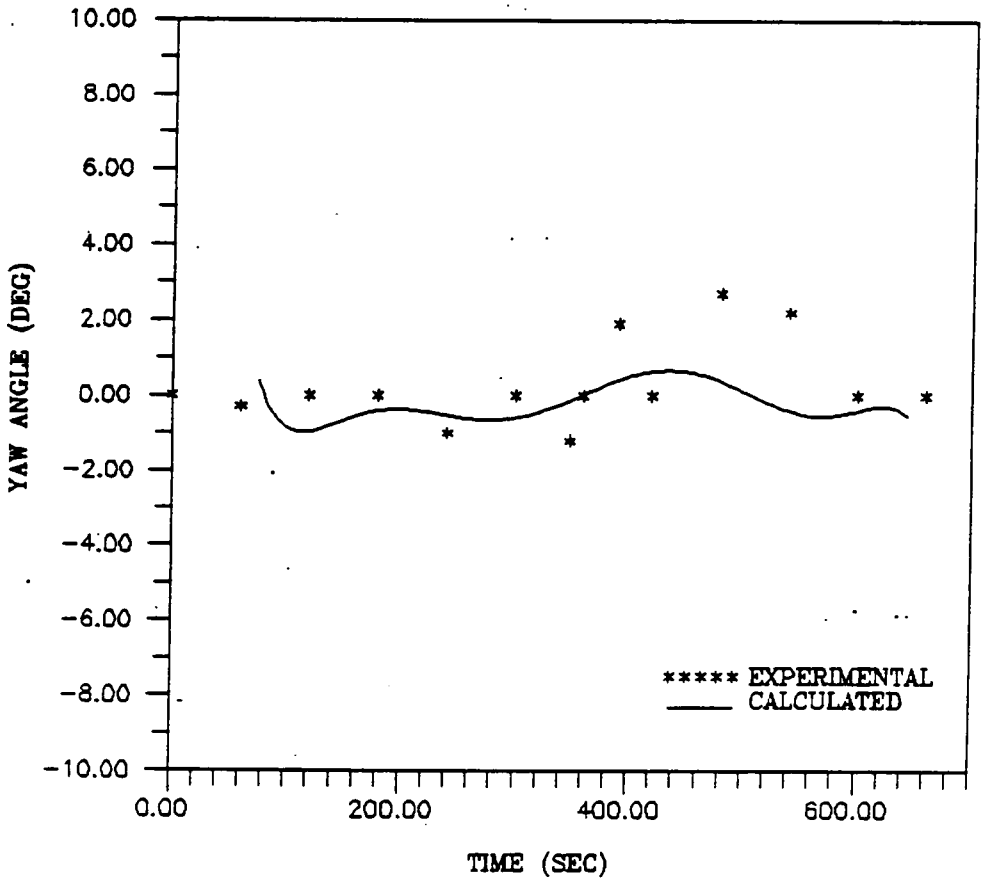

Fig-11(i): Heading Angle - UNREP Simulation - 3

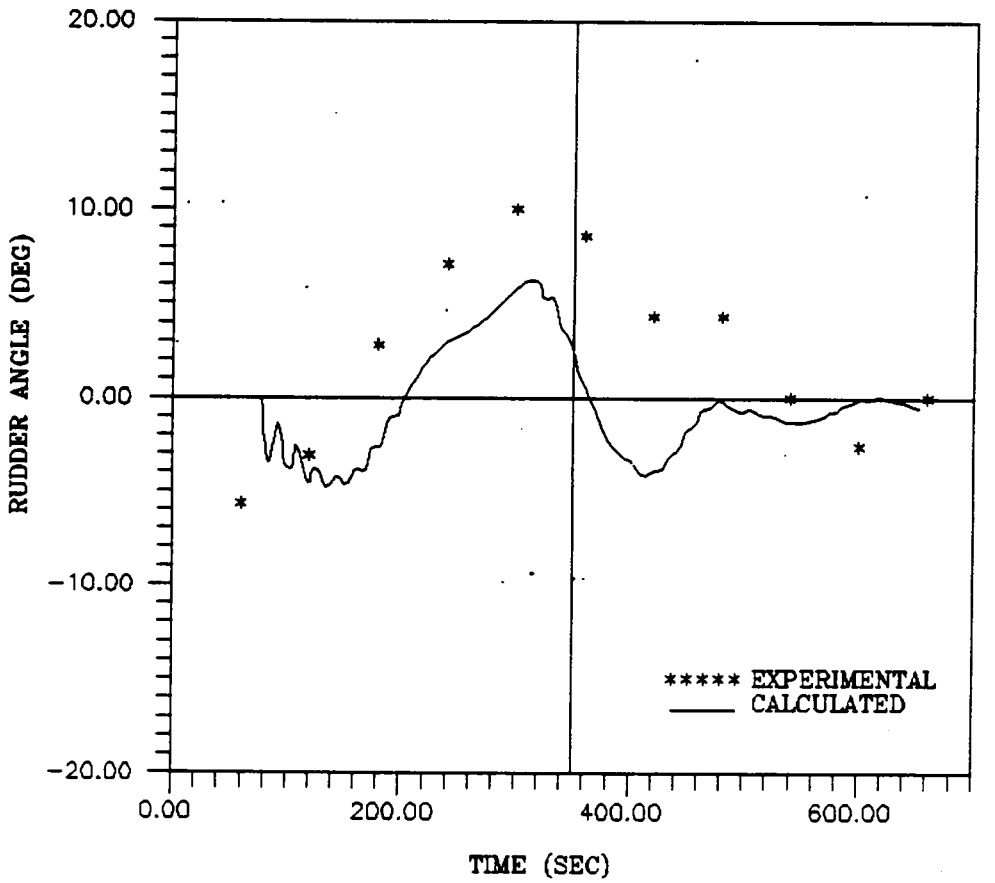

Fig-11(j): Rudder Angle - UNREP Simulation - 3

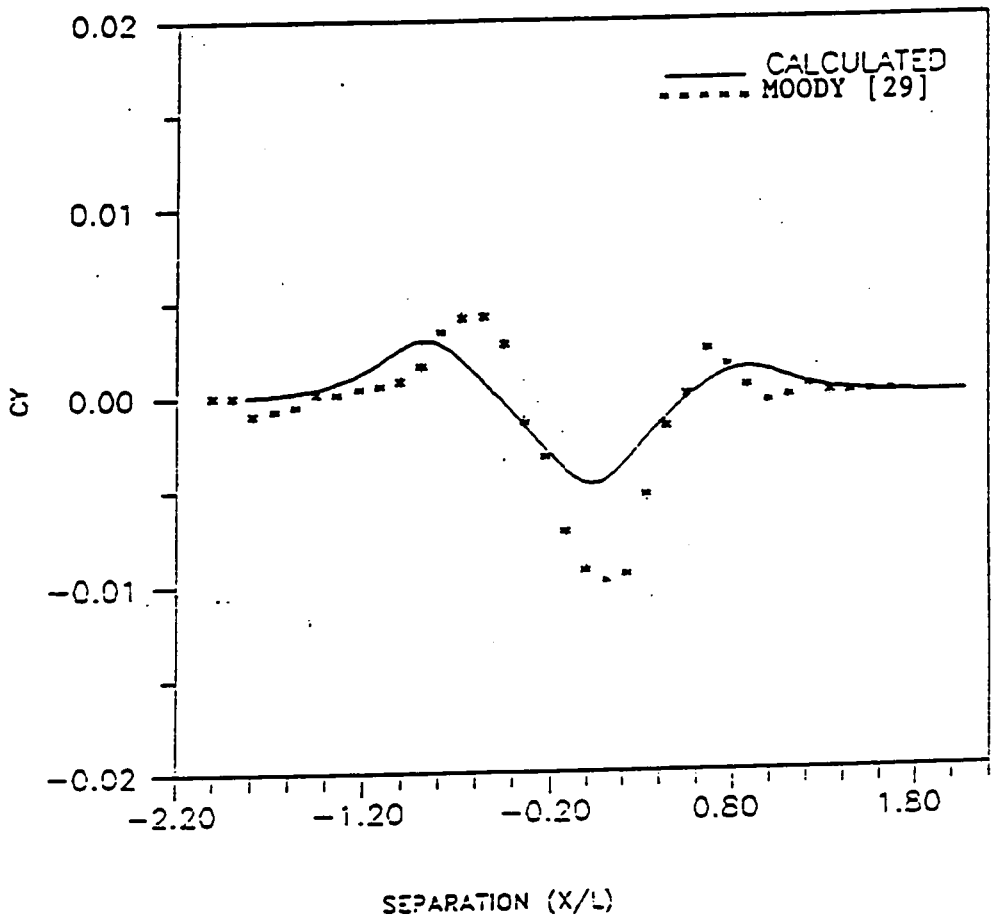

Fig-12(a): Lateral Force - Series-60 Ships Passing.

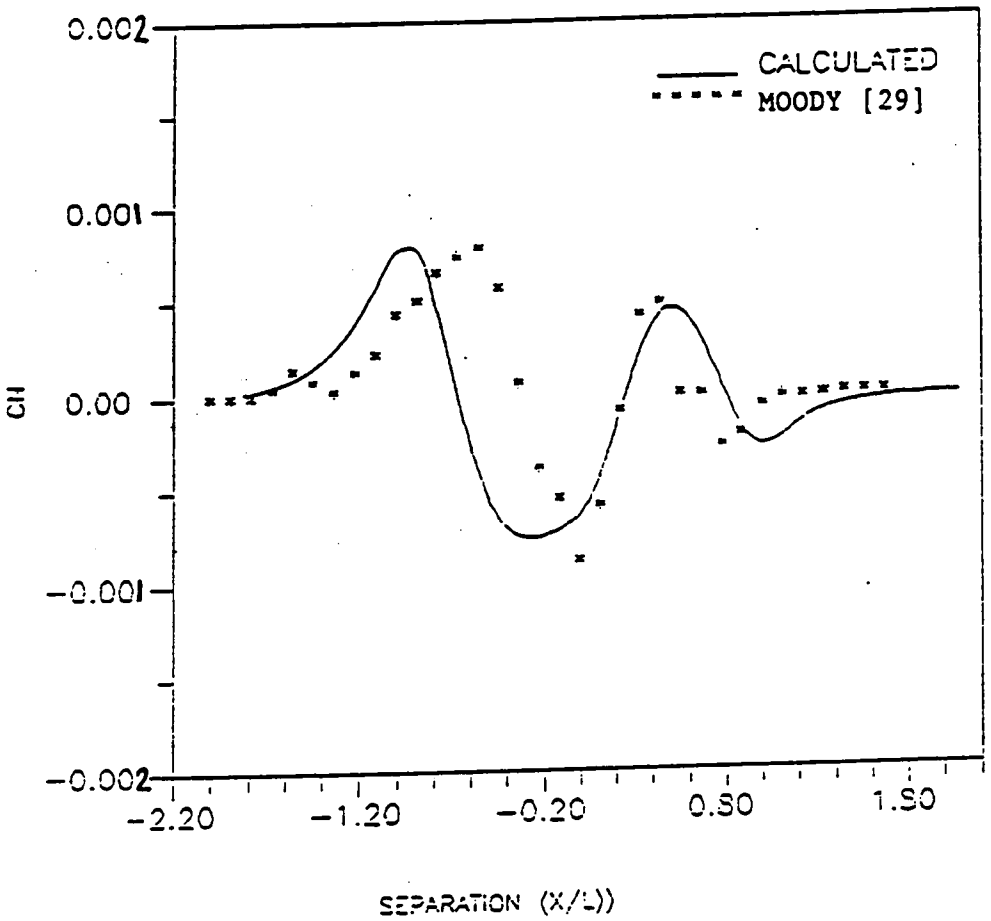

Fig-12(b): Yaw Moment - Series-60 Ships Passing.

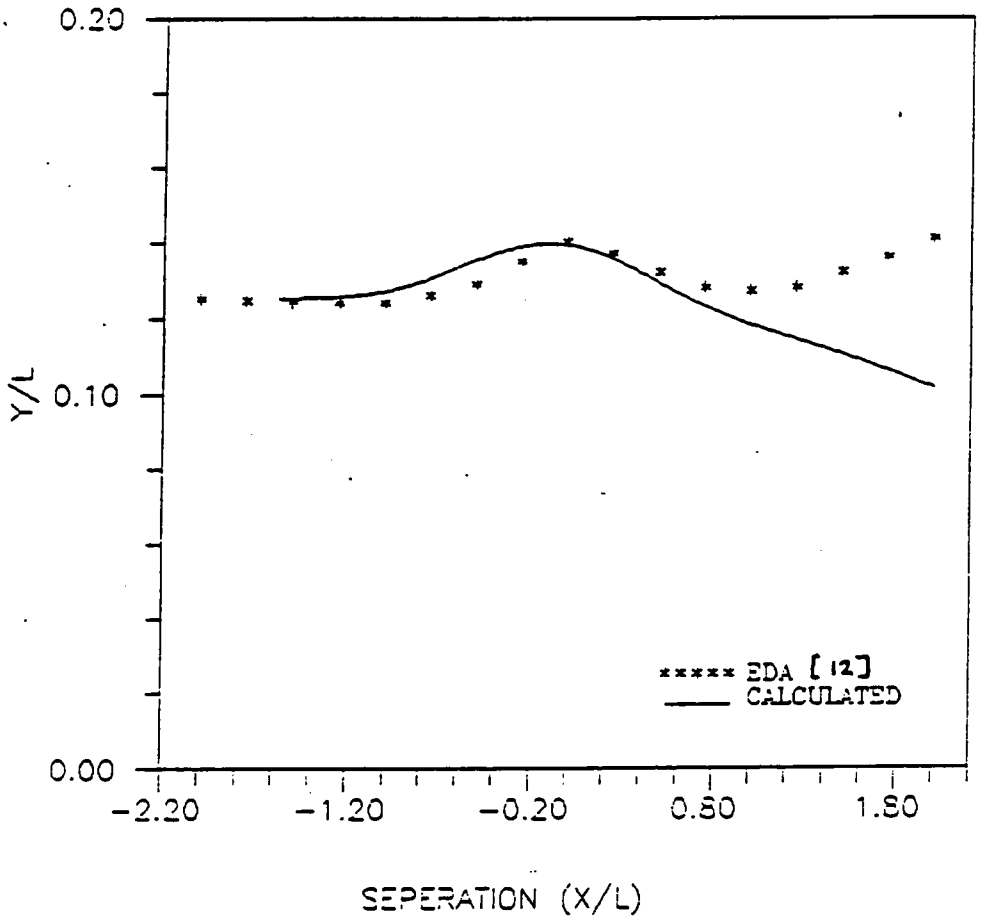

Fig-12(c): Lateral Position - Series-60 Ships Passing in a canal without steering control - A = B' = 0

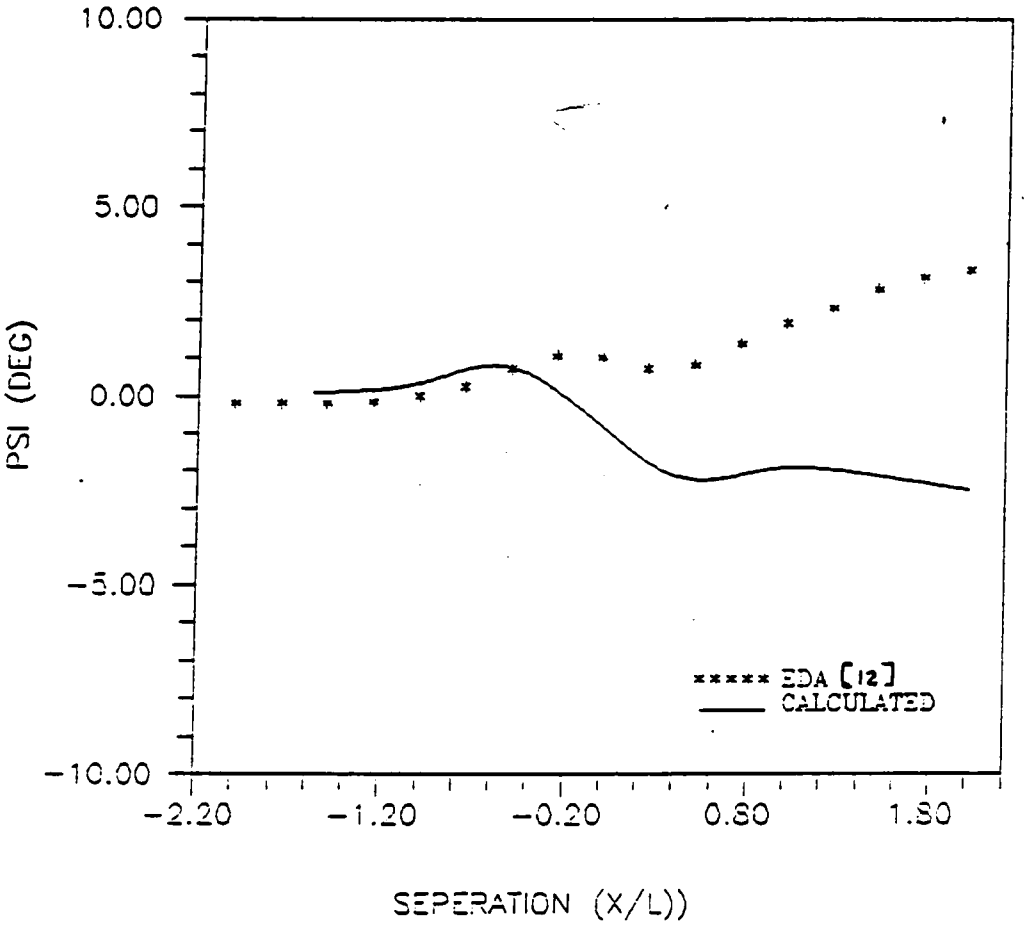

Fig-12(d): Heading Angle – Series-60 Ships Passing in a canal without steering control – A = B' = 0

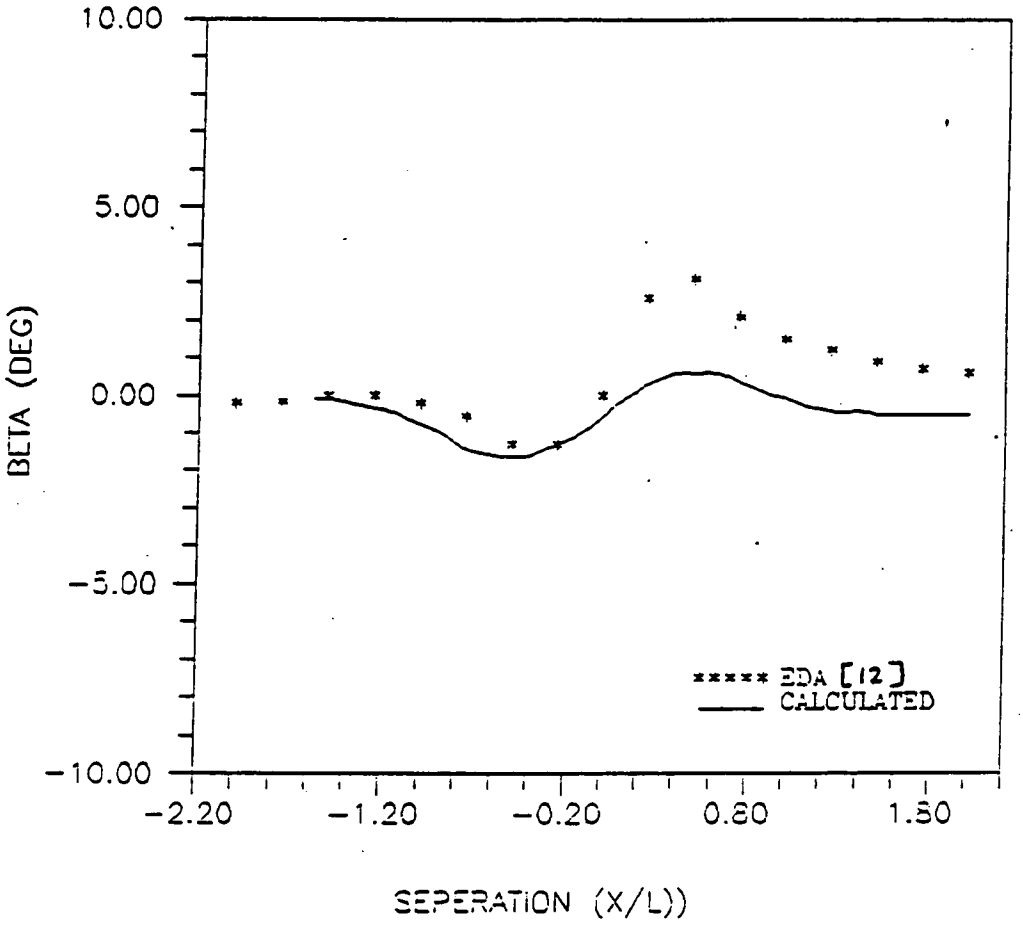

Fig-12(e): Drift Angle – Series-60 Ships Passing in a canal without steering control – A = B' = C

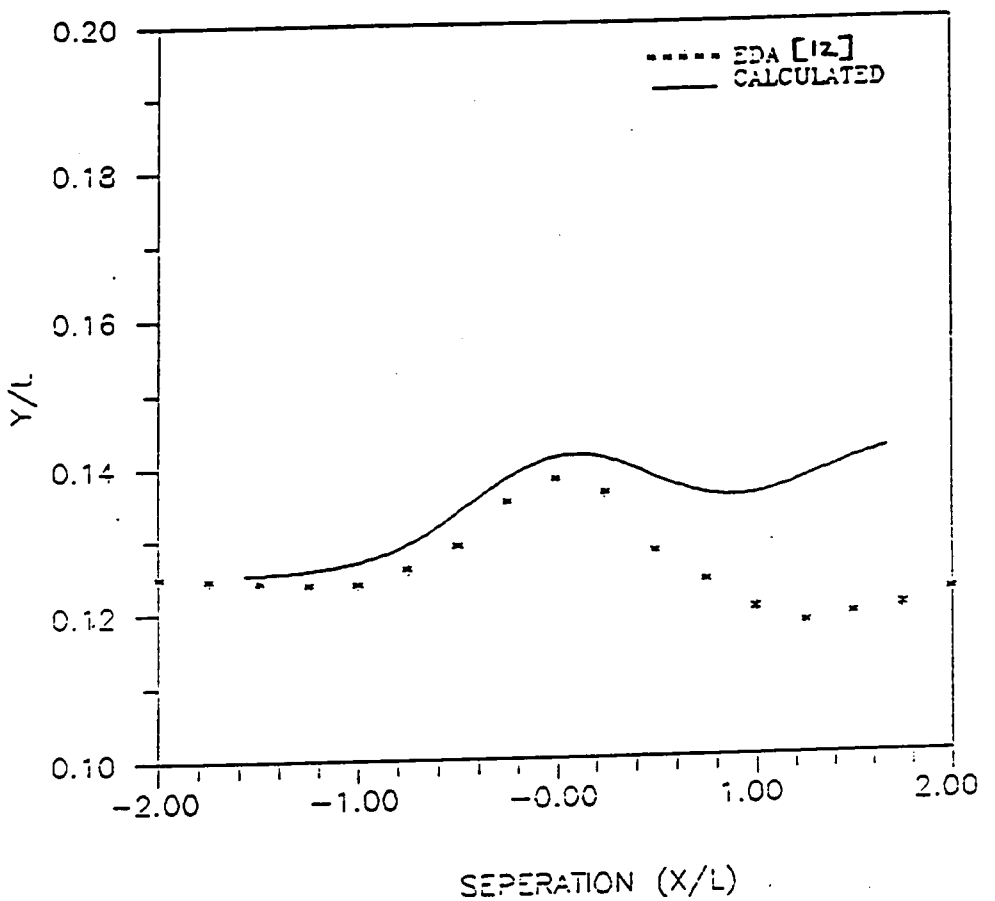

Fig-12(f) Lateral Position - Series-60 Ships Passing in a canal with steering control - A = B = 4

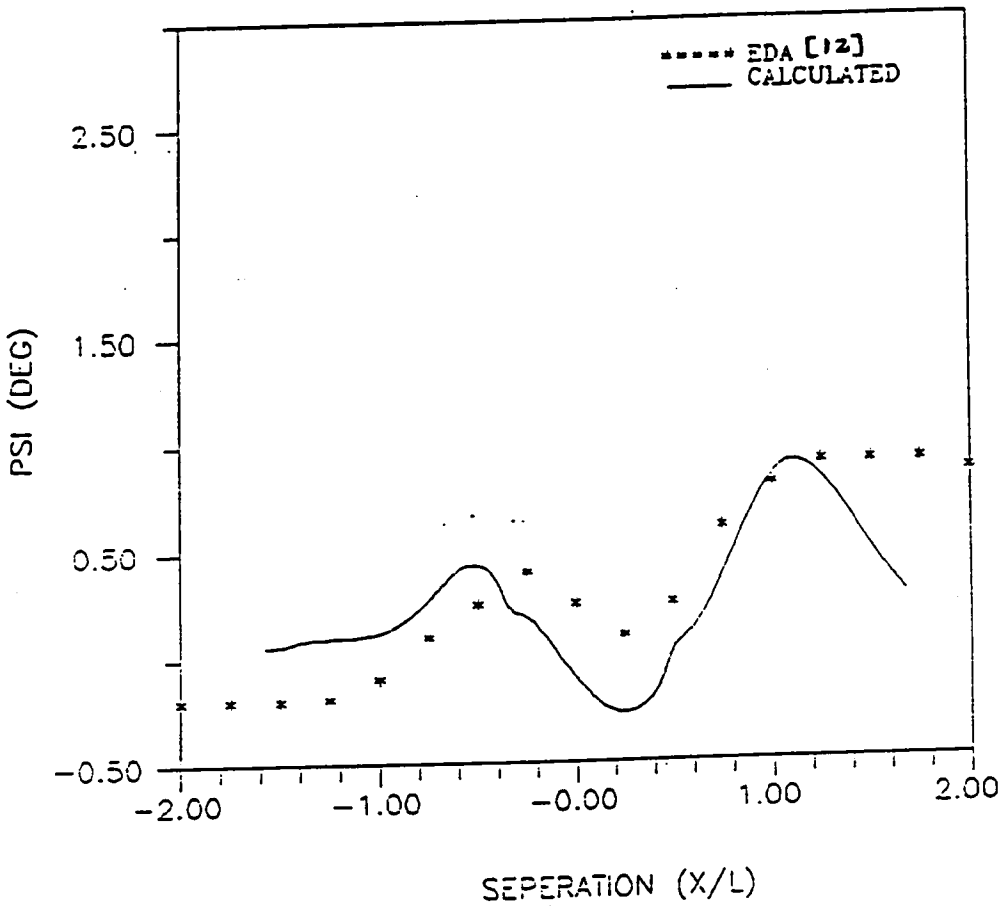

Fig−12(g): Heading Angle − Series-60 Ships Passing in a canal with steering control − A = B = 4

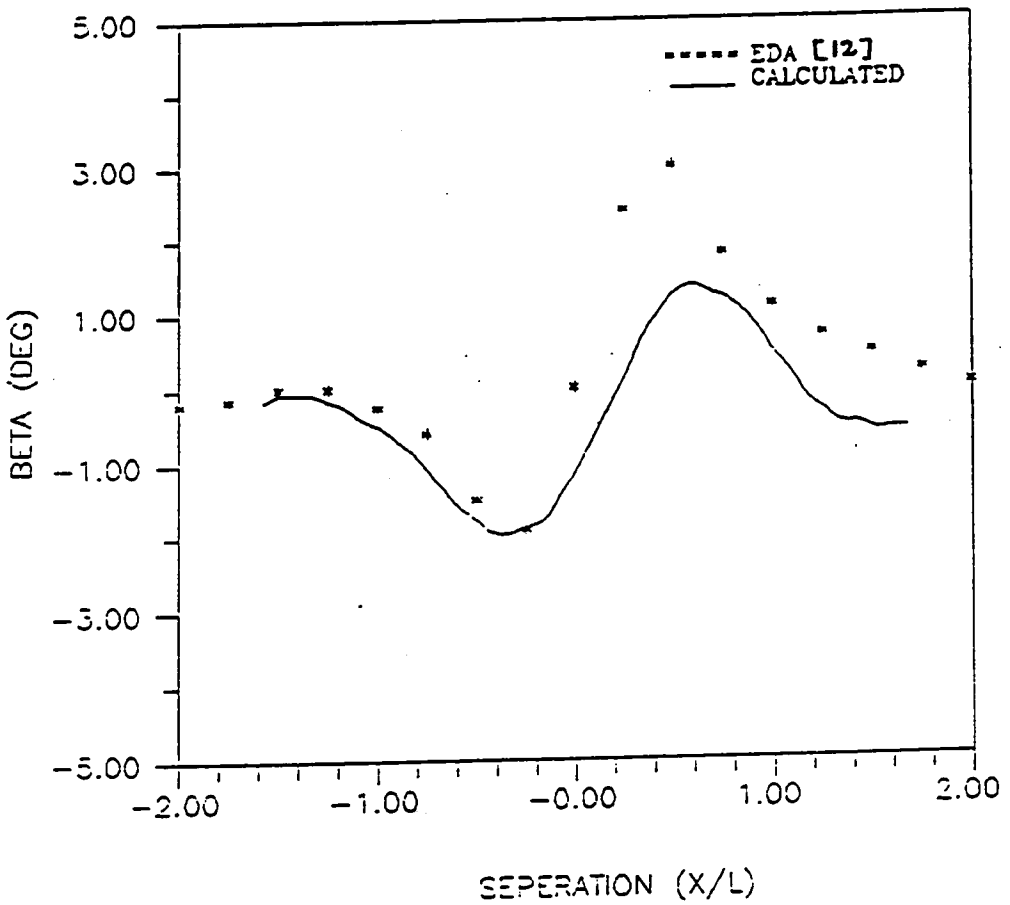

Fig-12(h): Drift Angle – Series-60 Ships Passing in a canal with steering control – A = B = 4

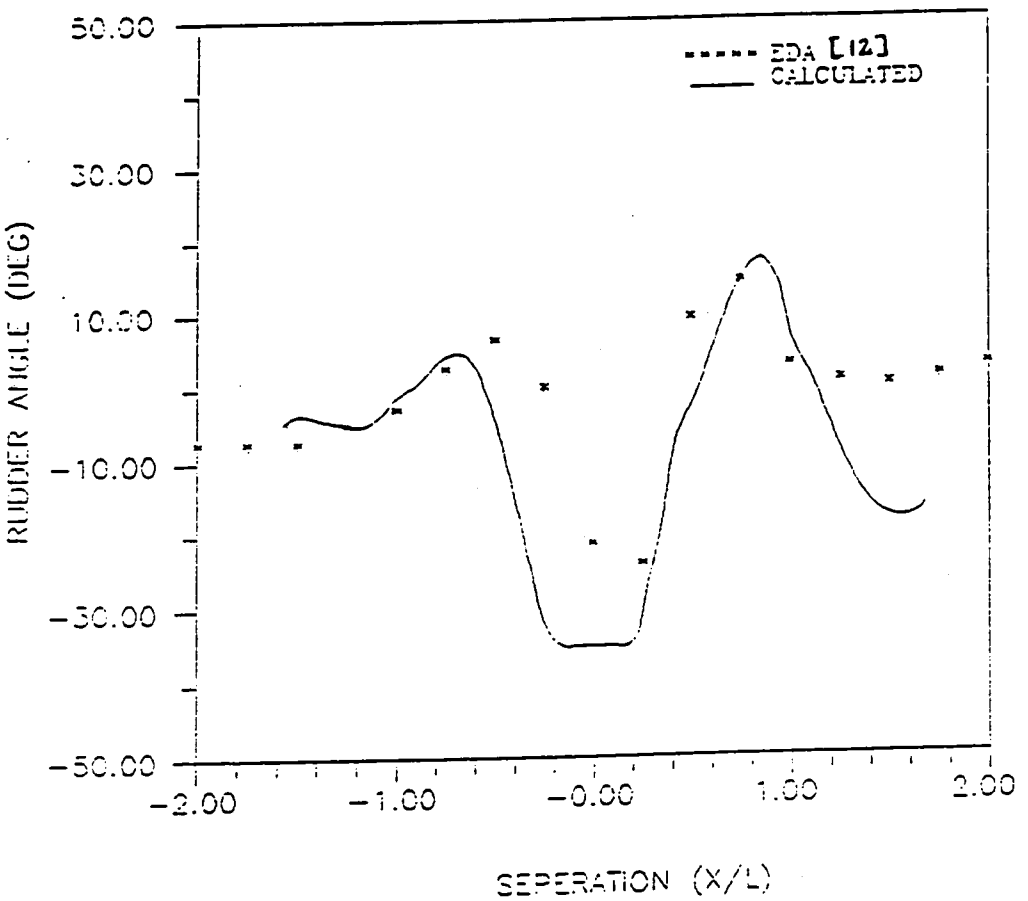

Fig-12(i): Rudder Angle - Series-60 Ships Passing in a canal with steering control - A = B = 4

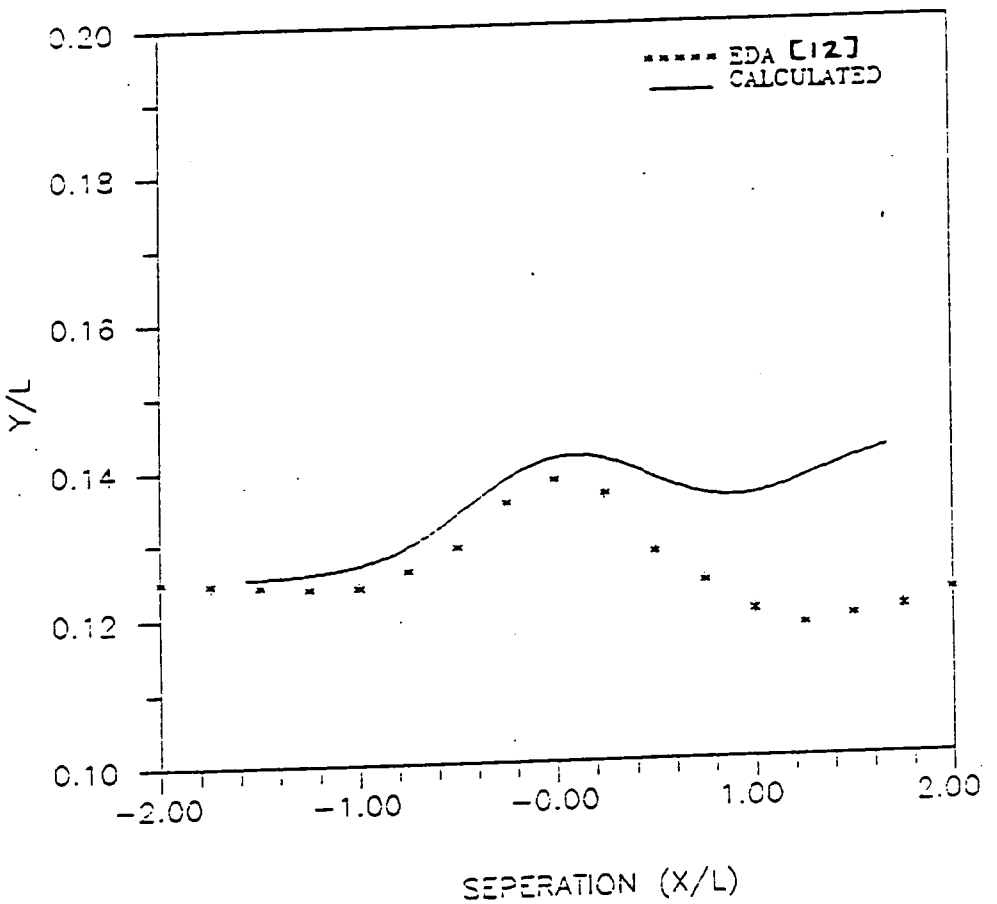

Fig-12(j): Lateral Position – Series-60 Ships Passing in a canal with steering control – A = B' = 6

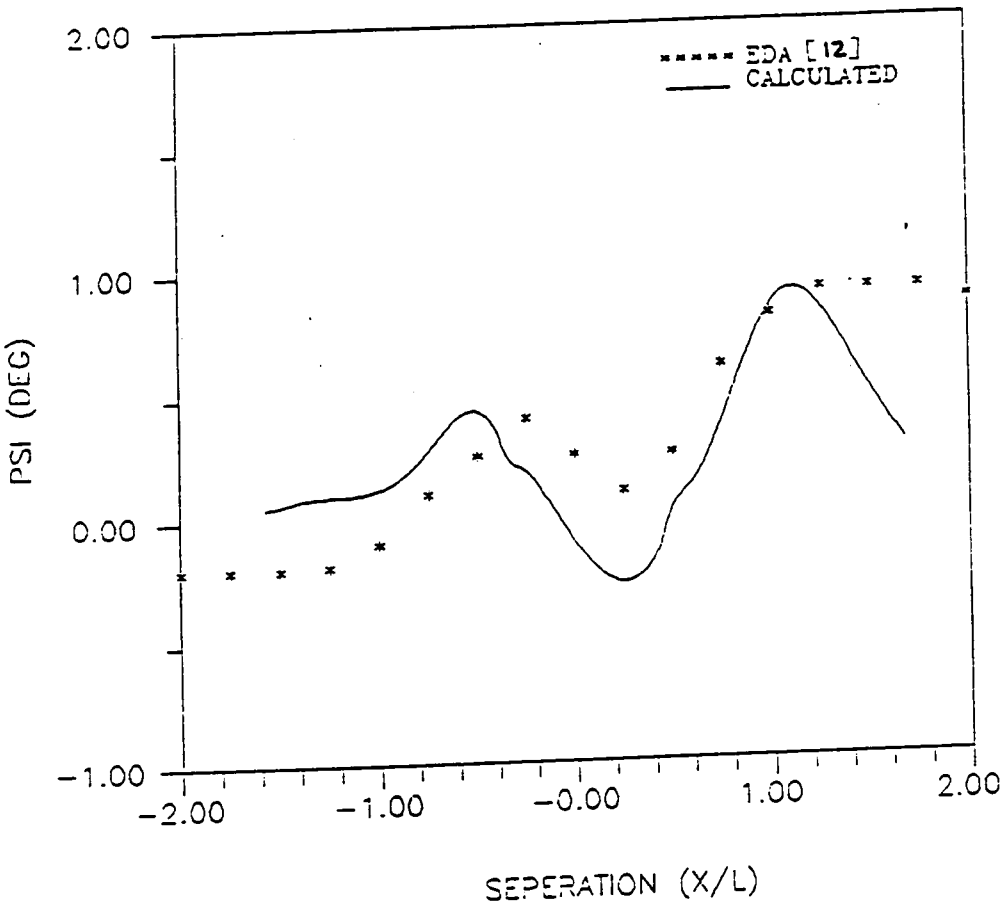

Fig-12(k): Heading Angle – Series-60 Ships Passing in a canal with steering control – A = B' = 6

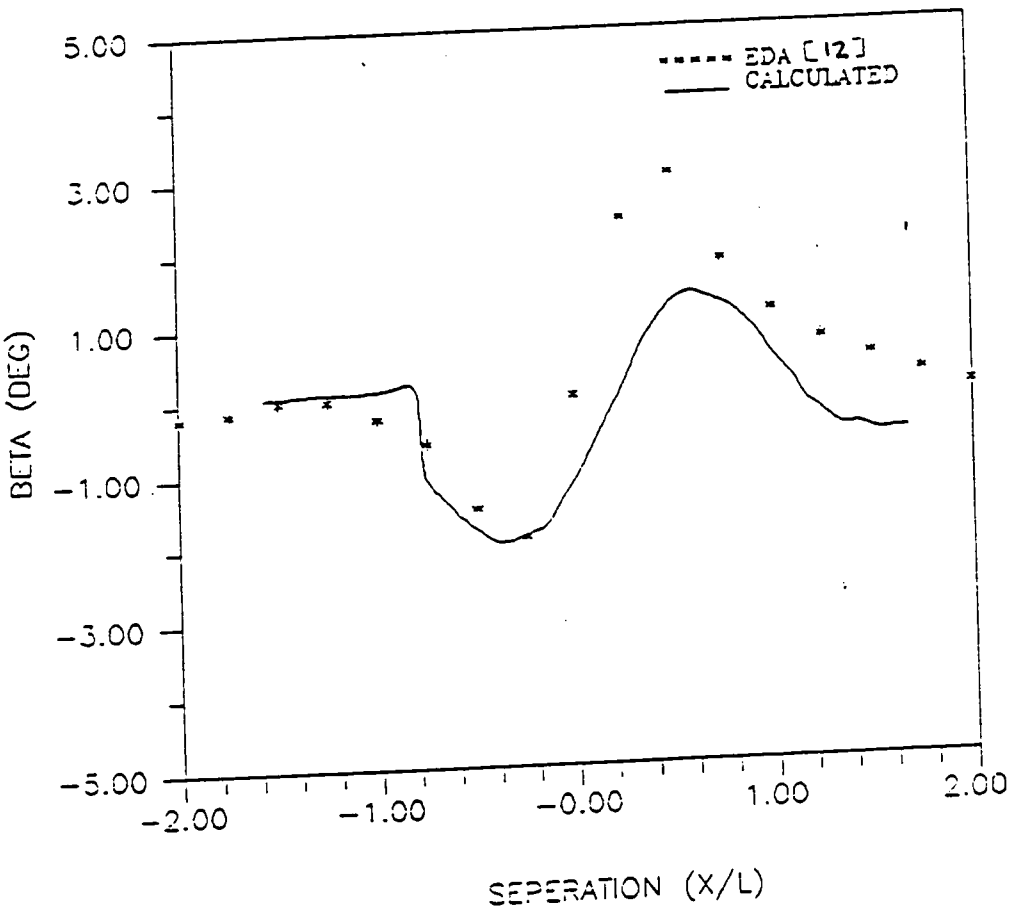

Fig-12(1): Drift Angle – Series-60 Ships Passing in a canal with steering control – A = B = 6

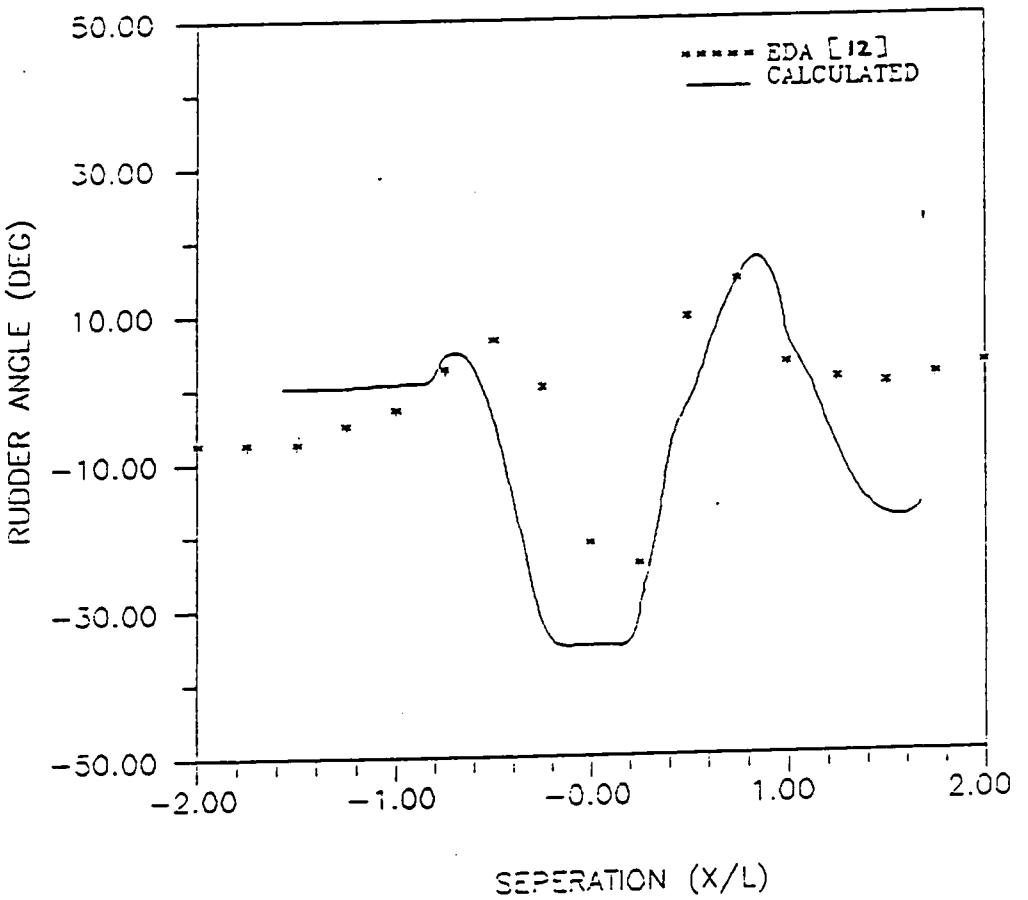

Fig-12(m): Rudder Angle – Series-60 Ships Passing in a canal with steering control – A = B = 6

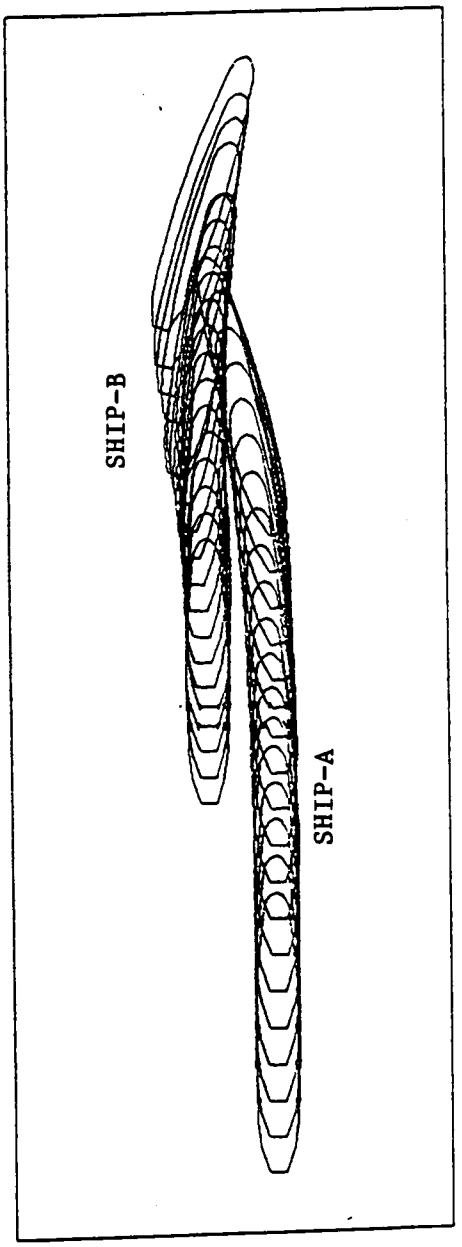

Fig. 13(a): 'NEWYORK' Overtaking in Shallow Water
Without Steering Control - Case-1

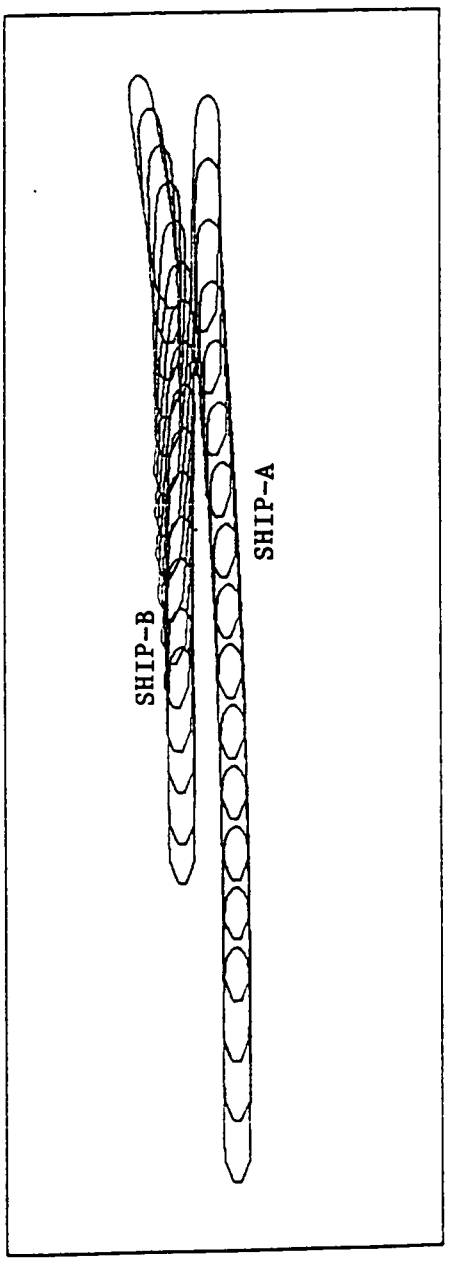

Fig. 13(b): 'NEWYORK' Overtaking in Shallow Water
With Automatic Steering Control - Case-2

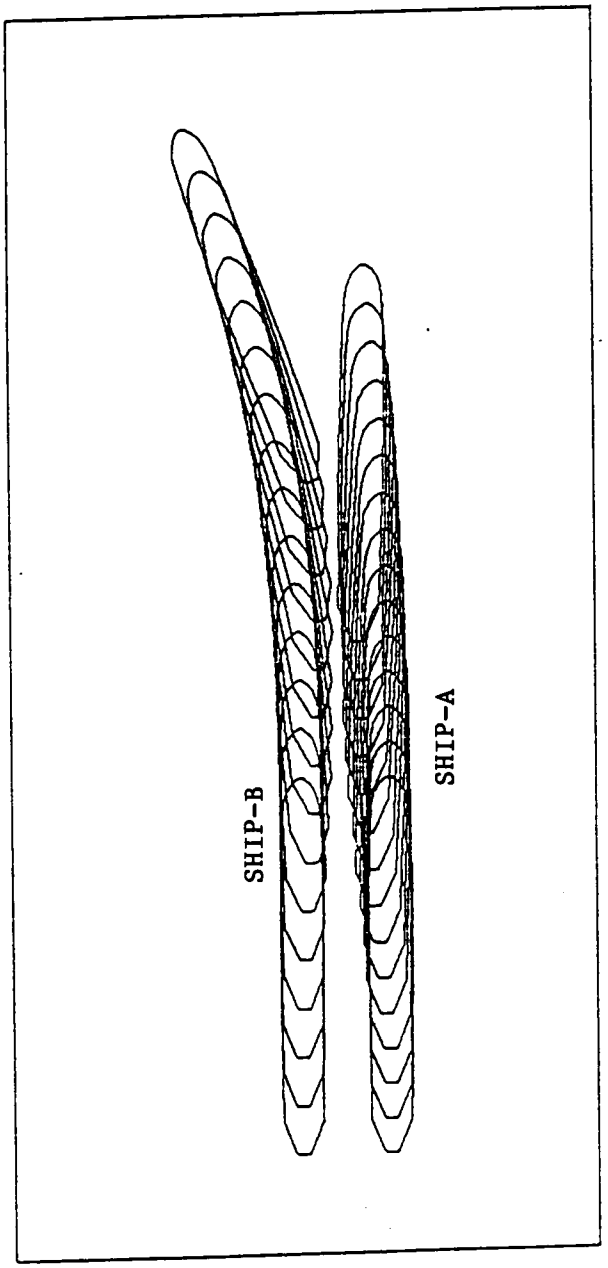

Fig. 13(c): 'NEWYORK' Overtaking in Shallow Water
Without Steering Control - Case-3

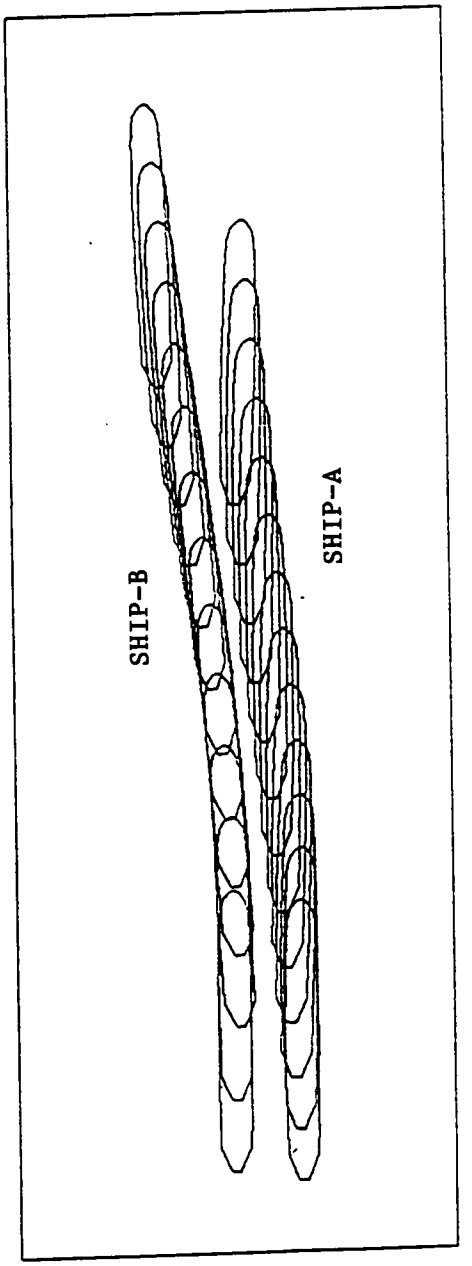

Fig. 13(d): 'NEWYORK' Overtaking in Shallow Water
With Automatic Steering Control - Case-4

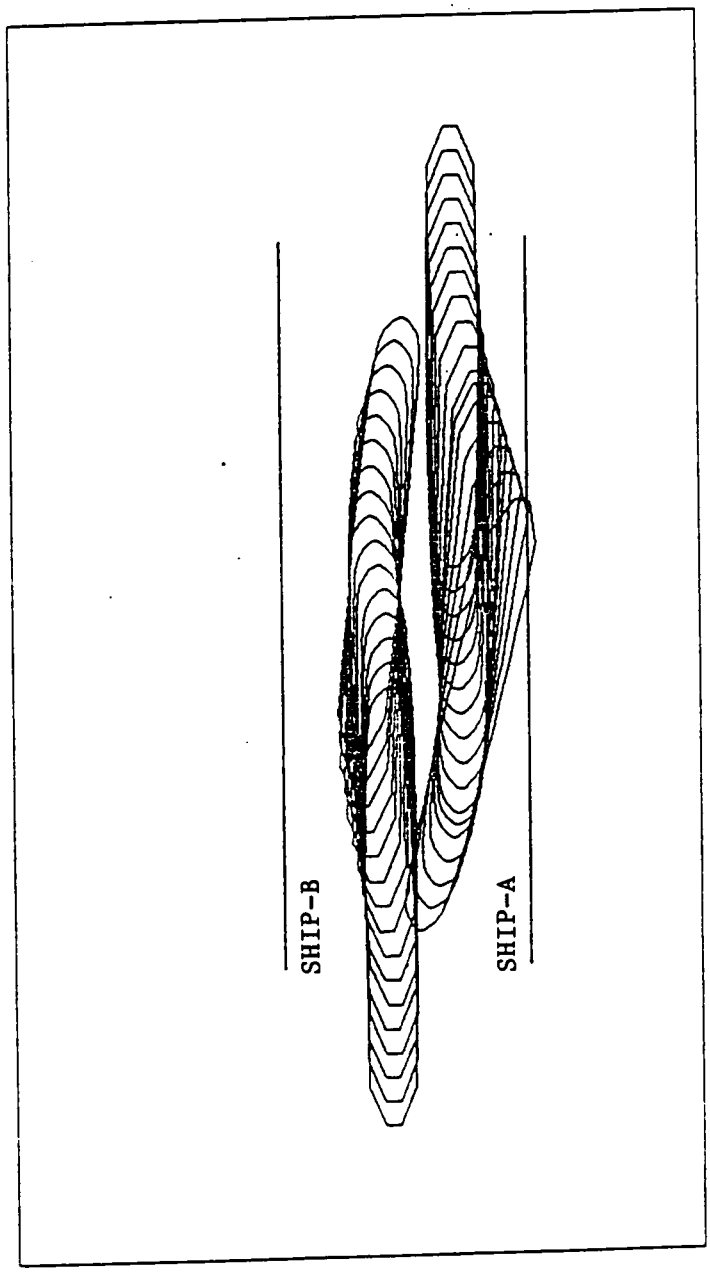

Fig. 13(e): 'NEWYORK' Passing in a Shallow Canal
Without Steering Control - Case-5

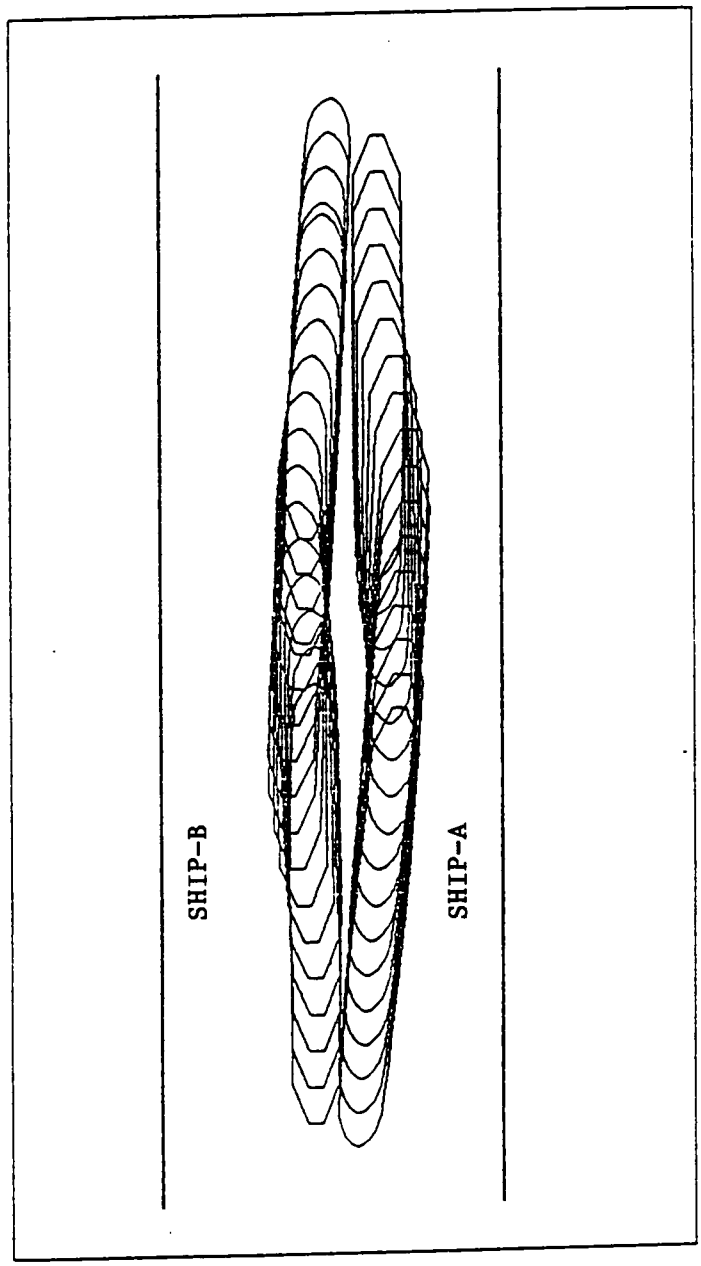

Fig. 13(f): 'NEWYORK' Passing in a Shallow Canal
With Automatic Steering Control - Case-6

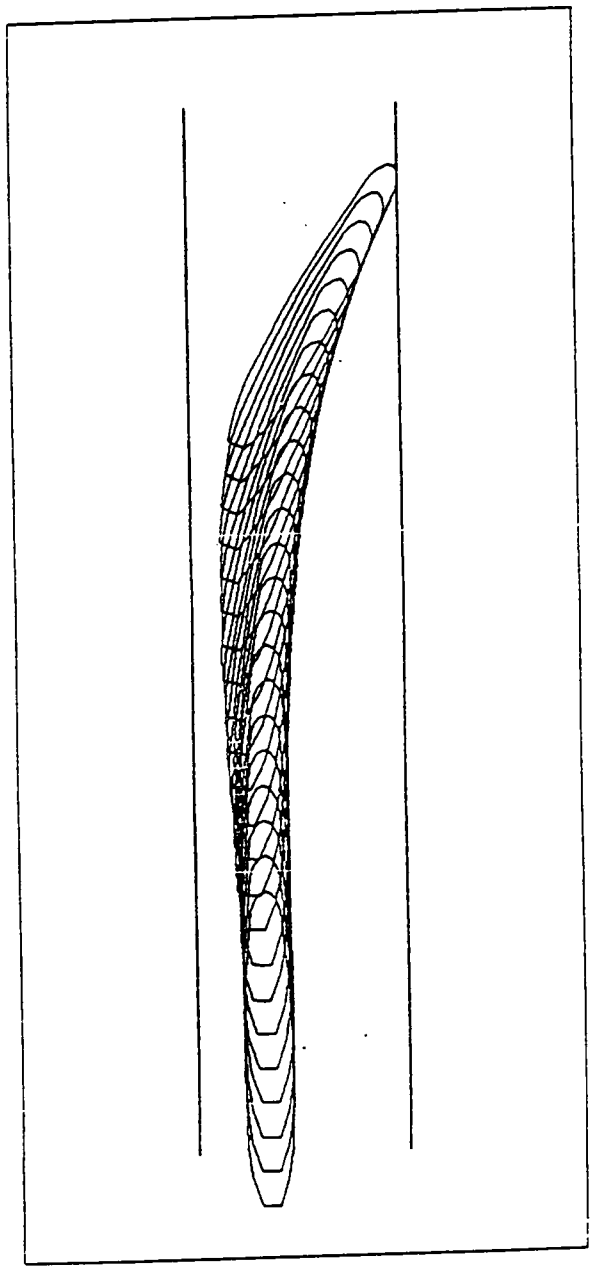

Fig. 13(g): 'NEWYORK' in a Shallow Canal
Without Steering Control - Case-7

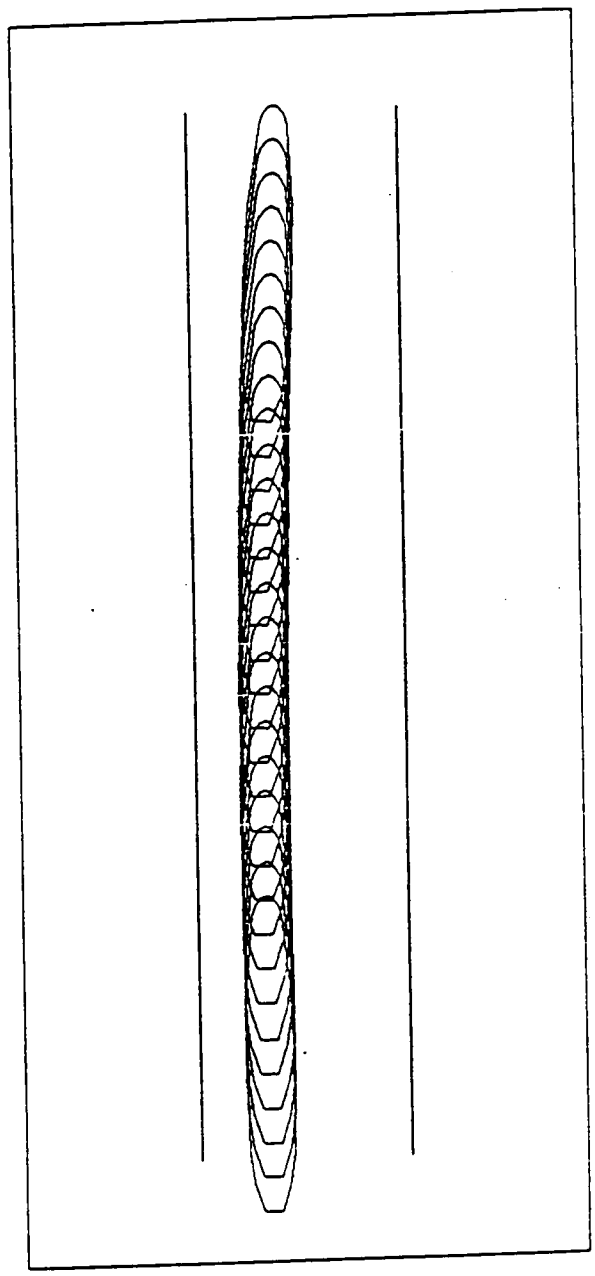

Fig. 13(h): 'NEWYORK' in a Shallow Canal
With Automatic Steering Control - Case-8

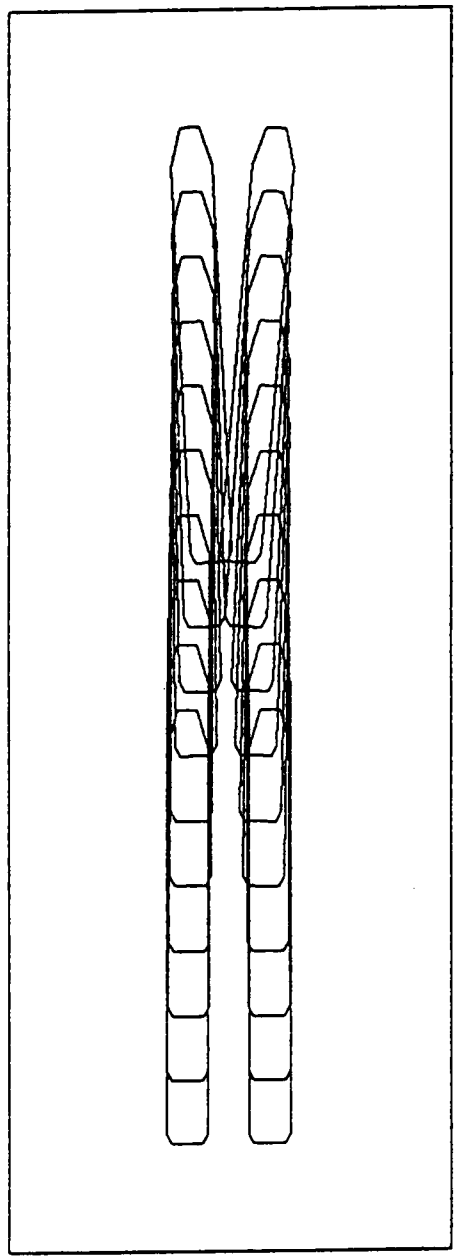

Fig. 13(1): 'Barge-Tow' Overtaking in Shallow Water
Without Steering Control - Case-9

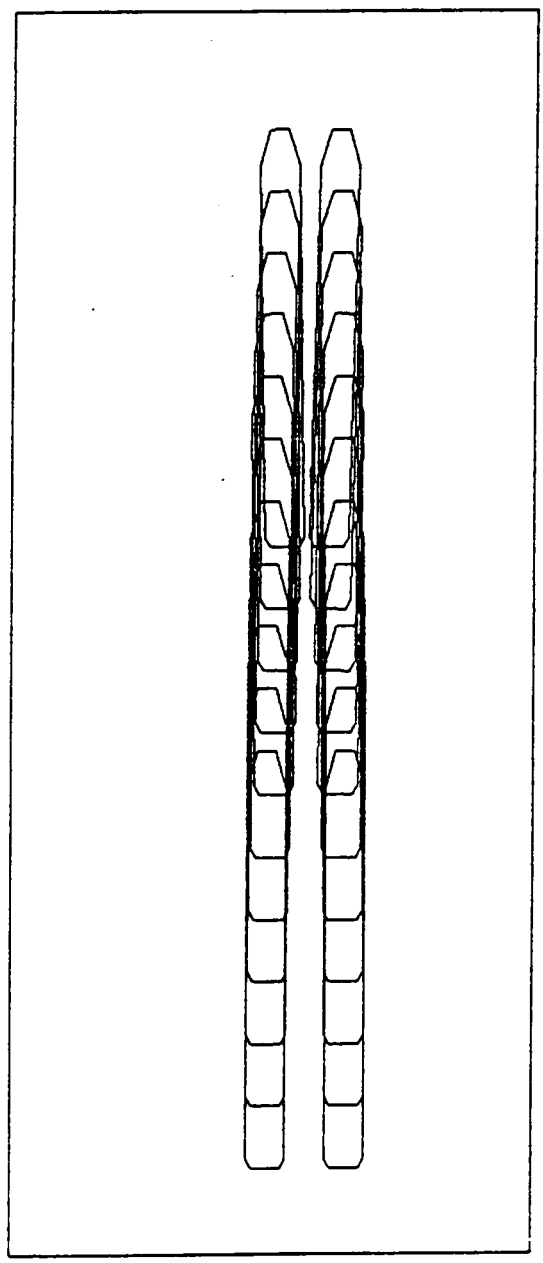

Fig. 13(j): 'Barge-Tow' Overtaking in Shallow Water
With Automatic Steering Control - Case-10

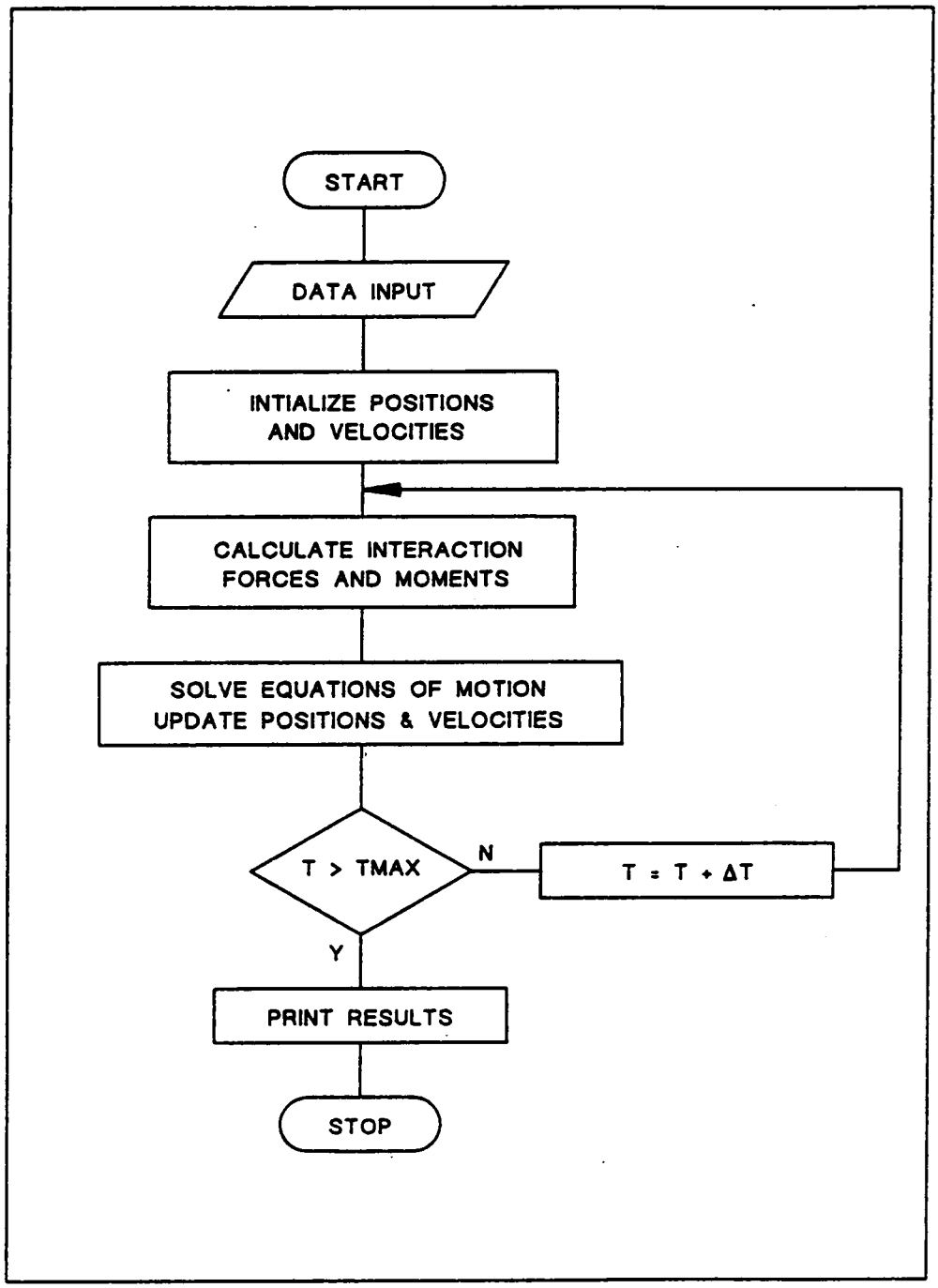

Fig. 14(a): Flow Chart of the Main Program.

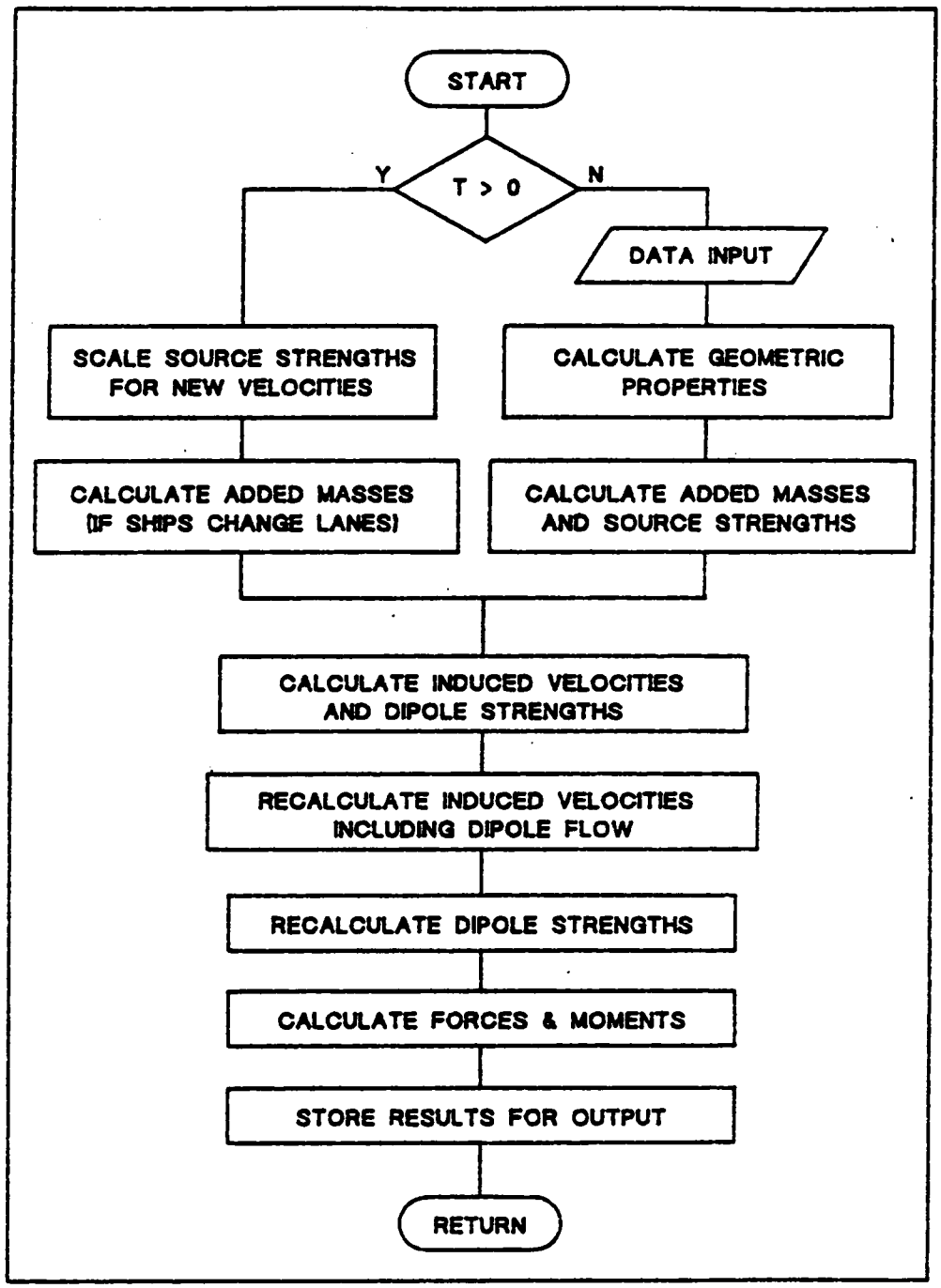

Fig. 14(b): Flow Chart of the Interaction Program.

Appendix-A

Solution of the analytical equation for added mass

For not intermediate water depth situations where T/H is less than 0.8, the asymptotic solution for added mass as given in Eqn. 4.3 cannot be used. These cases require complete solution of Gurevich's equation as given in Eqn.[4.5]. The solution can be obtained by finding the parameters α and q in terms of the geometrical parameters of the problem, viz: b/c and d/c.

Here we use a method first introduced by Flagg and Newman [13]. The procedure is an iterative search leading to the solution by a generalized Newton-Raphson scheme. Using the same notations as in Flagg and Newman [13], we have:

$$b/c = B \qquad d/c = D$$

$$\frac{\partial(b/c)}{\partial\alpha} = B_\alpha$$

$$\frac{\partial(d/c)}{\partial\alpha} = D_\alpha$$

$$\frac{\partial(b/c)}{\partial q} = B_q$$

$$\frac{\partial(d/c)}{\partial q} = D_q$$

Starting with the guess values for $\alpha=\alpha_1$ and $q=q_1$, calculate B_1 and D_1 using Eqn. [4.6] and [4.7]. Here it may be noticed that 'b' is the beam of the vessel, 'd' is the draft and 'c' is the water depth according to the notations of Chapter 4. repeat the calculations using $\alpha = \alpha_1 + \Delta\alpha$ and $q = q_1 + \Delta q$ to obtain $B(\alpha+\Delta\alpha,q)$, $B(\alpha,q+\Delta q)$, $D(\alpha+\Delta\alpha,q)$ and $D(\alpha,q+\Delta q)$. Then,

$$B_{\alpha 1} = \frac{B(\alpha+\Delta\alpha,q)-B(\alpha,q)}{\Delta\alpha}$$

$$B_{q1} = \frac{B(\alpha,q+\Delta q)-B(\alpha,q)}{\Delta q}$$

$$D_{\alpha 1} = \frac{D(\alpha+\Delta\alpha,q)-D(\alpha,q)}{\Delta\alpha}$$

$$D_{q1} = \frac{D(\alpha,q+\Delta q)-D(\alpha,q)}{\Delta q}$$

Then, using the first order Taylor expansion for B and D, we can write,

$$B = B_1 + \Delta\alpha\, B_{\alpha 1} + \Delta q\, B_{q1}$$

$$D = D_1 + \Delta\alpha\, D_{\alpha 1} + \Delta q\, D_{q1}$$

$$\Delta\alpha = \frac{D_{q1}\,[B-B_1] - B_{q1}\,[D-D_1]}{D_{q1}\,B_{\alpha 1} - B_{q1}\,D_{\alpha 1}}$$

$$\Delta q = \frac{B_{\alpha 1}\,[D-D_1] - D_{\alpha 1}\,[B-B_1]}{D_{q1}\,B_{\alpha 1} - B_{q1}\,D_{\alpha 1}}$$

and $\alpha = \alpha + \Delta\alpha$

$q = q + \Delta q$

Continue iteration until adequate convergence is obtained. Once α and q are known, added mass can be calculated using the infinite series solutions as given in Equations 4.5, 4.8, 4.13, 4.14 and 4.15.

Appendix-B

Non-dimensional hydrodynamic coefficients:

Mariner Class Ships

Coefficient	Value X 10^5
$X_{\dot{u}}' - m'$	-850.0
X_u'	-120.0
Y_v'	-1243.0
$Y_{\dot{v}}' - m$	-1500.0
Y_r'	-510.0
$Y_{\dot{r}}' - m'x_G'$	-27.0
Y_δ'	270.0
N_v'	-351.0
$N_r' - m'x_G'$	-227.0
$N_{\dot{r}}' - I_z'$	-68.0
N_δ'	-126.0
X_n'	4.62
Y_n'	-0.52
N_n'	0.26

APPENDIX-C

Non-dimensional hydrodynamic coefficients:

Series-60 Cargo Ships in Canal

(W/B=5.7, D/H=1.5)

Coefficient	Value X 10^5
$X_{\dot{u}}' - m'$	-874.7
Y_v'	-4437.9
$Y_{\dot{v}}' - m'$	-2684.2
$Y_r' - m'$	-113.6
Y_δ'	309.7
N_v'	-1445.8
N_r'	-650.1
$N_{\dot{r}}' - I_z'$	-137.9
N_δ'	-135.6
X_{uu}'	-85.9
X_{vr}'	2684.2
Y_η'	442.4
V_e'	380.70
β_e	-13030.1
δ_e	-7465772.0
Y_{oe}'	12500.0

APPENDIX-D

Non-dimensional Hydrodynamic Coefficients

Container Ship "NEWYORK"

Coefficient	Value
$X_{\dot{u}}'$	-0.0004
X_{rr}'	0.0001
X_{vr}'	0.0049
X_{vv}'	-0.00245
X_{vvn}'	0.00
$X_{\delta\delta}'$(steering)	-0.00172
$X_{\delta\delta}'$(flanking)	0.00
$Y_{\dot{r}}'$	-0.00035
$Y_{\dot{v}}'$	-0.0057
Y_{rr}'	-0.0005
Y_{vr}'	-0.0055
Y_{r}'	0.0026
Y_{v}'	-0.00725
Y_{rn}'	0.00065
Y_{vv}'	-0.0215
Y_{vn}'	-0.00116
Y_{vvn}'	0.0
Y_{*}'	0.00005
Y_{δ}'(steering)	0.00192
Y_{δ}'(flanking)	0.00
Y_{rv}'	0.00115

Non-dimensional Hydrodynamic Coefficients

Container Ship "NEWYORK" (CONTD.)

Coefficient	Value
$N_{\dot{r}}'$	-0.000322
$N_{\dot{v}}'$	-0.000255
N_{vr}'	-0.00316
N_{rr}'	-0.00048
N_{r}'	-0.00172
N_{rn}'	-0.00033
N_{v}'	-0.00378
N_{vv}'	0.000960
N_{vn}'	0.000580
N_{vvn}'	0.0
N_{*}'	-0.000025
N_{δ}'(steering)	-0.000960
N_{δ}'(flanking)	0.00
N_{rv}'	0.00122

APPENDIX-E

Non-dimensional Hydrodynamic Coefficients

1130 Feet Long Barge-Tow

Coefficient	Value
$X'_{\dot{u}}$	-0.000025
X'_{rr}	0.0000
X'_{vr}	0.000275
X'_{vv}	-0.000950
X'_{vvn}	0.00
$X'_{\delta\delta}$(steering)	-0.000244
$X'_{\delta\delta}$(flanking)	0.00
$Y'_{\dot{r}}$	-0.0000383
$Y'_{\dot{v}}$	-0.000403
Y'_{rr}	-0.000280
Y'_{vr}	-0.00189
Y'_{r}	0.00047
Y'_{v}	-0.00117
Y'_{rn}	0.000155
Y'_{vv}	-0.00505
Y'_{vn}	-0.000339
Y'_{vvn}	0.0
Y'_{*}	0.000008
Y'_{δ}(steering)	0.000329
Y'_{δ}(flanking)	0.00
Y'_{rv}	-0.0000750

Non-dimensional Hydrodynamic Coefficients

1130 Feet Long Barge-Tow (CONTD.)

Coefficient	Value
$N_{\dot{r}}'$	-0.0000249
$N_{\dot{v}}'$	0.0000380
N_{vr}'	-0.000257
N_{rr}'	-0.000101
N_{r}'	-0.000224
N_{rn}'	-0.0000670
N_{v}'	-0.000163
N_{vv}'	0.000445
N_{vn}'	0.000151
N_{vvn}'	0.0
N_{*}'	-0.000004
N_{δ}'(steering)	-0.000171
N_{δ}'(flanking)	0.00
N_{rv}'	0.0000550

The vita has been removed from the scanned document